AL-GA SACRIFICIAL ANODES:

UNDERSTANDING PERFORMANCE VIA SIMULATION AND MODIFICATION OF ALLOY SEGREGATION

Michael Scott Kidd Jr.

Thesis Submitted to The Faculty of the Virginia Polytechnic Institute and State University in Partial Fulfillment of the Requirements for The Degree of

Master of Science
In
Material Science and Engineering

Alan P. Druschitz
Bill T. Reynolds
Sean G. Corcoran

February 19, 2019
Blacksburg, Virginia

Key Words: Corrosion, Cathodic Protection, Sacrificial Anode, Al-Ga, Galvanostatic, Diffusion Simulation

Al-Ga Sacrificial Anodes:

Understanding Performance Via Simulation and Modification of Alloy Segregation

Michael Kidd

Abstract

Marine structures must withstand the corrosive effects of salt water in a way that is low cost, reliable, and environmentally friendly. Aluminum satisfies these conditions, and would be a good choice for a sacrificial anode to protect steel structures if it did not passivate. However, various elements can be added to aluminum to prevent this passivation. Currently, Al-Ga alloys are used commercially as sacrificial anodes but their performance is not consistent. In this research, Thermo-Calc software was used to simulate various aspects of the Al-Ga system in an attempt to understand and potentially correct this reliability issue. Simulations showed that gallium segregates to the grain boundaries during solidification and then diffuses back into the grains during cooling to room temperature. Simulations also suggest that faster cooling rates and larger grains cause the potential segregation of gallium at the grain boundaries to remain after cooling. A set of aluminum plus 0.1% weight percent gallium alloy plates were produced with varying cooling rates, along with a control set (cooled slowly in a sand mold). Some samples were later homogenized via annealing. Samples were subjected to a 168 hour long galvanostatic test to assess voltage response. The corrosion performance of samples was found to have both consistent and optimal voltage range when subjected to quick cooling rates followed by annealing. Testing samples at near freezing temperature seems to completely remove optimal corrosion behavior, suggesting that there are multiple causes for the voltage behavior.

Al-Ga Sacrificial Anodes:

Understanding Performance Via Simulation and Modification of Alloy Segregation

Michael Kidd

General Audience Abstract

Ships must withstand the corrosive effects of salt water in a way that is low cost, reliable, and environmentally friendly. Aluminum has properties which could allow a plate of it to rust instead of a ship it is attached to, thus protecting the ships from rusting. However, because aluminum usually does not rust, gallium can be added to aluminum to allow it to rust. Currently, aluminum-gallium alloys are used commercially to protect ships, but their performance is not consistent. In this research, various aspects of the aluminum-gallium system were simulated in an attempt to understand and potentially correct this reliability issue. Simulations showed that the gallium concentration may not be uniform in the alloy, and various conditions can cause the gallium concentration to be inconsistent. A set of aluminum-gallium alloy plates were cast in molds from liquid aluminum. Some of the plates were cooled quickly, and some cooled slowly. Some samples were later heated in an oven at high temperatures in an attempt to even out the gallium concentration. Samples were subjected to tests to observe corrosion behavior. The corrosion performance of samples was found to be best when subjected to quick cooling rates followed by the oven heating. Testing the samples in cold temperatures seemed to remove the desired corrosion behavior, suggesting that there are multiple reasons for the inconsistent corrosion behavior of aluminum gallium.

Table of Contents

List of Figures

List of Tables

Background and Introduction

All marine vessels and structures are under constant attack from the corrosive effects of seawater. Without protection from corrosion, our mightiest constructions would have an unacceptably short lifespan. There are various ways to protect iron and steel from corrosion, including paint and other coatings, as well as active and passive cathodic protection measures.[1,2,3] Often, more than one of these measures are used together.

One particular form of cathodic protection is a sacrificial anode. This anode corrodes such that the structural elements it is attached to remain unharmed. The anode is composed of a metal, typically magnesium or zinc, with a lower electropotential than the metal it is designed to protect. These anodes are effective only for certain sized areas and must be occasionally replaced.[3] Thus, there is an endless demand for sacrificial anodes which are low cost, reliable, and environmentally friendly.

Previous work suggested that aluminum alloys might fulfill all of these qualities, as it is both lower cost than zinc, and has a higher efficiency due to aluminum's current capacity of 2974 A-hr/kg vs 795 A-hr/kg for zinc.[3,4] Pure aluminum, however, passivates by forming a layer of aluminum oxide on its surface preventing further oxidation, and thus prevents its use as a sacrificial anode. Alloying elements, however, can be added to break, bypass, or otherwise stop this passive oxide layer from preventing oxidation.[2] One aluminum-based sacrificial anode currently in use today is Al-Zn-In.[4] However, Al-Zn-In anodes have significant drawbacks in that indium is relatively expensive, and some of its compounds are considered toxic.[5,6] They also operate at voltages which may generate hydrogen gas, potentially embrittling many types of high strength steels.[7]

One potential solution is aluminum gallium (Al-Ga) anodes. Gallium is negligibly harmful to the environment, and at the start of this research, was cheaper than Al-Zn-In, though cost depends upon the volatile metal markets.[8] However, Al-Ga anodes have proven to be frustratingly unreliable with respect to their operating voltage.[7,9] Optimally, a low voltage aluminum anode would operate at a consistent voltage between -0.78 V and -.83 V vs saturated silver/silver chloride in seawater, or -0.80 to -.85 V against a Saturated Calomel Electrode (SCE) in sea water.[10] This research seeks to improve the understanding of the variability in Al-Ga anode performance and develop methods to improve performance consistency.

Literature Survey

The literature on aluminum alloys and their corrosion is extensive. Below is a short summary of several papers which directly influenced this work and the direction taken.

The first hints that Al-Ga could be used as a sacrificial anode started in 1966, with Reding and Newport extensively investigating many aluminum alloys, and showed that Mg, Zn, Ga, Sn, Cd, In, and Hg, could interfere with the passive aluminum oxide layer, and allow aluminum alloys with these impurities to corrode.[2]

Pautasso et al. in 1998 looked for new ways to cathodically protect steels in such a way to prevent hydrogen evolution and thus hydrogen embrittlement.[9] They found that the Al-Zn-In anodes created an excessively low voltage, which had the potential of hydrogen gas being generated, and instead wanted to create an anode with a potential of around -0.8 V vs SCE. They found that Al-0.1 wt% Ga held promise for this purpose.

At Virginia Tech in 2014, Monzel et al. extensively investigated low voltage aluminum alloys, including Al-0.1 wt% Ga, and the effects of various additions on the voltage.[11] These tests showed extreme differences in post-corrosion microstructures depending upon alloying elements, and testing conditions. This research continued in 2015, by Baker et al., involving galvanostatic tests on Al-0.1 wt% Ga samples and found that after variable periods of time the voltage behavior changed from a steady state behavior to an erratic behavior.[12] Remelting the alloy seemed to increase the time the alloy was well behaved (Figure 1). The same source material used from Baker's tests was also used for this research.

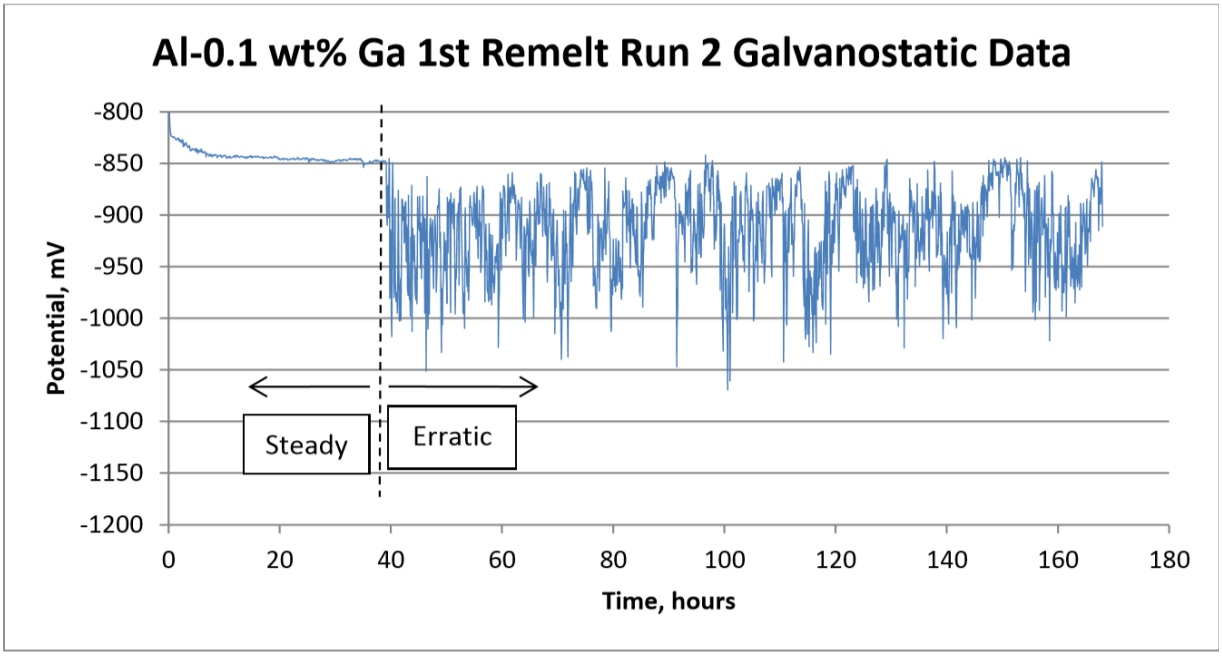

Figure 1: Galvanostatic voltage behavior change from previous work[12]. Used with permission.

There have been competing hypothesis for how and why Al-Ga alloys corrode.[13,14] There have been various methods proposed, some contradictory, and due to the difficulty of direct observation of the corrosion as it happens, it is hard to completely prove or disprove the various theories. No papers containing direct microscopic observation of the corrosion of Al-Ga alloys were found during the course of this work.

Uruchurtu noted that pure aluminum, if managed to be activated, would only corrode at certain local sites, while the rest of the anode would be passive.[13] This pitting mechanism showed significant noise of the recorded voltage, referred to in the work as potential deviation, and was attributed to a healing and reforming of the oxide layer (Figure 2).

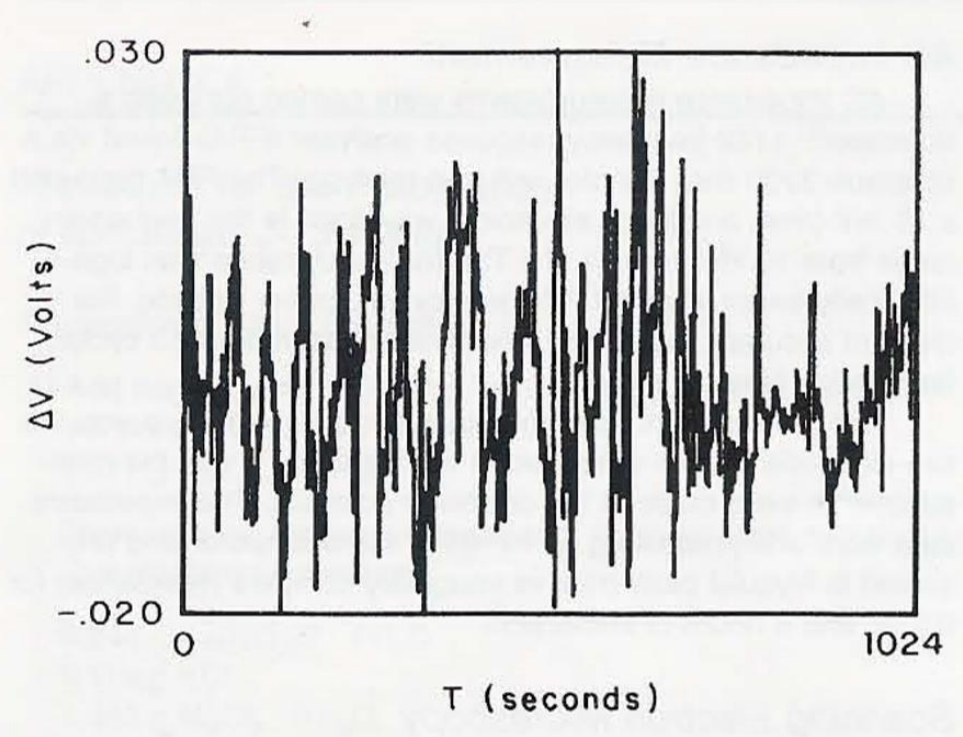

Figure 2: Potential deviation of pure aluminum in salt water from literature[13]. Used under fair use.

Tuck et al. proposed that a critical amount of gallium must accumulate on the surface of the aluminum alloy to allow for activation.[15] They proposed that as the anode corrodes, gallium built up particles via deposition of the gallium back on the surface as super-cooled liquid drops. These drops of liquid gallium then allowed aluminum to diffuse through the drops to the surface, and created pits. Tuck's findings were supported by Aragon et al., which showed that gallium can partition and supercool in aluminum alloys.[16] Murer and Buchheit showed that a Monte Carlo simulation is effective in predicting the pitting behavior of aluminum alloys due to corrosion.[17] This modeling also helped support the Tuck et al. findings.

Hunter later showed that at gallium concentrations above 2.3% a different mechanism corroded Al-Ga alloys.[18] Hunter's mechanism caused corrosion primarily at the grain boundaries and showed no pitting.

Flamini et al. proposed that in Al-Ga alloys, the redepositing gallium forms a surface amalgam-like liquid film which thins and detaches the oxide layer.[14] This liquid surface film had to be maintained with sufficient heat generated by a certain minimum corrosion rate, else the film would solidify.

McPhail, while working on Al/air batteries, showed that in his method of casting Al-Ga, he was able to detect significant segregation of gallium to grain boundaries.[19] McPhail noted that this contradicted Hunter's results but mentioned heat treatment could be the cause of the differences. Senel et al. investigated bulk properties of Al-Ga alloys, and found that brittleness caused by liquid gallium could be removed by annealing, which was attributed to the anneal removing the gallium from the grain boundaries.[20] Keyvani et al. correlated current capacity and potential of Al-Zn-In alloys with cooling rate.[21] They attributed optimal corrosion behavior to homogenized impurities, which they achieved by casting their alloy in a mold kept at a temperature of 400^{o}C. These findings partially lead to the investigations of the heat treatment on the effects of Al-0.1 wt% Ga anodes in this research.

Straumal et al. in 1995 determined that Al-0.1 wt% Ga exhibits abnormal grain growth when recrystallizing from cold rolled alloys.[22] This paper is of interest, as at least one of the samples exhibited abnormal grain growth when heat treated.

While many of these papers gave data on corrosion testing of Al-Ga, with the exception of the Baker paper, none were found which had both a sufficiently long time scale and data resolution to display or refute the potential erratic corrosion behavior of Al-0.1 wt% Ga alloy. Worse, if the erratic corrosion behavior shown by Baker et al. was present but unseen in the previous papers, it potentially could have caused unseen errors. Thus, the primary goal of this research was to collect more complete data to better understand the corrosion behavior transition between the erratic behavior and the steady-state voltage behavior.

Initial Hypothesis

If the process in which the sacrificial anode is cast and heat treated causes a difference in the bulk properties of the of Al-0.1 wt% Ga sacrificial anodes, perhaps that could explain some of the differences seen in the corrosion behavior. To start, we must have some idea of how the alloy solidifies, and how the gallium is distributed within that alloy. For this we attempted to simulate the solidification and heat treatment of an individual grain within the anode.

Once we have an idea of how the gallium distributes, we can then focus on how that distribution effects the voltage behavior of the anode. Since the Baker galvanostatic tests seem to show the most variance of voltage behavior, this test was applied to a variety of samples which underwent various solidification and heat treatment conditions. The voltage responses were then compared.

Experimental Methods

Simulations

Understanding of Al-Ga sacrificial anodes starts with understanding a thermodynamic description of the Al-Ga binary system. A commercial program, Thermo-Calc,[23] was used to understand this binary system and to make predictions of the bulk material of Al-Ga anodes. This software package uses thermodynamic databases which contain equations that determine Gibbs free energy of elemental phases with respect to temperature and composition, and other thermodynamic properties are calculated from these equations. It is important to be aware that differences or simplifications in the databases can create errors in results. These differences are usually small, but have been noted in this research.

The phase diagram of the Al-Ga system is fairly straight forward. The liquid phase is a homogenous solution, and the solid phase is also a homogenous solid solution up to ~20 wt% Ga concentrations at room temperature. The liquidus starts at 660.3°C at 100% aluminum and gently curves to 29.76°C at the gallium side. The solidus curves steeply down to room temperature at ~20 wt% Ga. The triangular region between the liquidus and solidus is a face centered cubic + liquid region, with the majority of the gallium remaining in the liquid region.

There is a eutectic point which the software package calculates to be at 98.98 wt% Ga and 299.43°C using the Aluminum v4.0 Database (Figure 4) and 98.96 wt% Ga and 299.36°C using the Binary Solutions v1.1 Database (Figure 5). These can be compared to the literature diagram in Figure 1. Below the eutectic point, is a two phase region, where the aluminum rich phase is face centered cubic, and an orthorhombic gallium phase.

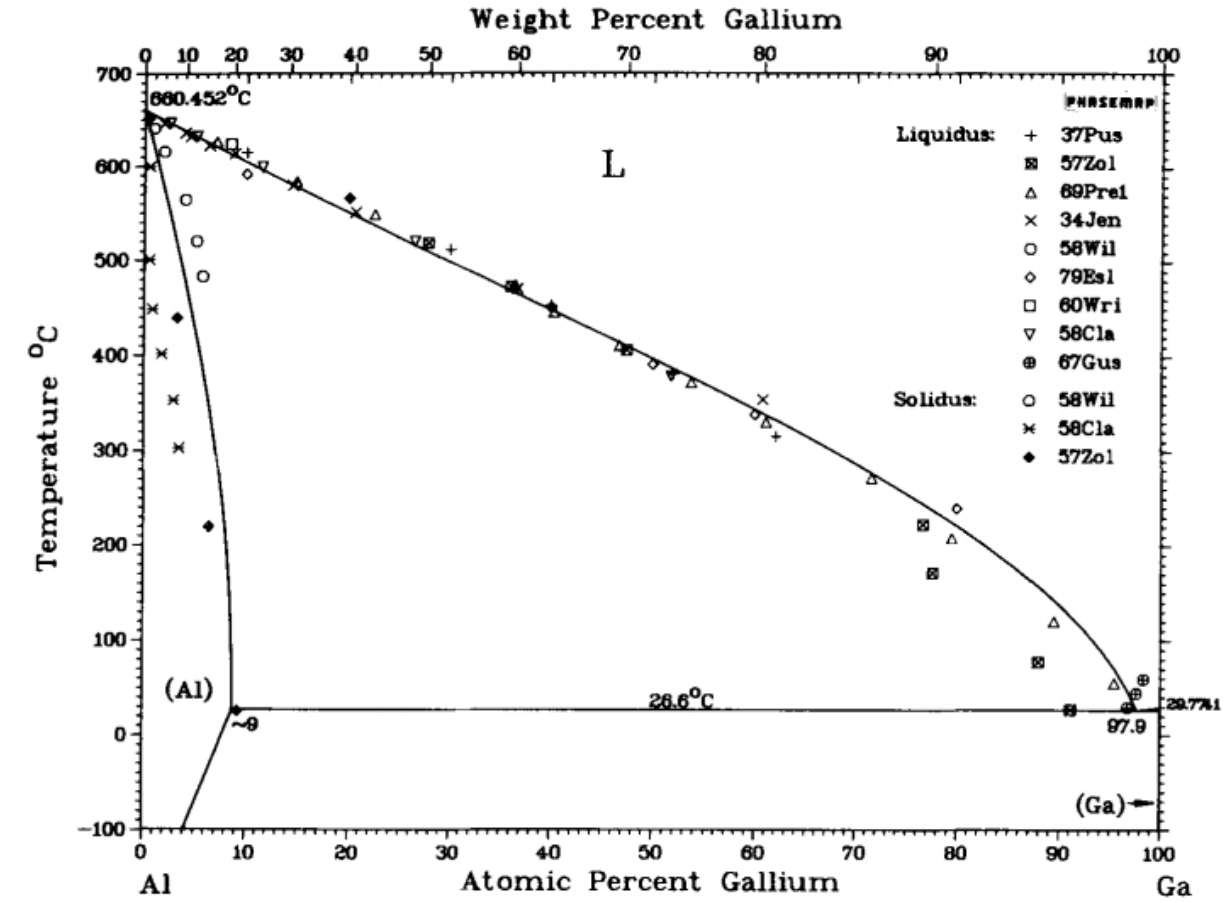

Figure 3: Al-Ga phase diagram from literature[24]. Used under fair use.

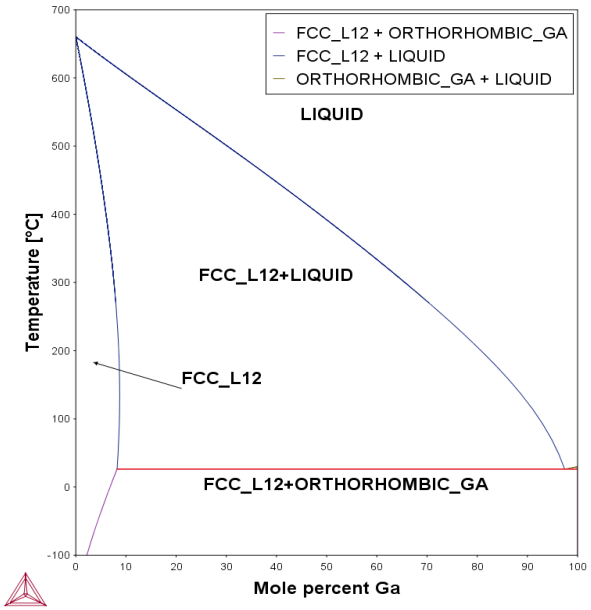

Figure 4: Al-Ga phase diagram generated using the Aluminum v4.0 Database.

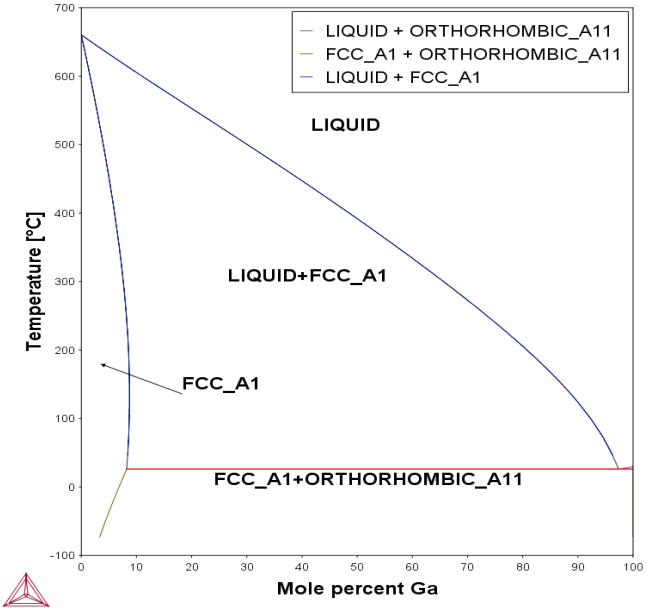

Figure 5: Al-Ga phase diagram generated using the Binary solutions v1.1 database.

The differences are negligible between the two calculated phase diagrams and the published phase diagram.

Over the time period this research was done, many of these simulations were repeated with identical parameters but different software versions. Originally some of these simulations were run in Thermo-Calc 2015b, using the TCAL4: AL-Alloys v4.0 Database produced by the Thermo-Calc Company. Later, simulations were run on the 2017a version of the software, using the same database. At the time of completion of this research, the software is on version 2018b, and uses the TCAL5: AL-Alloys v5.1 Database. This should have little to no effect on any results, and a few simulations were redone with the new version to confirm this, but it is worthy of note for anyone attempting to replicate this work in the future.

Initial Cooling Simulations

The Thermo-Calc software package can do both equilibrium cooling simulations, and Scheil simulations. Equilibrium cooling assumes that the cooling process will be at thermodynamic equilibrium throughout the entire process. The equilibrium simulation used in Thermo-Calc is based on the minimization of the Gibbs free energy of the system. Equilibrium cooling tends to overestimate the temperature of the liquidus and solidus curve temperatures compared to real-world cooling.[23] The Thermo-Calc Scheil simulation is another useful model for solidification. This model has a few assumptions, namely that the liquid is always homogenous (diffusion occurs infinitely fast.), and no diffusion happens in the solid.[25,26] This Scheil simulation is based up the Schiel-Gulliver equation, which predicts:

Equation 1: Scheil-Gulliver equation[25,26]

$$C_s = kC_o(1 - f_s)^{k-1}$$

Where C_s is the solute dissolved in the solid, C_o is the initial concentration, f_s is the solid fraction, and k is the partition coefficient. The Scheil simulation tends to underestimate liquidus and solidus curve temperatures compared to real world cooling results due to its assumptions.[23]

Comparing these models creates two extreme bounds within which real cooling resides. Thus, they can be used to verify results; either of an experiment, or the underlying inputs of the model calculations. They can also be used to check that more complex cooling models are within reasonable bounds.

Both Scheil and thermodynamic equilibrium cooling models remove time as a factor. When time and thus diffusion are taken into account, the simulation would change. Since aluminum and gallium have vastly different melting temperatures, the usual assumption of a homogenous solid after casting may not be correct, as the gallium may remain in the liquid as the alloy cools. The first initial hint that cooling rate might affect Al-Ga sacrificial anodes came from a simple diffusion simulation. The diffusion module for Thermo-Calc, DICTRA, effectively solves a diffusion equation governed by both kinetics and thermodynamics across a one dimensional set of user defined nodes. The differences of the cooling curves of these three different models is shown in Figure 6.

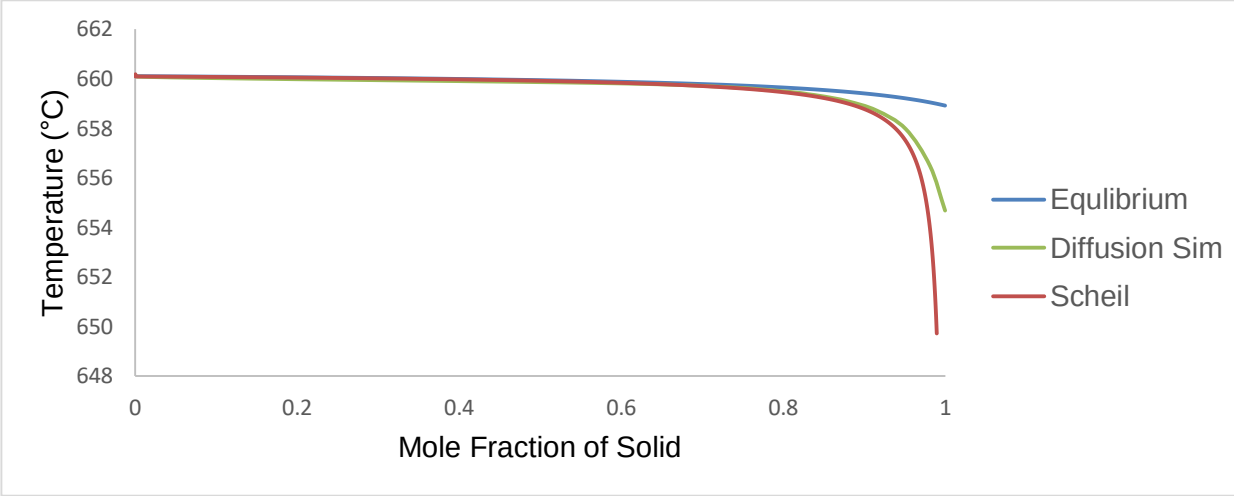

Figure 6: Simulated solid fractions as a function of temperature for Al 0.1wt% Ga using thermodynamic equilibrium, the Scheil approximation, and a representative diffusion simulation.

The diffusion simulations are significantly different than the equilibrium and Scheil simulations, as they must simulate many points across a weighted one dimensional region. The left side of the region is chosen to be the grain nucleus, where the first material solidifies. The solid region then expands as the material cools, till it reaches the right side of the simulation, which is chosen to be the grain boundary, the last material of the grain to solidify. Figure 7 shows how the growth of a grain might be simulated in this way.

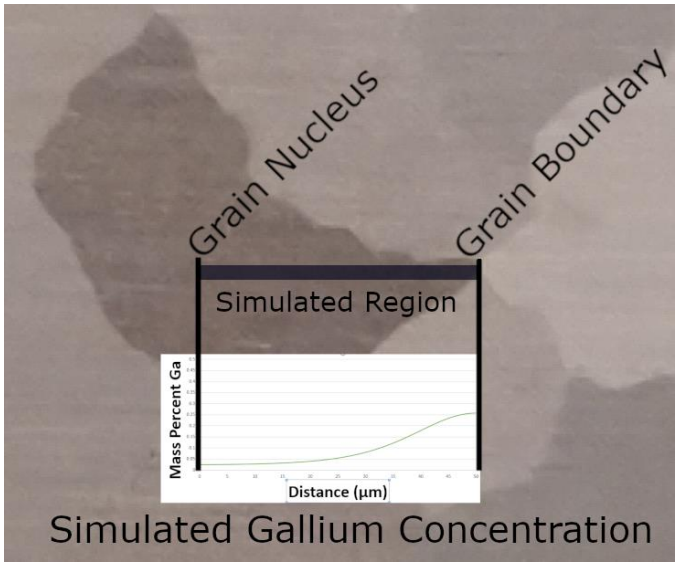

Figure 7: Schematic of a theoretical diffusion simulation imposed on a grain. This diagram shows how the left side of the simulation corresponds to an assumed grain nucleus, and the right side corresponds to the edge of a grain. The simulation shows how the gallium concentration may change as one moves from the material first solidified to the material which solidified last.

When diffusion simulations were run of a simple steady rate cooling of Al-Ga (Figure 8), the results showed a very striking movement of the gallium away from the nucleus of solidification as it prefers to partition to the liquid. After solidification has ended, the simulation showed that gallium diffuses throughout the solid until homogeneity is achieved. This effect happens over a few dozen seconds depending upon the initial simulation conditions. This homogenization can be stopped if temperature drops rapidly, or conversely, be forced to continue if temperature is held close to but below the solidus temperature.

Thermo-Calc's simulations are not perfect. Many aspects of the simulations must be set before running the simulation, particularly, the grain radius. Grain size, however, is dependent on cooling rate, and so one cannot simply change those variables independently and expect reliable results. Moreover, there is no function, at time of this writing, within the software package to simulate grain sizes during solidification from a liquid. Thus grain size and cooling rate must be determined experimentally.

The first diffusion simulation performed for this project was a simple Al-Ga alloy cooling simulation which assumed a steady rate cooling of 0.5°C per second, and a grain 'radius' of 50 µm. This simulation assumed a flat infinite plane, as opposed to spheres or dendrites. Figure 6 shows that the gallium concentration changed over the course of the simulation by almost two orders of magnitude from grain center to edge.

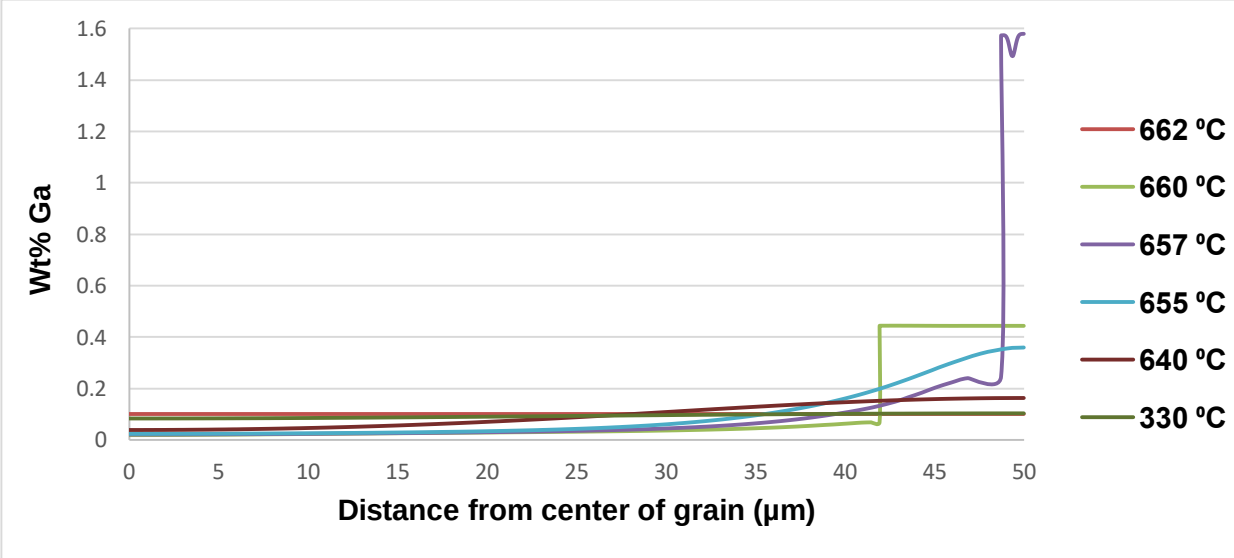

Figure 8: Movement of Ga through a cooling simulation at 0.5°C/sec of an Al 0.1%Wt Ga grain of 50 µm radius. One can distinctly see the boundary between liquid and solid regions at a particular temperature by the vertical line in the gallium concentration.

Both cooling rate and grain size strongly affect the resulting final gallium concentration profile. When the cooling rate of the simulation was varied, it was found that generally the final variance in gallium concentrations is quite substantial for faster cooling rates, and almost eliminated by a slower cooling rate. If simulated grain size is instead varied, the simulated gallium segregation would tend to remain for larger grains, while it would tend to vanish for smaller grains. Figures 9 and 10 compare these effects. There are

many ways to control grain size in aluminum alloys during casting, such as adding an element as a grain refiner, but for the thermodynamic software package used, grain size must be assumed.

These two effects often work against each other. Slower cooling usually means larger grains and vice versa. From this we can hypothesize that there are optimal cooling rates which maximize or minimize gallium segregation. Given the previously proposed mechanisms of Al-Ga anode activation that involves increased surface gallium concentration,[14,15,27,28] it can be hypothesized that increased segregation would make a better anode, as certain areas of the anode would immediately have the required gallium concentration required for activation. However, to the contrary, a segregated anode could also create passivated regions which don't corrode, which would be detrimental to anode performance.

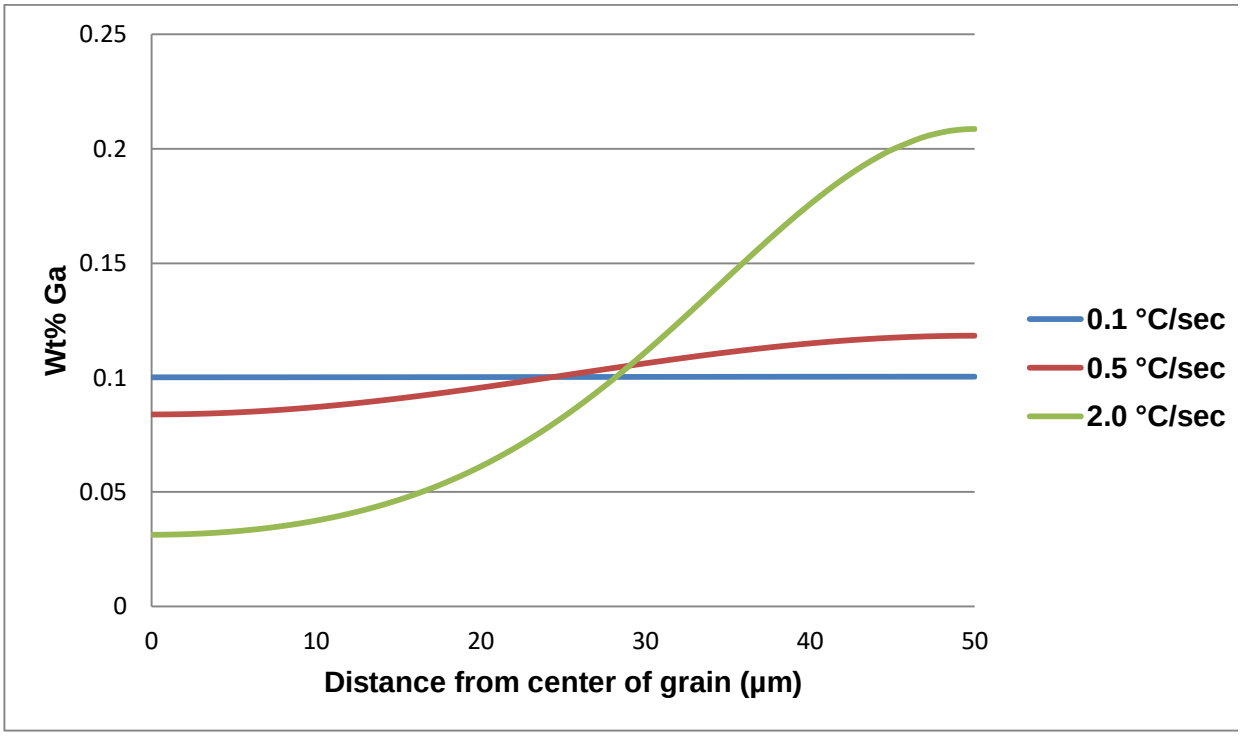

Figure 9: Simulated gallium segregation of Al-0.1% Ga alloy for 50 µm grain sizes at different cooling rates.

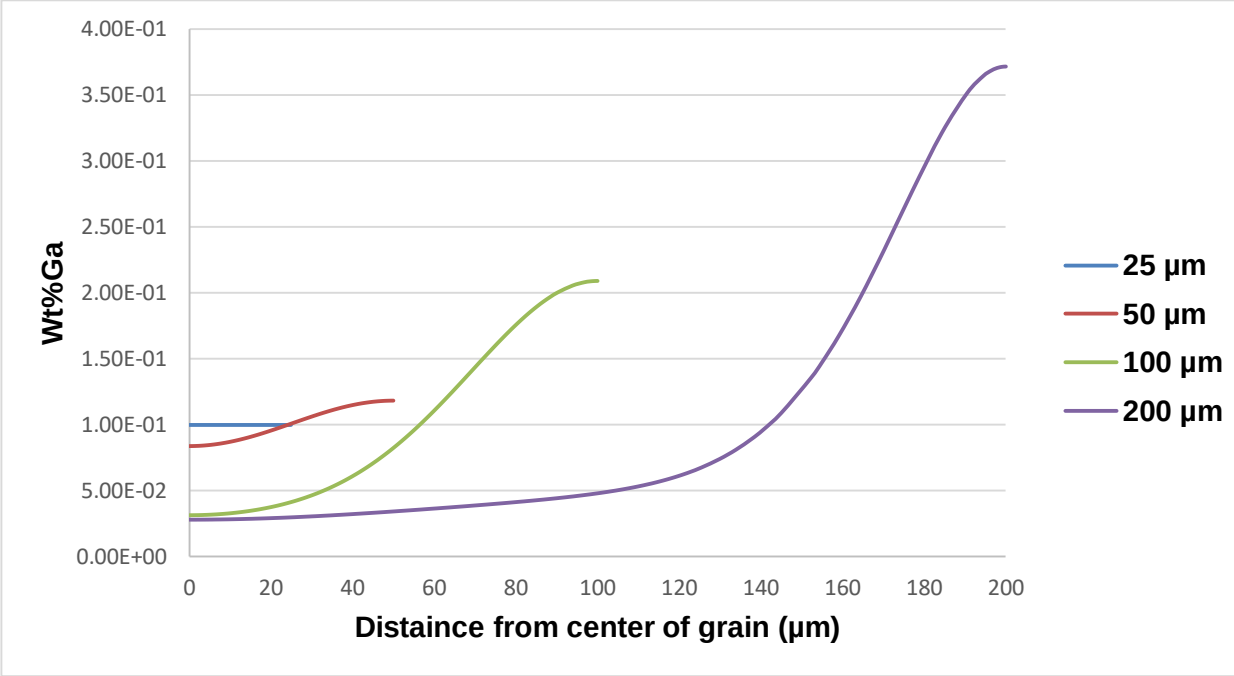

Figure 10: Simulated gallium segregation of Al-0.1% Ga alloy for various gran sizes at 0.5°C/sec cooling rate.

First Experimental Verification Attempt

With the knowledge that the software package's simulations predict potential segregation of the gallium within the anode and previous work suggests that increased surface gallium may be required for anode activation, experiments were performed to verify the simulation results.

In order to replicate, and thus improve on the previous work, galvanostatic tests were chosen to gauge the effectiveness of the sacrificial anodes. These tests measure the voltage response of the anode to a steady current as it corrodes. The weight of the samples before and after was also recorded in an attempt to measure anode efficiency.

Two sand molds were prepared. Each mold had cavities for four plates. 3.18 mm thick copper and steel chills were placed inside one mold, while the other was only sand. Figure 11 is a picture of the molds containing both copper and steel chills. An induction furnace was used to melt the Al-0.1 wt% Ga alloy and heat it above 725°C. The Al-Ga alloy used for these tests was the same metal used in previous work at Virginia Tech.[12] The composition was checked by an optical emission spectrometer shown in Appendix B. The molten Al-Ga was poured into the chilled molds, followed by pouring into the sand molds. Additional material was poured into a Heraeus electro-nite Qc4010 Quik-Cup to generate a cooling curve, and the excess poured into pig molds for future use. The downsprues, the cup, and the pig molds all experienced visible shrinkage.

The chilled molds were broken and the castings quenched in water immediately after the downsprues had solidified, ~110 seconds after pouring. Figure 12 shows the chilled molds broken open, and the conventional sand molds in the process of cooling slowly.

Nine square samples were cut from the middle of each plate using a water jet. During this process the samples did not exceed 40°C. Samples were then labeled based upon position on the original plate. The labeling system used to keep track of these samples is described in Figure 13. A period of months passed between when the plates were cast, and when the samples cut, during which the samples were stored at room temperature.

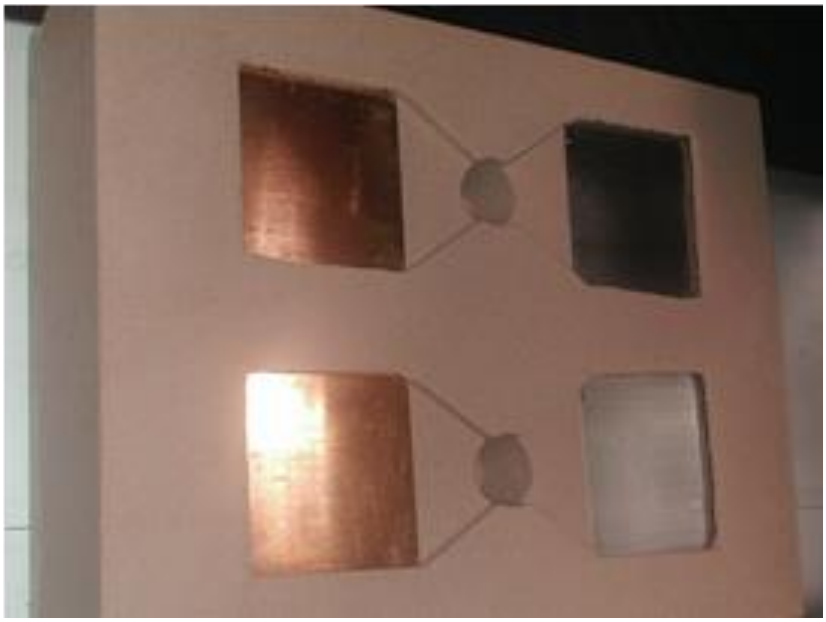

Figure 11: Picture of mold, containing copper (left) and steel (right) chills.

Figure 12: Picture of molds after casting. The left mold contains the slow-cooled plates, while the chilled samples from the right mold have been removed and quenched in water.

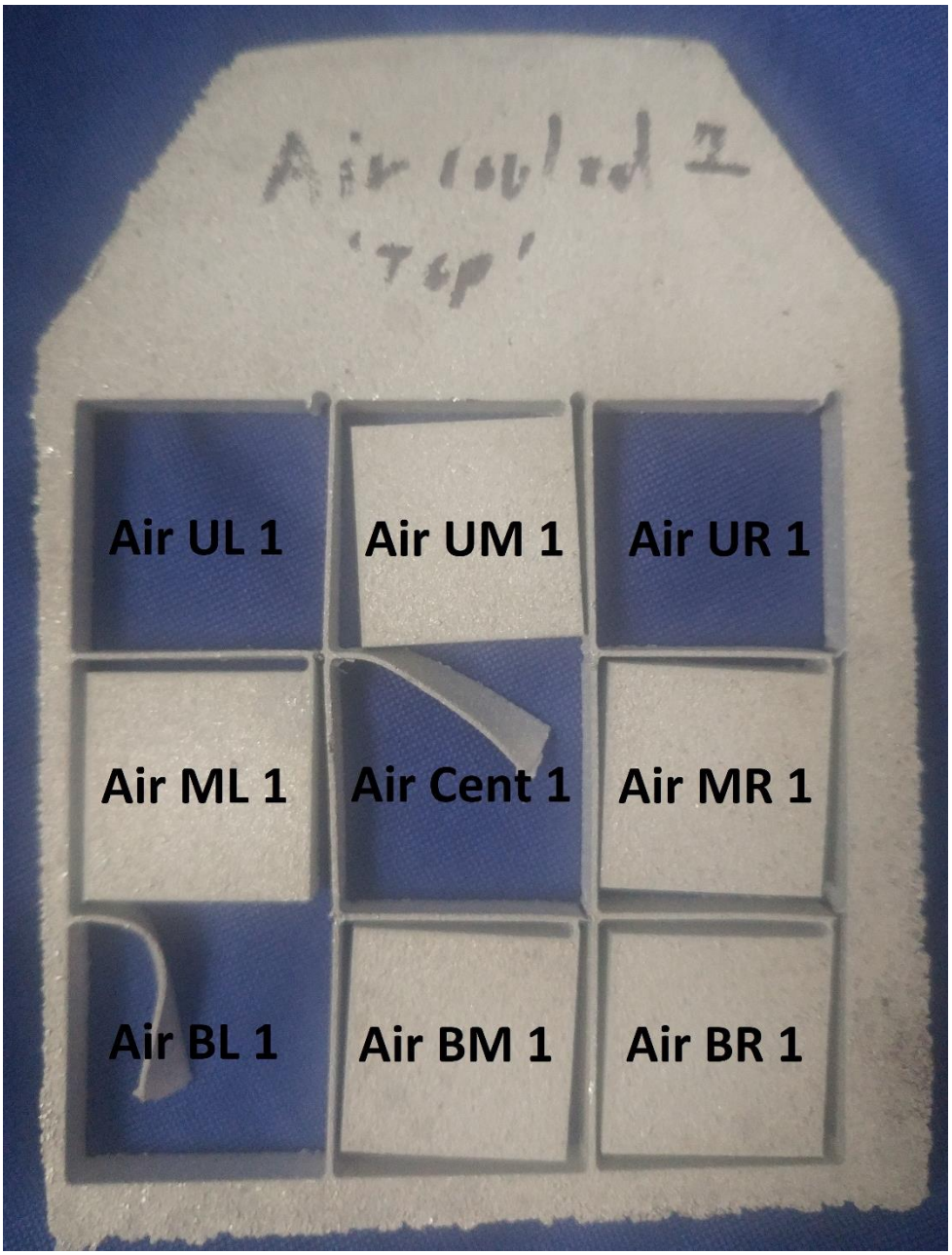

Figure 13: Labeling system for samples. Each sample is labeled based upon its position in the 3x3 grid made by the water jet cutter. 'Upper' (U) samples are closer to the downsprue, and thus cooled slightly slower than the bottom (B) samples, which were farther from the downsprue. The 'top' side for chilled samples, is the face touching the chilled side of the mold. 'Air' samples are the samples which remained in the sand molds to cool slowly. 'Cu' and 'Steel' samples were subjected to the copper and steel chills respectively.

Samples were taken from various positions from each plate, and the side of each sample, a mark was placed which indicated the back of each sample. (The front of each sample is the face which was against the chill for chilled samples, and arbitrarily picked in case of the slow cooled samples.) The fronts of these samples were then sanded using 600 grit silicon carbide paper, until any surface defects were

eliminated. Each sample had final approximate dimensions of 22 mm length and width, and 6 mm thick. This 6 mm final thickness varied slightly due to differences in sanding time. This variable grinding depth is a potential source of error if gallium segregated with respect to the entire sample, instead of the expected segregation with respect to grains, as more or less gallium may have been lost during grinding. However, the goal of this research was to determine effects of segregation within the grains of the alloy, thus removing the surface of the samples should have eliminated more variables than it added.

The galvanostatic tests were performed in three different electrochemical testing cells. The cells used were Model K0235 flat cell from Princeton Applied Research (PAR). Each test cell had a working electrode area of 1 cm^2, 250 ml volume, and 80 mm distance between electrodes. The electrolyte used was ASTM D 1141[29] substitute ocean water without heavy metals.

Each cell was hooked up to a different channel of a PAR 'VersaStat MC' unit, designed for potentiostatic and galvanostatic electrochemical corrosion testing. The same channel was used for each cell for each set of tests. The cells were cycled, such that each cell did one test each of steel, copper, and slow cooled to randomize the effects of test equipment variation. No systematic difference between the cells was noticed over the course of the experiment. Tests were done at room temperature in a heated building in the winter, so over the course of three weeks it is unlikely that temperature variance during testing contributed significant error.

The primary test of interest was a galvanostatic test with a steady 0.62 mA forced though the sample area of 1 cm^2, for a nominal current density of 0.62 mA/cm^2 and the voltage with respect to a saturated calomel electrode (SCE) was measured. Voltage was measured every 30 seconds for 7 days. For consistency, each test used a different sample.

Corrosion Testing

Test results strongly suggested that there was indeed a difference in performance between the rapidly cooled samples and the slowly cooled samples. Both the copper chilled samples and the steel chilled samples for the most part behaved similarly, with the steel chilled samples perhaps behaving with a more consistent voltage. Both copper and steel chilled samples rarely registered a voltage below -1.00 V_{SCE}, while two of three air cooled samples often dropped below that voltage. Complete charts of each experiment are in Appendix B.

Both the steel and copper samples maintained an average voltage of about -0.80 V_{SCE} slightly dropping over the course of the experiment, while the slow cooled samples, while initially starting at a similar -0.80 V_{SCE}, ended the test approaching an average voltage of less than -0.95 V_{SCE}. This data strongly suggests that the Al-Ga anodes which had chilled molds will generate less hydrogen compared to slow cooled anodes, and experience less voltage change as a function of time.[9] The difference between the fast cooled and slow cooled samples is shown in Figure 14 and 15.

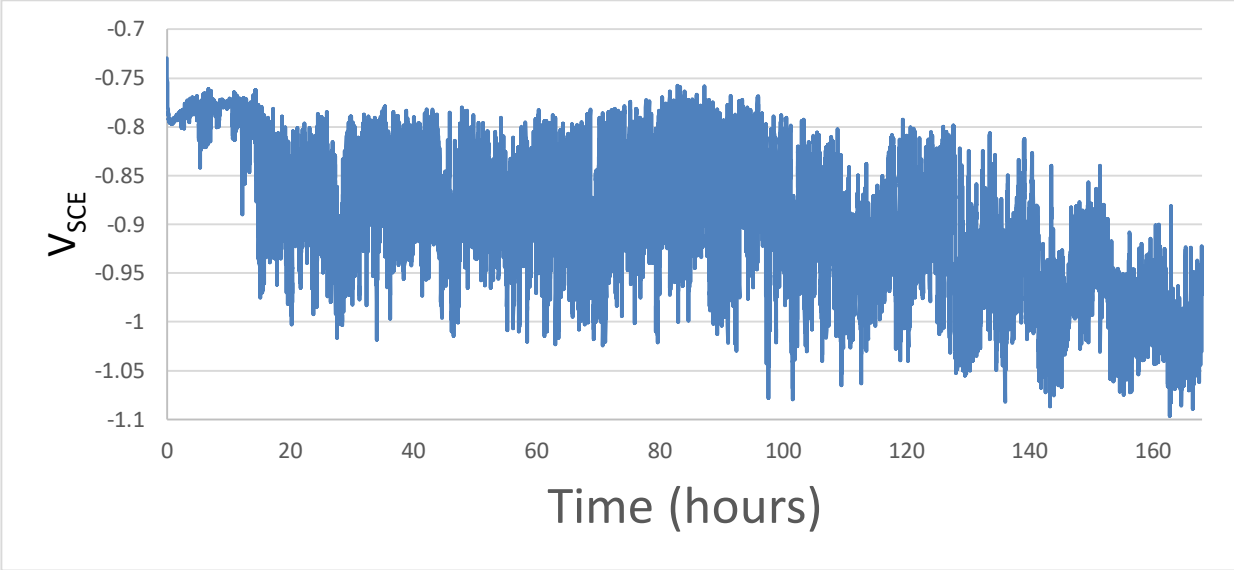

Figure 14: Voltage data for 'Air UR1', showing representative voltage behavior of slow cooled samples.

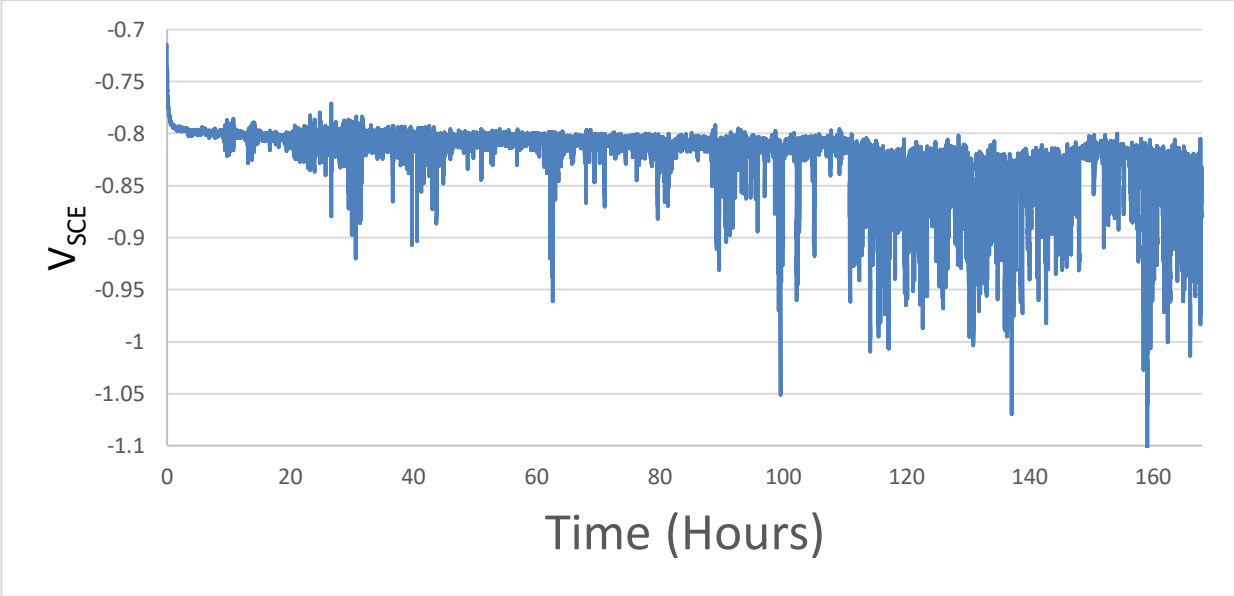

Figure 15: Voltage data for 'Copper BL1', showing representative voltage behavior of rapidly cooled samples.

The two slow cooled samples which had erratic voltages both had one massive hole due to corrosion while most of the chilled samples had many scattered and comparatively smaller holes due to corrosion. A representative sample of the slow cooled erratic samples after the one-week test is shown in Figure 16 and a representative chilled sample in Figure 17.

One of the copper cooled samples maintained a significantly different average voltage than the rest of the chilled samples. Since the sample types were cycled through the same pieces of equipment, and the same voltage difference was never seen in other tests, it is highly unlikely to be an equipment related or other systemic error. Visually, this sample was quite different from most other samples, with large fissures extending out of the tested area (Figure 18).

One of the air cooled samples exhibited the most consistent behavior of all the samples, maintaining a voltage similar to the average of the chilled samples, but with almost no voltage spikes. This visual difference of the corrosion of this sample was striking compared to the rest of the samples, as the visible holes are mere pin-pricks despite the sample losing just as much mass as all the others (Figure 19). Either the bulk of the corrosion happened in cavities beneath the visible pinpricks, or instead there was a relatively uniform corrosion across the surface. This samples existence means more tests needed to be done to determine if this was an anomaly.

One of the steel chilled sample data was unfortunately lost due to a combination of user and software failures. This is why only two steel samples are shown in Appendix A and D.

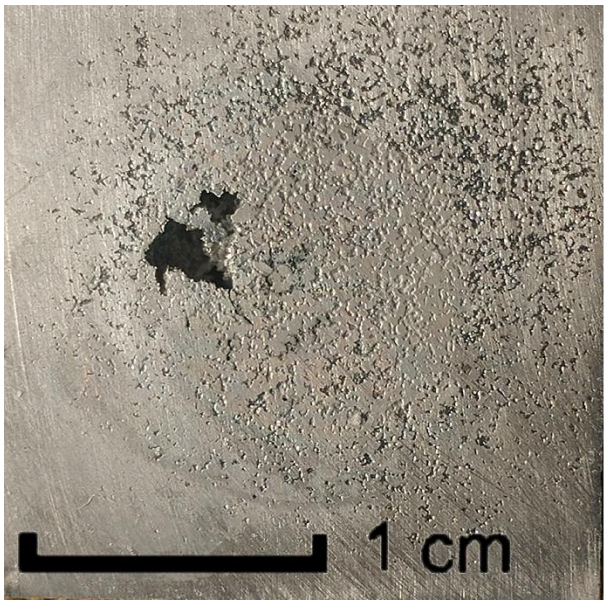

Figure 16: Photograph of corroded surface of sample 'Air UR 1': representative of the slow cooled samples.

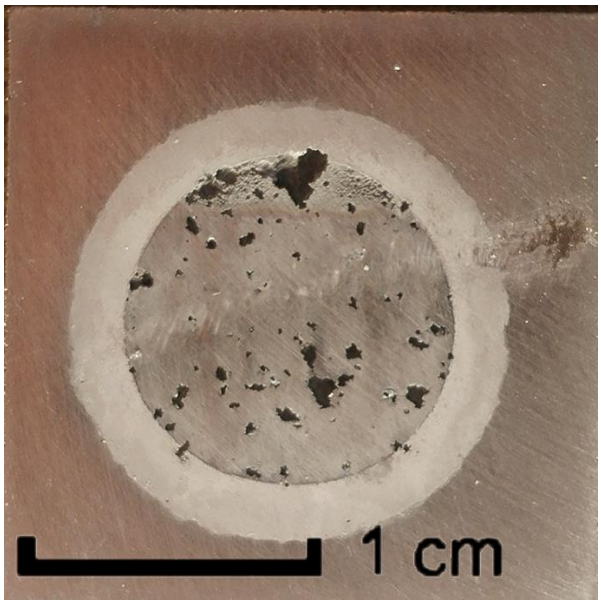

Figure 17: Photograph of corroded surface of sample 'Copper BL 1': representative of the chilled samples.

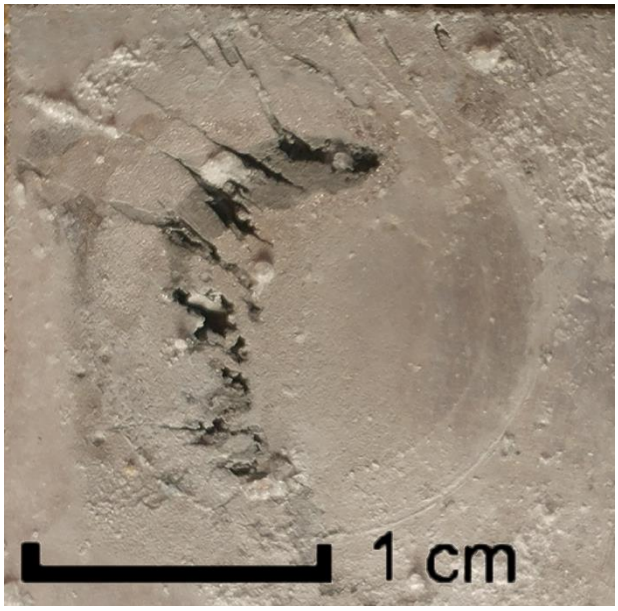

Figure 18: Photograph of corroded surface of sample 'Copper BR 2', the chilled sample with abnormally low voltage.

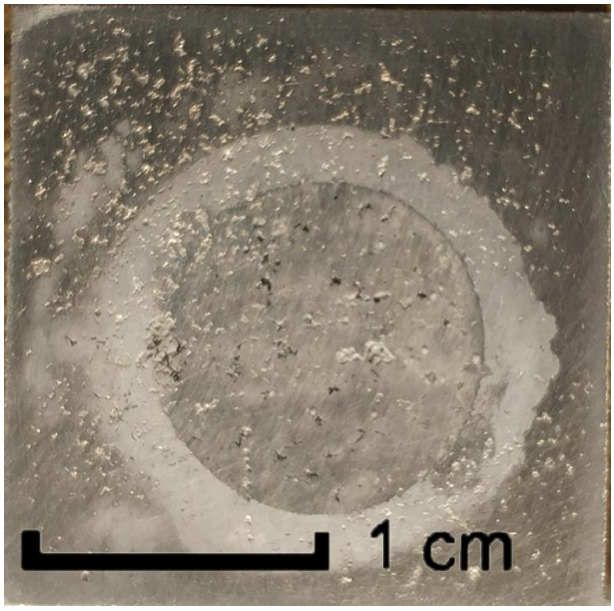

Figure 19: Photograph of corroded surface of sample 'Air BL 1', the slow cooled sample with almost perfect voltage response.

Further Testing

These initial tests and simulations gave insight that there indeed might be some sort of effect of segregation on the electrochemical properties of the anode; they certainly gave insight that cooling rate affected the galvanostatic performance, but was far from sufficient to really show what was happening with the voltage behavior. To gather more data surrounding this behavior, and potential segregation, more tests were conducted. These include an accurate determination of the gallium composition, cooling curve tests using thermocouples placed in the sample molds, and etching of samples to gather grain size information. These tests give more information for the purposes of better simulating the alloy within Thermo-Calc. In addition, more galvanostatic tests were completed to include the testing of annealed samples, which should better reveal the effect of segregation, and cold water tests, to help determine if the voltage behavior has a temperature dependence.

Alloy Composition Verification

While the alloy used for these tests was targeted to be 0.1%wt Ga during the original process of casting of the alloy, this was done in previous work at Virginia Tech and the alloy had gone through multiple melting and solidification processes before finally being used in this research.[12] Two elemental composition tests were performed to verify the alloy's composition.

The first compositional test was done using an optical emission spectrometer in the Virginia Tech Foundry. These results showed that all measured impurities except Si, Mg, Cu, B, Ca, and Mo were below the detection threshold. Work has been done with the effect of these impurities.[2,11] In particular, in the previous work there was evidence that both Si and Cu influenced measured voltage response in galvanostatic tests.[11] However, the amount of these impurities measured in the cast alloy is only 0.0082wt% and 0.0063wt% respectively, and should have negligible effect. Some of these measured impurities, can in theory form thermodynamically stable phases in very negligible quantities, but the kinetics required to form these phases is certainly lacking. Even so, these potential impurity phases can be simulated in Thermo-Calc, and their thermodynamically stable quantities and impurity ratios are shown in Figure 20 and 21. This spectrometer can only measure impurities within a certain range, and the expected gallium percentage is about twice what the machine can read. The complete results are in Appendix B.

In order to verify the gallium percentage of the alloy, a commercial service, NSL Analytical, was used to perform a second test. NSL used an inductively coupled plasma mass spectrometry test to measure the gallium content. This test measured a gallium concentration of 0.092% by weight. The full report from this test is in Appendix C.

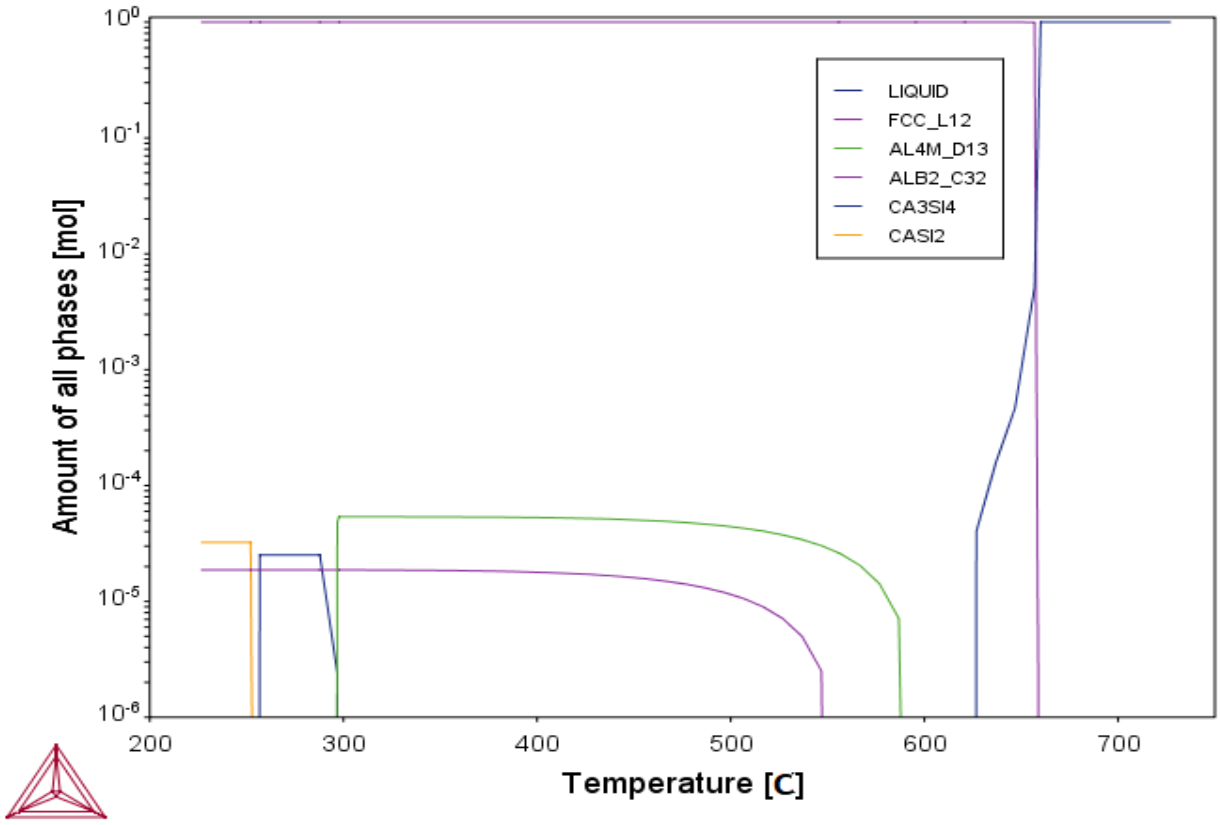

Figure 20: Theoretical thermodynamically stable phases of measured impurities as a function of temperature. AlB2_C32 is a potential boron containing precipitate, and AL3M-D13, CA3Si4, and CASi2 are potential silicon and calcium containing precipitates.

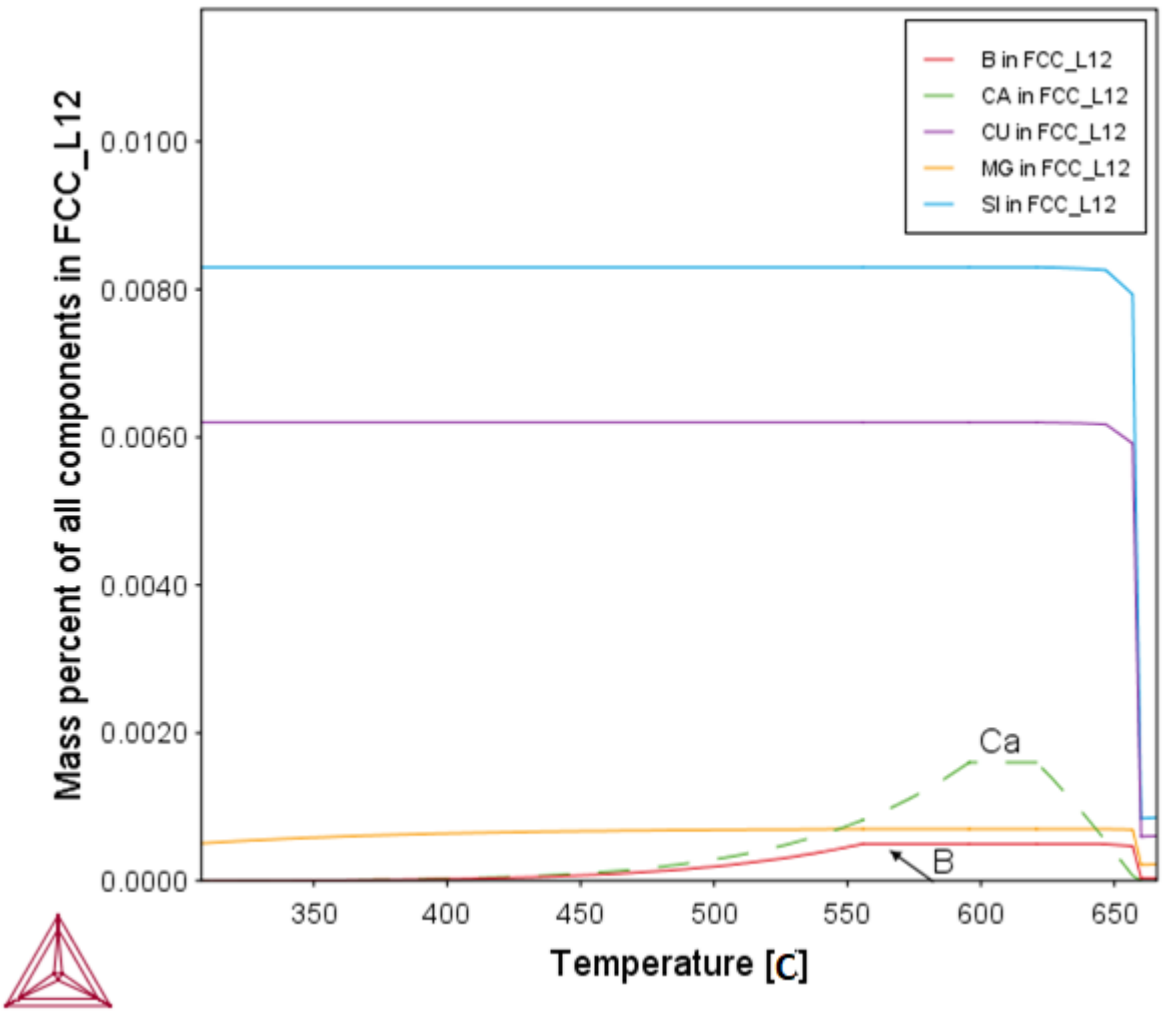

Figure 21: Theoretical thermodynamically stable concentrations of impurities within the bulk alloy with respect to temperature. This shows that Si and Cu never leave the bulk material, while B and Ca would leave the bulk material for a new separate phase if kinetics allowed.

Cooling Curves

In order to accurately simulate the solidification of the anodes, the temperature of the alloy as it cools must be known. To accomplish this, four Al-Ga 0.1wt% alloy plates were cast. The casting process was identical to the previously cast plates, with the exception that four Omega Engineering Type K grounded thermocouples were inserted into the molds. These thermocouples were hooked up to a data acquisition system and laptop which recorded the data for each thermocouple every 0.1 seconds. The setup is shown in Figure 22. During the process of casting, it was noted that the chilled samples quickly fell below temperatures critical for significant gallium diffusion (about 500^{o}C), and so the molds were not immediately broken as previously, such that the thermocouples could continue to record data for a longer period of time.

Figure 22: Picture of thermocouples imbedded within samples after solidification. The plates on the left had no chills, while the plates on the right had one copper chill and one steel chill. The plate on the bottom right of this image had the steel chill.

The results of these tests were quite different compared to the previously assumed cooling rates. Even the samples left in the mold cooled very quickly compared to the material used to measure the solidification temperature. Figures 23, 24, and 25 show the measured time-temperature data of the plates. This data was placed into Excel, and the zero mark for each data set was adjusted to when the thermocouple began recording a temperature spike, as the time at which the thermocouples began recording data, and the time they came into contact with the molten metal was not identical. The results of this test determined that there was very little difference between the cooling curves of the copper chill and steel chill, which means there should be little difference between the copper and steel chilled samples. This correlates nicely with the corrosion data showing no significant difference between the steel chilled samples and the copper chilled samples.

It is quite interesting that one of the slow cooled samples remained at the melting temperature for nearly 5 seconds, or 20% longer than the other, as well as how the chilled samples cooled so quickly that the thermocouples were unable to react fast enough to record a temperature above the melt temperature. This is due to the fact that the thermocouple wires are housed in an Inconel alloy tube, which while more responsive than ungrounded thermocouples, still absorbs some heat, and prevents an instantaneous response.

It is important to note that the thermocouples also acted as a heat sink for the samples, slightly increasing the rate at which the cooled, in addition, the thermocouples measured the center of the sample, which will also cool at a different rate than the edges. This, in addition to the lag time

mentioned previously, means that the measured time temperature data cannot be relied on as perfectly accurate, but for the purposes of running the simulations, it is a drastic improvement over the assumption of the previously used Quik-Cup cooling curves.

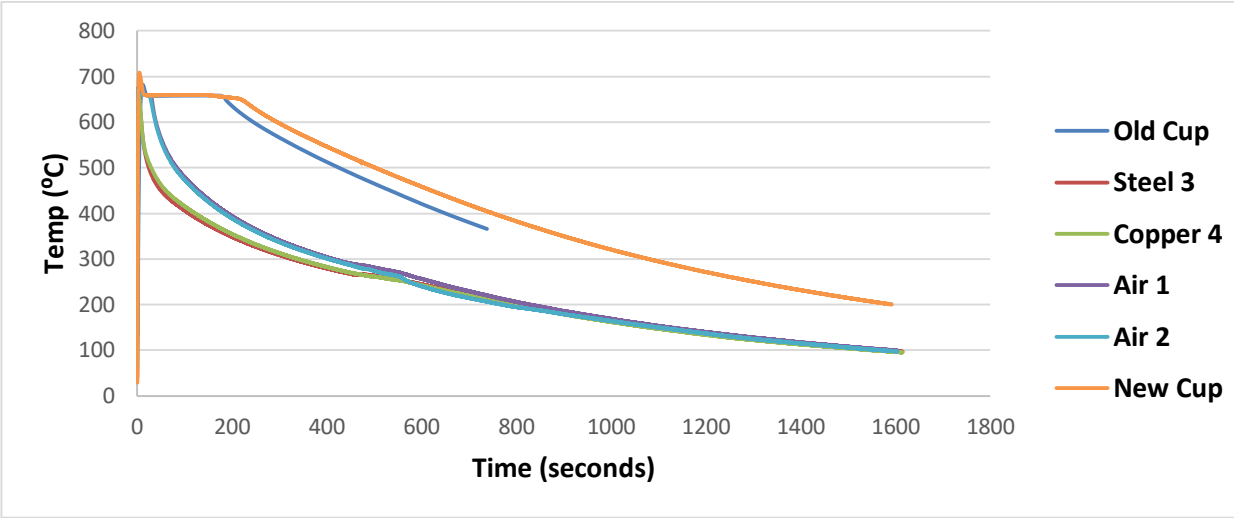

Figure 23: Comparison of recorded time vs temperature data of all thermocouples. The first two thermocouples were placed in the slow cooled plates, the third thermocouple in the steel-chilled plate, and the fourth thermocouple in the copper-chilled plate. The excess material was poured into a fifth Quik-Cup mold, labeled 'new cup' on this chart to compare it to the original cooling data from the original pour, labeled 'old cup'.

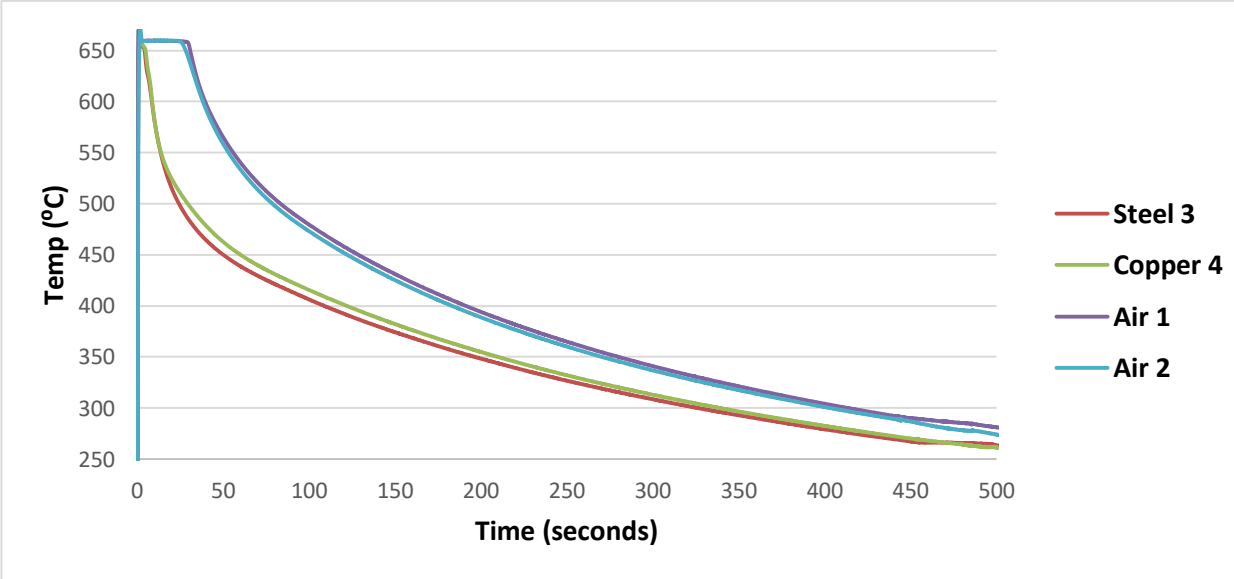

Figure 24: Comparison of recorded time vs temperature data of just the plate thermocouple results for which the data is meaningful. The bump at approximately 470 seconds of the four plate's thermocouple data is when the plates were deemed to be a low enough temperature to be removed from the molds, but the thermocouples continued to record data.

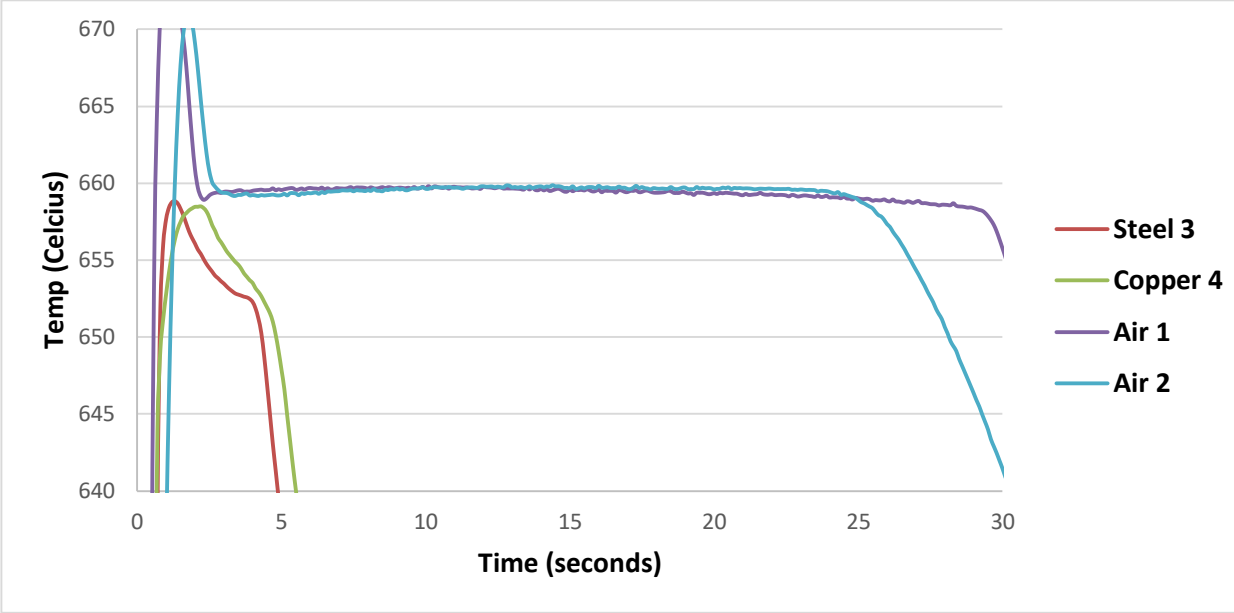

Figure 25: Close up of the first 30 seconds of the plate thermocouple tests. The chilled samples cooled so quickly, that the thermocouples failed to react fast enough to record a temperature above the solidification temperature of the alloy.

Etching and Grain Size

Several samples were etched to determine the approximate grain size of the samples. Al-Ga 0.1wt% is nearly pure aluminum, and is a single phase, so it requires very specific etching procedures as the aluminum oxide film protects the sample. Several failed attempts were made before a successful process was found. One sample of each type, steel chilled, copper chilled, and slow cooled, in addition to annealed variants of each, for a total of six samples were etched.

This final process was as follows: First, the samples were polished to 600 grit using 3M Silicon carbide sandpaper, followed by 9 and 1 micron diamond paste with Precision Surfaces International PSI 541-1 diamond extender lapping solution and a PSI 605-10 nylon polishing cloth on a Buehler Ecomet3 variable speed polisher/grinder. Once the samples were as smooth as possible, the oxide layer was removed by immersing the sample in a 10:1 mixture of water and hydrogen fluoride for approximately 45 seconds. Next, the aluminum was etched by immersing the sample in a 2:1:1 mixture of water, nitric acid, and hydrogen chloride for one to two minutes, until the grains became visible. Finally, the samples were rinsed with deionized water and dried with pressurized nitrogen gas.

As this process requires hydrogen fluoride, and Virginia Tech requires significant safety precautions when using it, this process, save for the polishing, was done by the Micro and Nano Fabrication Laboratory at Virginia Tech. Figure 26 and 27 are representative pictures of the final etched sample, all raw etched pictures are in Appendix F. While the samples were only prepped to be etched from the top side, since the etching process involves the emersion of the sample, some of the samples did reveal grains on the back side of the sample.

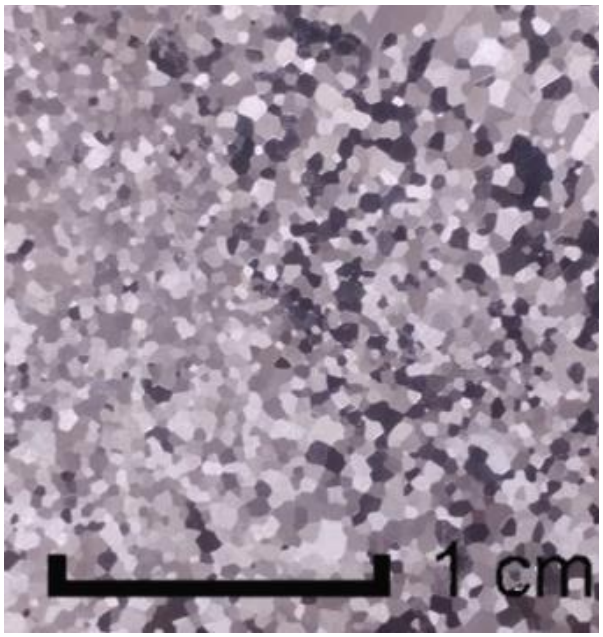

Figure 26: Etched surface of sample 'Steel Cent 2' with scale.

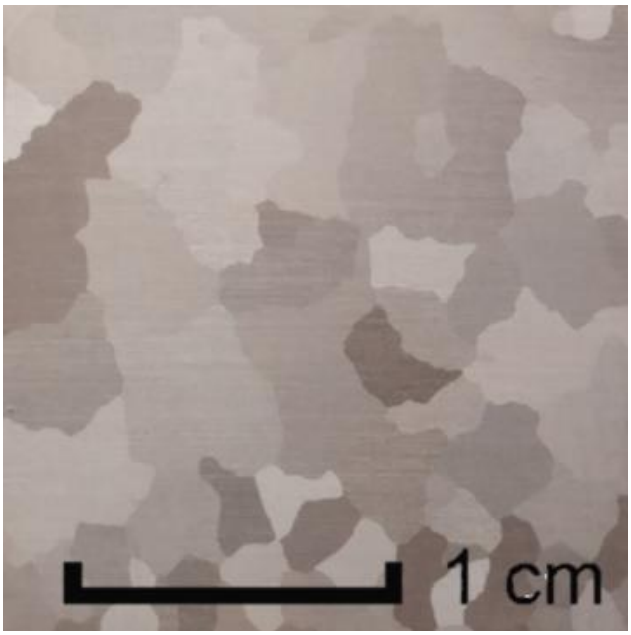

Figure 27: Etched surface of 'Air Cent 2' with scale.

Grain Size

Grain size was calculated using the average grain intercept method[30] on pictures of the front of etched samples within ImageJ[31]. Some of the samples etched better than others, and the copper and steel samples were similar enough to be considered the same for this purpose. One sample exhibited abnormal grain growth and was omitted from this measuring process.

Table 1: Grain Size Measurements

Sample Type	Chilled	Chilled+anneal	Slow cooled	Slow cooled + anneal
Sample Name	Steel Cent2	CU ML1	Air CENT2	AIR MR2
Average Diameter	0.50 mm	0.88 mm	2.3 mm	1.1 mm
Error[30] via $\frac{\sigma_d}{\sqrt{N}}$	±0.0054 mm	±0.027 mm	± 0.22 mm	±0.044 mm

Grains of the slow cooled samples were significantly larger than the chilled samples, which seemed to hold true whether or not the sample was annealed. With little or no driving force beyond grain boundary interfaces, the annealing grew grains only slightly or not at all, with the one exception of the sample which experienced abnormal grain growth. Strangely, the measured annealed+slow cooled sample had smaller grains than the measured slow cooled sample. While samples for the purpose of grain size measurement were picked to minimize differences of cooling rate based upon distance to the downsprue, it is possible that the differences in cooling rate still exist.

Abnormal Grain Growth

At least one of the samples exhibited abnormal grain growth after the annealing process. In Straumal et al.'s work, it was found that Al-Ga alloys can and do exhibit abnormal grain growth, for much less extreme annealing time and temperatures than used in this research[22]. Straumal et al.'s samples all had a driving force created by the cold rolling of the samples. This cold working encouraged the recrystallization and eventual abnormal grain growth, but the samples used in this research had no such cold working. However, the part of the chilled sample touching the chill solidified almost immediately, while the back side cooled slower. Metal farther away from the downsprue also cooled faster than metal close to the downsprue, which unfortunately acted as a massive heat source. It might be possible that, due to the rapid cooling, residual stresses could have developed and persisted in some parts of the anode, before it was cut into pieces. This possible residual stress could explain how one of the samples that went through the annealing process exhibited abnormal grain growth.

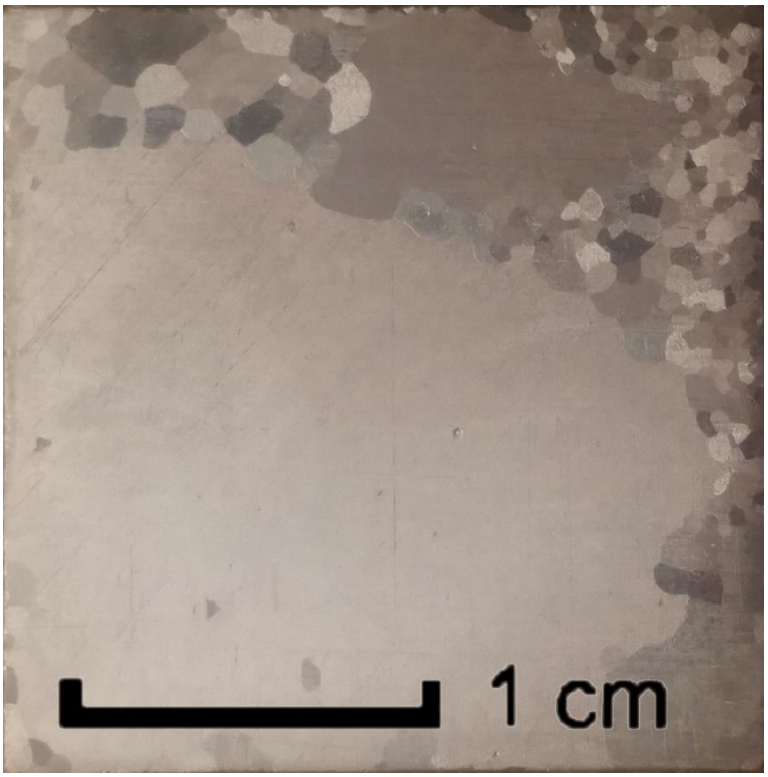

Figure 28: Picture of sample exhibiting abnormal grain growth.

Revised Solidification Simulations

With a better idea of the grain sizes, and cooling curves, the solidification simulations were revised to be more representative. Thermo-Calc can only handle a limited number of time temperature pairs, so the time-temperature data had to be simplified from ten data points per second, to a set which best maintains the overall cooling curve, and time of solidification. Because the time-temperature data from the chilled plate thermocouples never measured a temperature above the melt temperature, an

estimated starting temperature above the melt temperature must be added for those data sets. These revised simulations drastically changed in their results from the initial simulations. It turns out that the differences in grain sizes between the chilled and slow cooled samples far outweighed the extra time the slow cooled samples have at high temperatures to desegregate the gallium. Because the time temperature data is the same despite grain size, the simulations of larger grains are forced to grow at a faster rate in the simulation than the smaller grains. This has an interesting effect on the simulations of the particularly large grains for which the gallium does not have sufficient kinetics to completely outrun the advancing solid phase. These simulations also assume that the grain growth matches with the cooling data, and not faster or slower. Figures 29-34 show revised solidification simulations for various sized grains, using the different time temperature data sets. These graphs show the grain radius, with the left side of the graph representing the grain nucleus, and the right side of the graph representing the grain boundary. Programs to run these simulations in Thermo-Calc are in Appendix G.

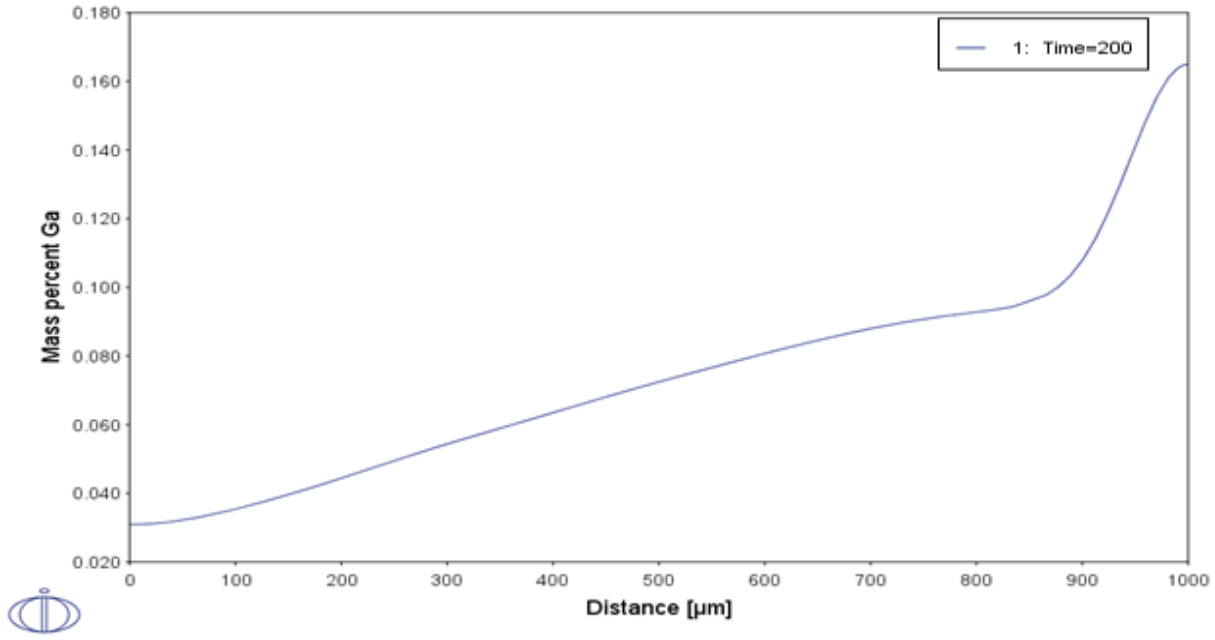

Figure 29: Predicted gallium distribution of a large 2 mm diameter grain using the slow cooled time-temperature dataset. Final distribution goes from nearly twice the nominal gallium percentage near the grain boundary, to nearly one third the nominal gallium percentage at the center of the grain.

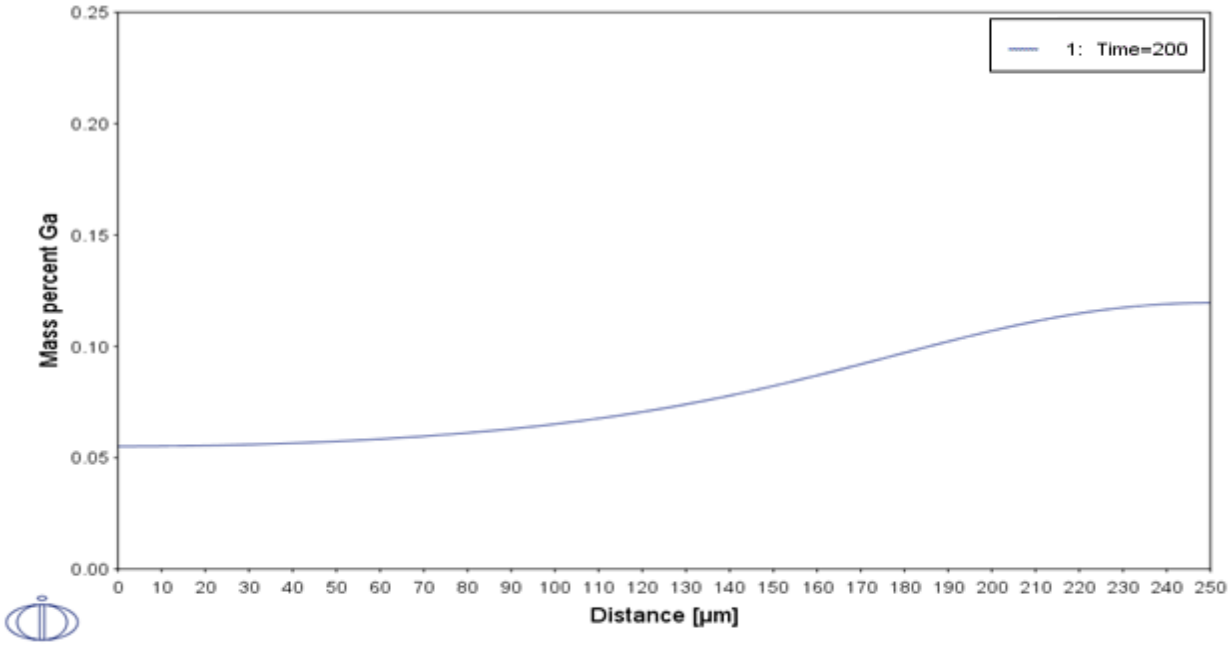

Figure 30: Predicted gallium segregation in an average sized, 0.5 mm diameter chilled grain. The predicted gallium depletion is significantly less at the grain center compared to the slow cooled sample, and the gallium rich zone is expected to be less than 25% above the nominal composition.

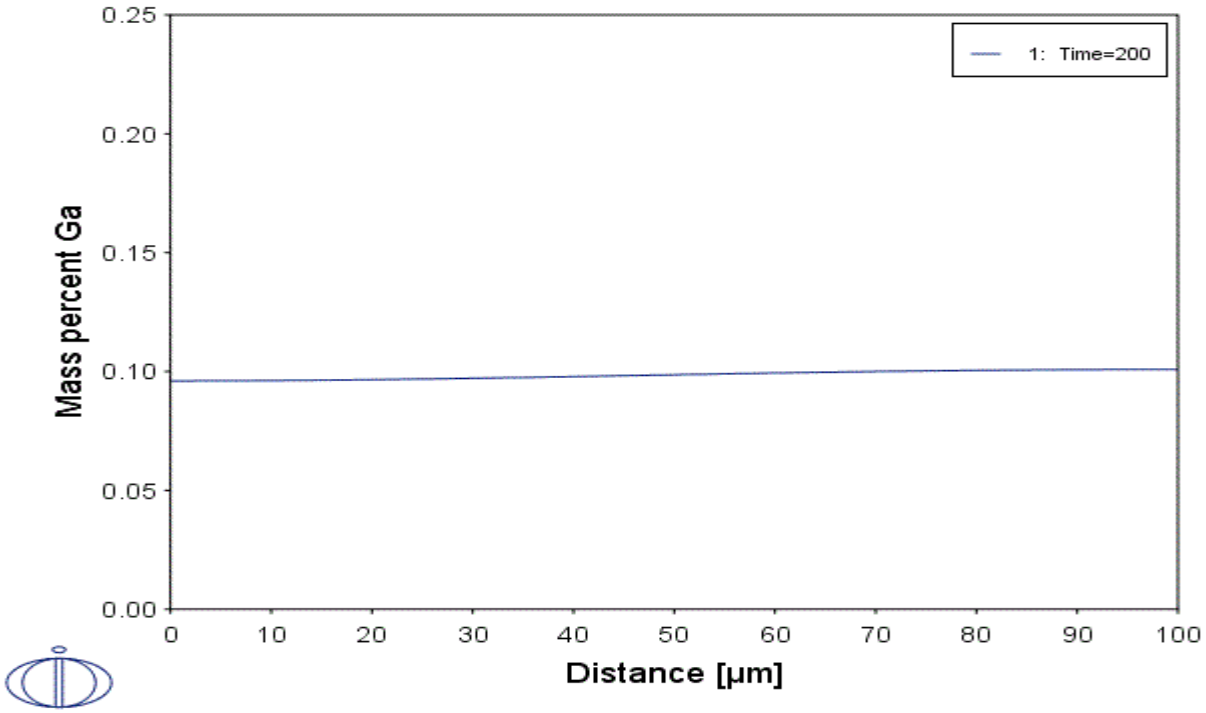

Figure 31: Estimated gallium distribution of a below average 0.2 mm diameter chilled grain. If a grain formed this small, the gallium distribution should be almost effectively uniform at the nominal composition.

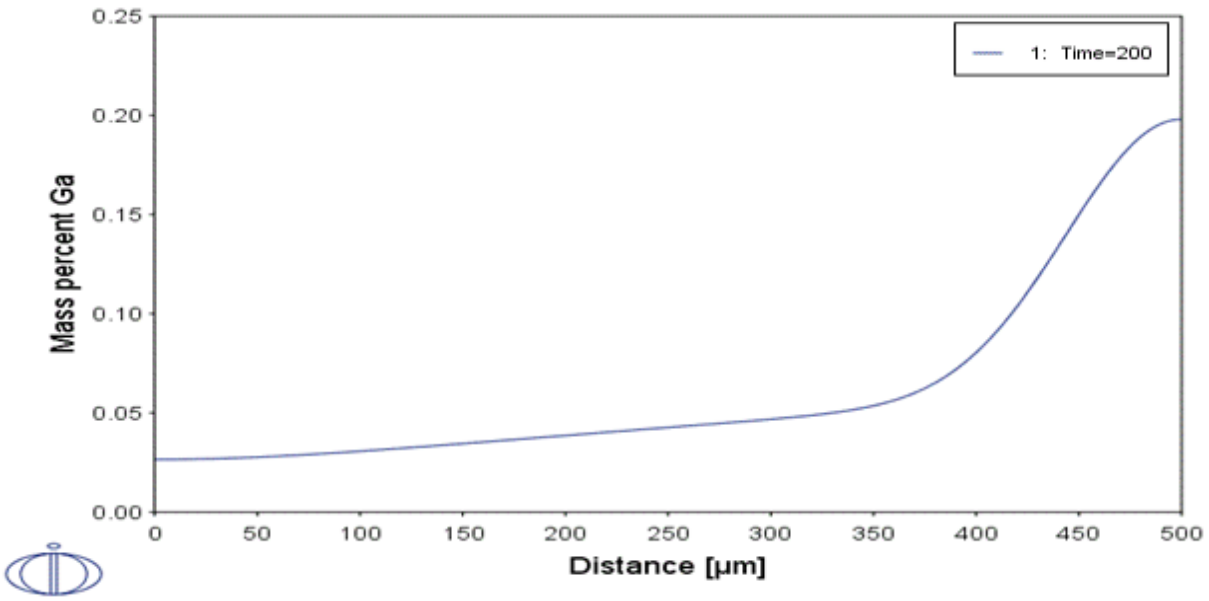

Figure 32: Estimated gallium distribution of a below average 1 mm diameter slow cooled grain. The gallium depletion region of this grain is not as extreme as the 2 mm grain, but the gallium rich region is similar.

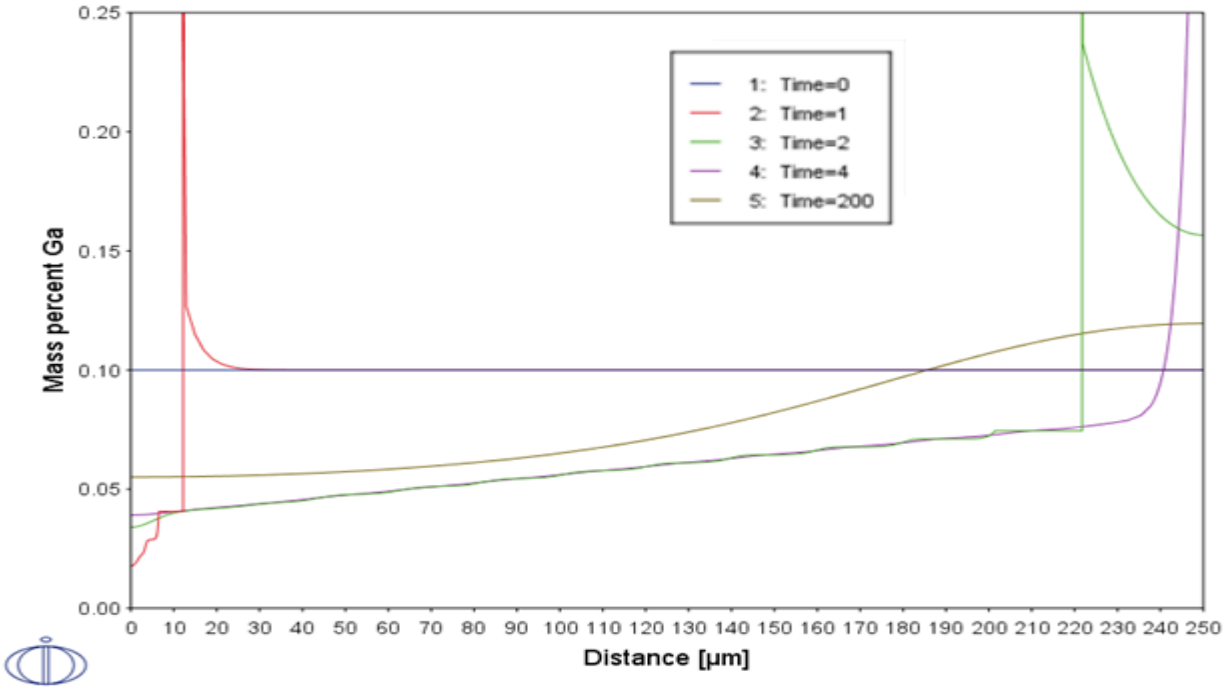

Figure 33: Estimated gallium distribution during simulated solidification of a chilled 0.5 mm diameter grain. At time zero the area which will become the grain is liquid, at T= 1 second, the nucleus has formed, and the gallium is being pushed into the remaining liquid. By T=2 second, the solid-liquid transition has almost made it to the edge of the grain. At T=4, the grain is simulated to be completely solid and the gallium begins moving back into the bulk, to which it is partially successful by the time the simulation ends.

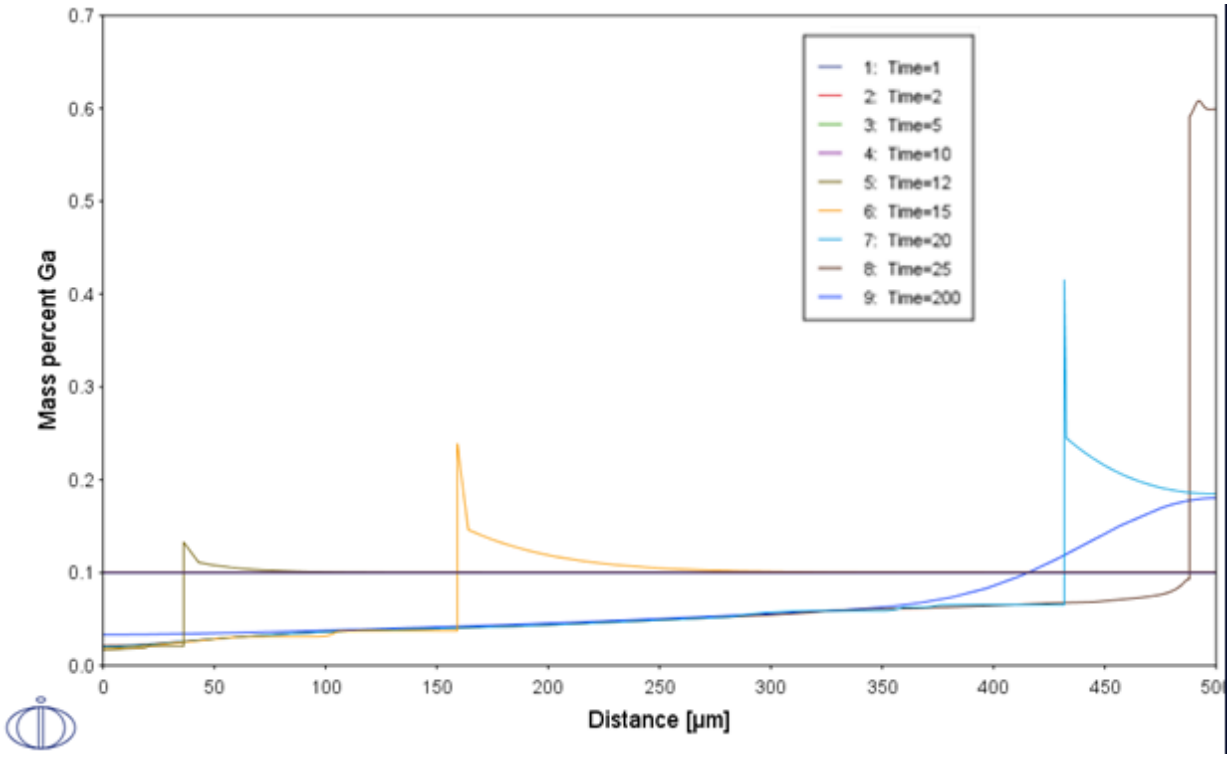

Figure 34: Estimated gallium distribution during simulated solidification of a slow cooled 1 mm diameter grain. At T=0, the area which is to become the grain is completely liquid still. At T=2 the grain nucleus has formed, and the gallium is being pushed by the solid liquid interface to remain in the liquid. As in the cooling data, it takes just over 25 seconds for the grain to completely form, and then the gallium begins to re-homogenize. While the dwell time at the higher temperatures is longer, the larger grain prevents the gallium from traveling back to the core of the grain.

Anode Lifespan

Many aluminum alloys are known to age at or near room temperature. If maintaining gallium segregation is important for Al-Ga anode effectiveness, then any room temperature diffusion would be a concern, and perhaps put a maximum lifespan upon these anodes. Fortunately, Thermo-Calc can be used to simulate years of time at constant temperatures in minutes.

Figure 33 shows a diffusion simulation of a low temperature long time anneal. The gallium does not migrate in significant fashion below 175°C, even at time periods of one year. Below about 150°C the software shows no diffusion whatsoever. This could be either hardware or software limitations due to small numbers. Once the temperature was raised to 275°C, significant diffusion did begin to take place, Figure 34. These diffusion simulations were done using the error function to create a simulated initial gallium distribution similar to the predicted gallium distributions seen in other simulations.

Equation 2: Chosen Initial gallium distribution for annealing simulations

$$Wt\%\ Ga = 0.1 + 0.05 * erf(2000000 * \frac{x - 0.000025}{25})$$

This assumed initial distribution was created using the above equation, with x in meters, and an assumed grain diameter to be 0.10 mm. This is below the average grain size of all the measured grain sizes, but was picked because such a grain would be the worst case scenario: A smaller grain radius means the gallium has less distance to travel to re-homogenize.

There are perhaps better ways to estimate initial distributions, but this is a decent estimate when compared to the sorts of supposed gallium distributions created by the solidification simulations, and is a reasonable grain size based upon the measured grain sizes.

Even if these estimates were unreasonable, Al-Ga lacks the typical driving forces of aluminum aging processes. The gallium percentages in the alloy are far below the gallium saturation limit, which Thermo-Calc calculates to be 18.66% by weight at 25^{o}C, even in the most extreme simulations of preservation of segregation. So no super saturation and thus precipitation of secondary phases will take place. Thus, the gallium diffusion should negligible.

These simulations are supported by the test data. The test results do not seem affected based upon the time between casting and the galvanostatic testing date. It is thus safe to conclude that no significant redistribution of gallium in Al-Ga anodes occurs at any reasonable storage temperature.

If the situation may be that segregation in the Al-Ga alloy is wanted to be removed, we can similarly simulate temperature and times for which the diffusion goes to completion in the bulk. Doing this, we find that 600^{o}C should be sufficient to effectively eliminate segregation in even the largest of grains over the course of five days.

Figure 35-37 do not take into account any potential affects from other alloying elements, or grain boundaries, but these should be negligible.

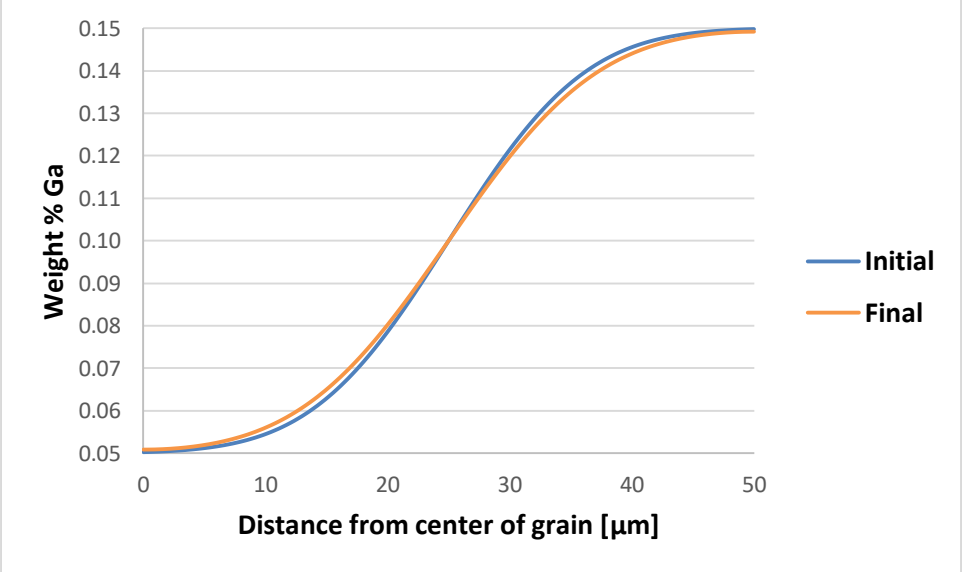

Figure 35: A simulated yearlong anneal at 175^{o}C for an estimated gallium gradient. The program used for this simulation can be found in Appendix 8.

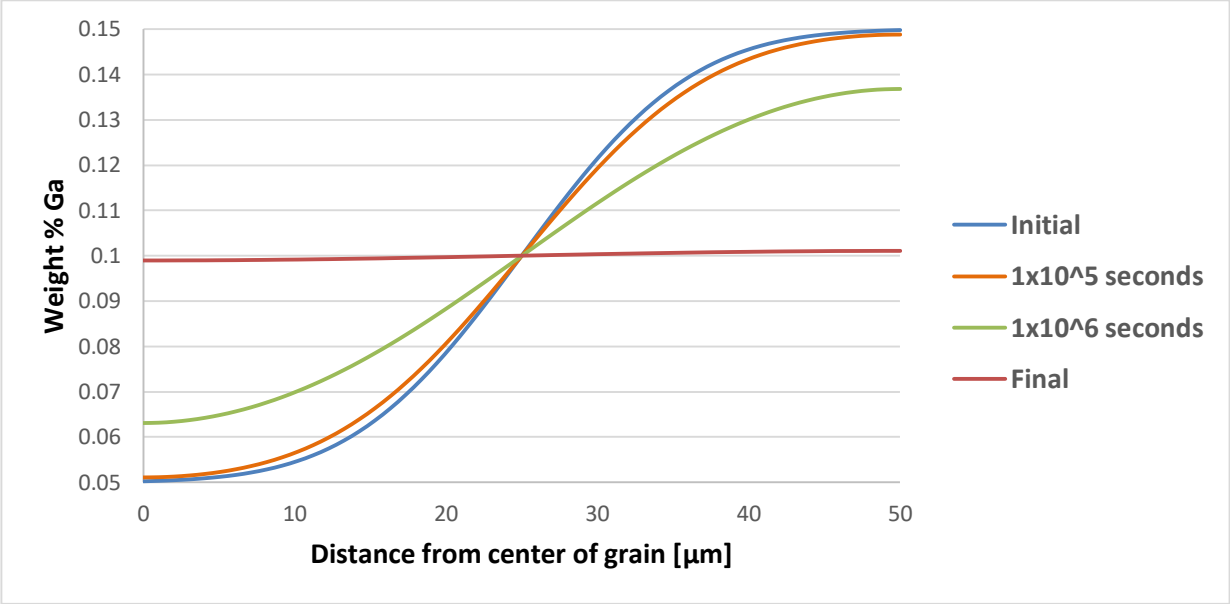

Figure 36: A simulated yearlong anneal at 275°C for an estimated gallium gradient. The program used for this simulation is essentially identical to the one in Figure 31.

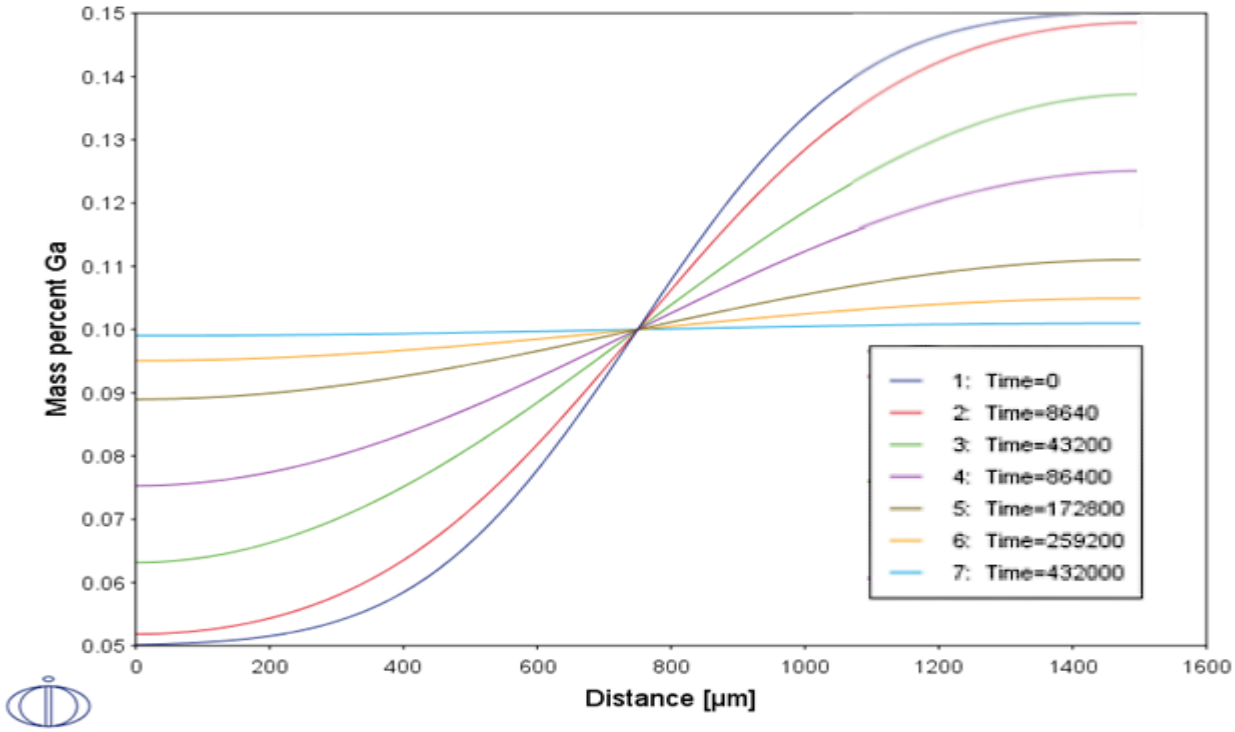

Figure 37: Simulated five day anneal at 600°C for an exceptionally large grain size of 3.2 mm with an initial gallium distribution based upon the ERF function. This is also the approximate width of the sample, so if there is a difference in gallium percentage between the front and back of the sample, this anneal should significantly reduce that variance.

Annealed Galvanostatic Testing

The updated simulations predict that gallium segregation persists in both the chilled and slow cooled plates. We also know that the chilled samples, with their predicted lower segregation of gallium, performed better than the slow cooled plates in the corrosion tests. It thus becomes obvious to ask how well perfectly homogenized samples would perform.

An anneal schedule of 5 days at 600°C was chosen after modeling the system within Thermo-Calc. This anneal was done using a Barnstead/Thermolyne model fa1730 furnace using a Thermolyne Furnatrol type 53600 temperature controller. The temperature was maintained using this controller.

During annealing, samples were placed on a ceramic tile, and the tile placed inside the furnace. The furnace then heated the samples to temperature at approximately 10°C per minute to 600°C, where the furnace maintained 600°C for 120 hours. The furnace was then turned off, and the ceramic tile removed. The samples were then allowed to air cool to room temperature. The annealed samples were then run though the same galvanostatic test used previously, and the data recorded. The results of these tests are shown in Figures 38-40, and Appendix B.

All samples seemed to generally exhibit better voltage behavior after the anneal. However, the samples which originally were slow cooled generally exhibited a more erratic voltage behavior to the samples which were chilled, then annealed; despite that the anneal schedule was designed to be excessively long compared to what should have been necessary for complete homogenization based upon the simulations. Further work could be done to optimize the annealing time and temperature.

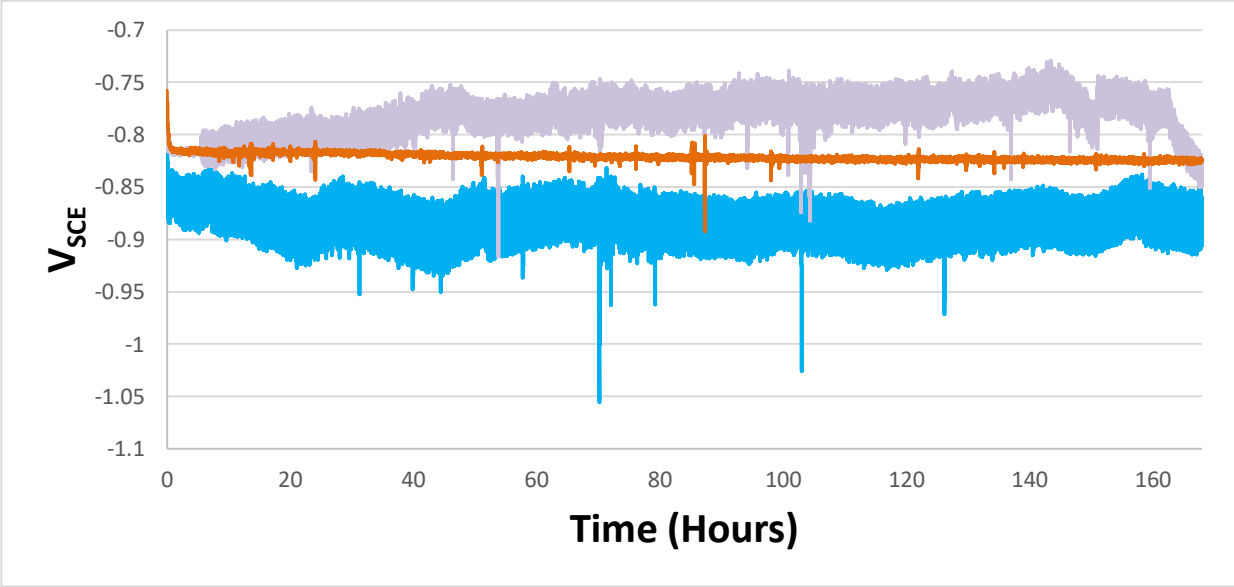

Figure 38: Voltage behavior of the three slow cooled + annealed samples. Like the non-annealed counterparts, two samples behaved erratically (substantially less so than the non-annealed samples, however), while one behaved perfectly.

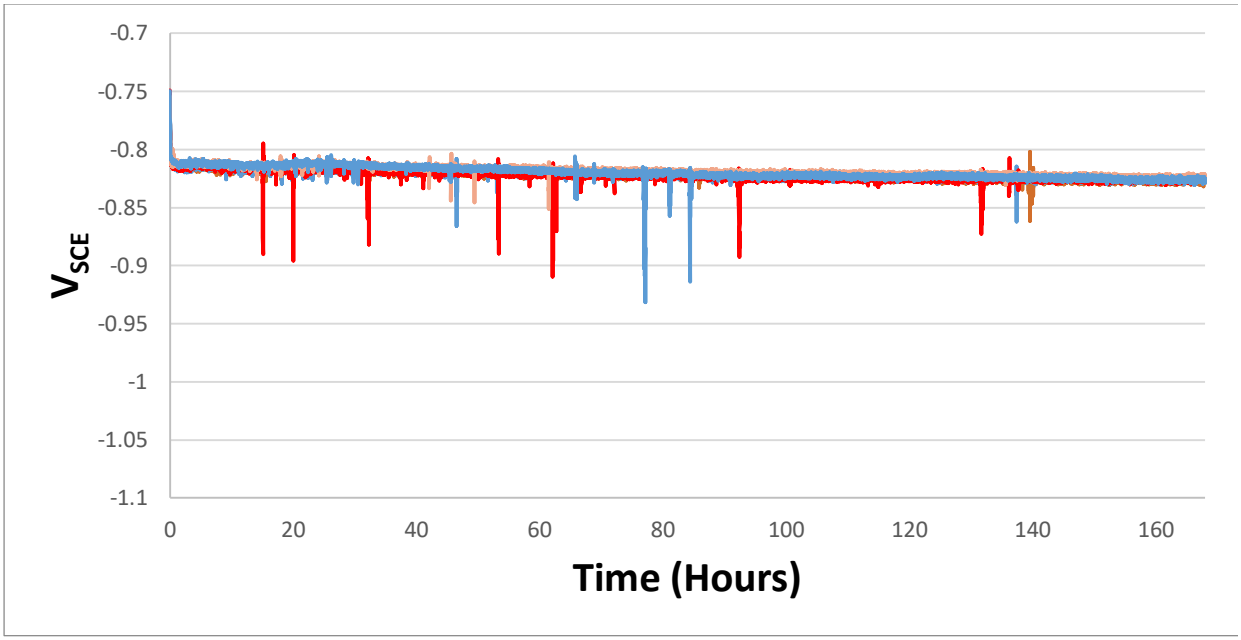

Figure 39: Voltage behavior of all five chilled and annealed samples, exhibiting nearly identical and near perfect behavior.

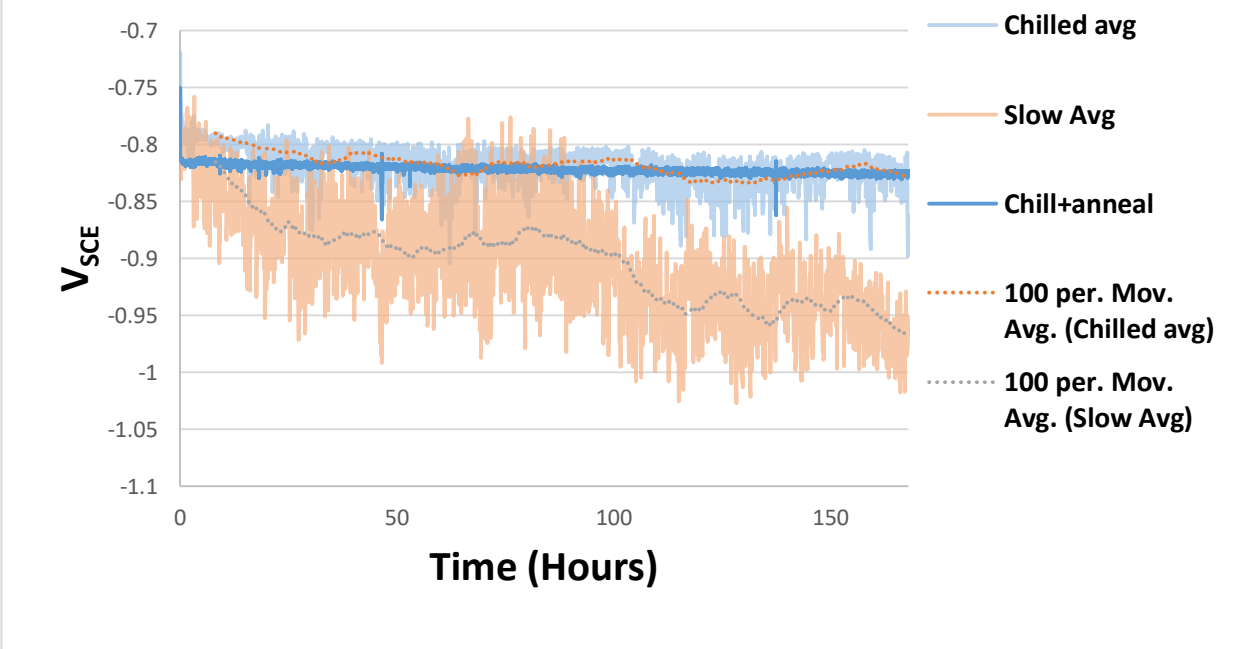

Figure 40: Comparison between a representative chilled+annealed samples against the previous 'as cast' samples.

Cold Water Galvanostatic Testing

If there are two different mechanisms for the corrosion of Al-Ga, we might be able to force the dominate mechanism to occur. The proposed super-cooled gallium mechanism[15], if indeed present,

would potentially be significantly affected by temperature. By cooling the environment in which the experiment takes place, we can increase the difference in Gibbs free energy of the liquid phase and solid phase, thus preventing a liquid phase from being present.

In order to test this, five more samples were run through a series of galvanostatic tests identical to the setups previously used, with the exception that the testing apparatus was placed inside a cooler filled with fresh water ice. The ice was replaced two times a day for 4 days, and then left to melt. This created two temperature gradients, from room temperature to approximately 0^oC, and then from 0^oC to room temperature after four days of near freezing temperature. Due to this method, there is no risk of the salt water in the test chamber freezing, which has a freezing point of ~-2^oC[32].

The process of replacing the ice did cause minor agitation to the otherwise still testing apparatus, it is unlikely this affected the results. The temperature of the test chamber was not directly measured during the test. This is unnecessary, as thermodynamics demands that melting ice at 1 atm maintains a steady temperature of 0^oC. The results of the tests suggest a change in the voltage behavior of the Al-Ga anode when the temperature is low, compared to room temperature.

All of the samples showed at least a slight improvement of the voltage behavior after the low temperature environment was removed, though some of the samples recovered move than others. A comparison of two of the datasets is shown in Figure 41, and the rest of the datasets are in Appendix B. Even the sample which did not go through the annealing process recovered somewhat, but mostly stayed erratic, once the erratic behavior manifests. The sample which showed a recovery to steady state voltage behavior, and then a reverting to erratic behavior helps highlight the meta-stable nature of the alloy's behavior.

It is possible that the colder temperatures could have other unforeseen effects, and thus it is not necessarily the case that it is indeed a super-cooled liquid gallium mechanism which has been shut off, but the results of the experiment are consistent with the hypothesis. In particular, the amalgam-like theory could also be affected by temperature if the lower temperature was sufficient to solidify the layer of gallium.

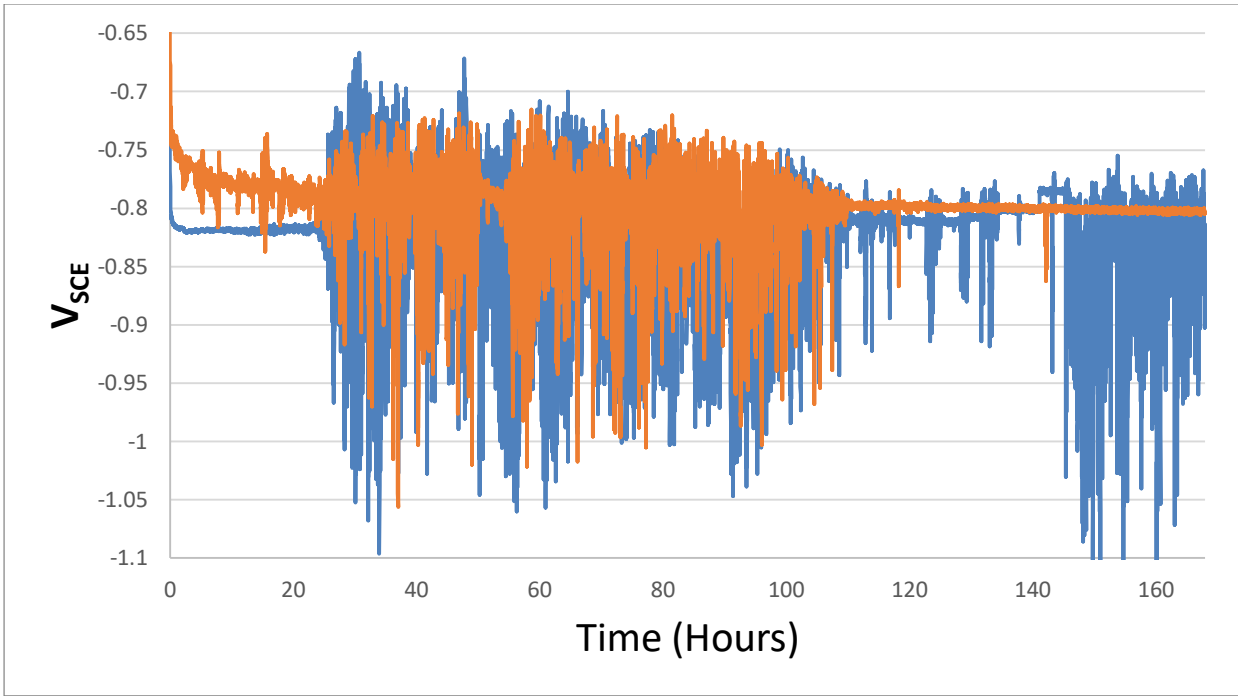

Figure 41: Galvanostatic voltage comparison of two of the chilled and annealed samples which underwent the cold water testing. One sample (steel BM2) recovered completely once the cold environment was removed, while another sample seemed to almost recover, (Steel UM1), and then returned to erratic behavior.

Optimizing Annealing Time

An annealing process of 600 ^{o}C for five days is very long, and should be excessive for the purposes of eliminating segregation. However, previous work with cooler and shorter annealing showed little to no effect on the voltage behavior.[12] As the results clearly show, the anneal used did change the voltage behavior at the 0.62 mA current used. To help show this, a sample was put though a 5 day, 500^{o}C anneal, and the voltage behavior tested, in an otherwise identical fashion to previous samples. The results of this test are shown in Figure 42. While a single sample is not statistically significant, it does strongly suggest that annealing temperatures at or below 500^{o}C are insufficient to affect voltage behavior.

It is of note that at 500^{o}C, some of the impurity phases which Thermo-Calc predicts with the material used for these tests could have sufficient kinetics to form. Attempting to verify the presence of these impurity phases is out of scope of this work, however.

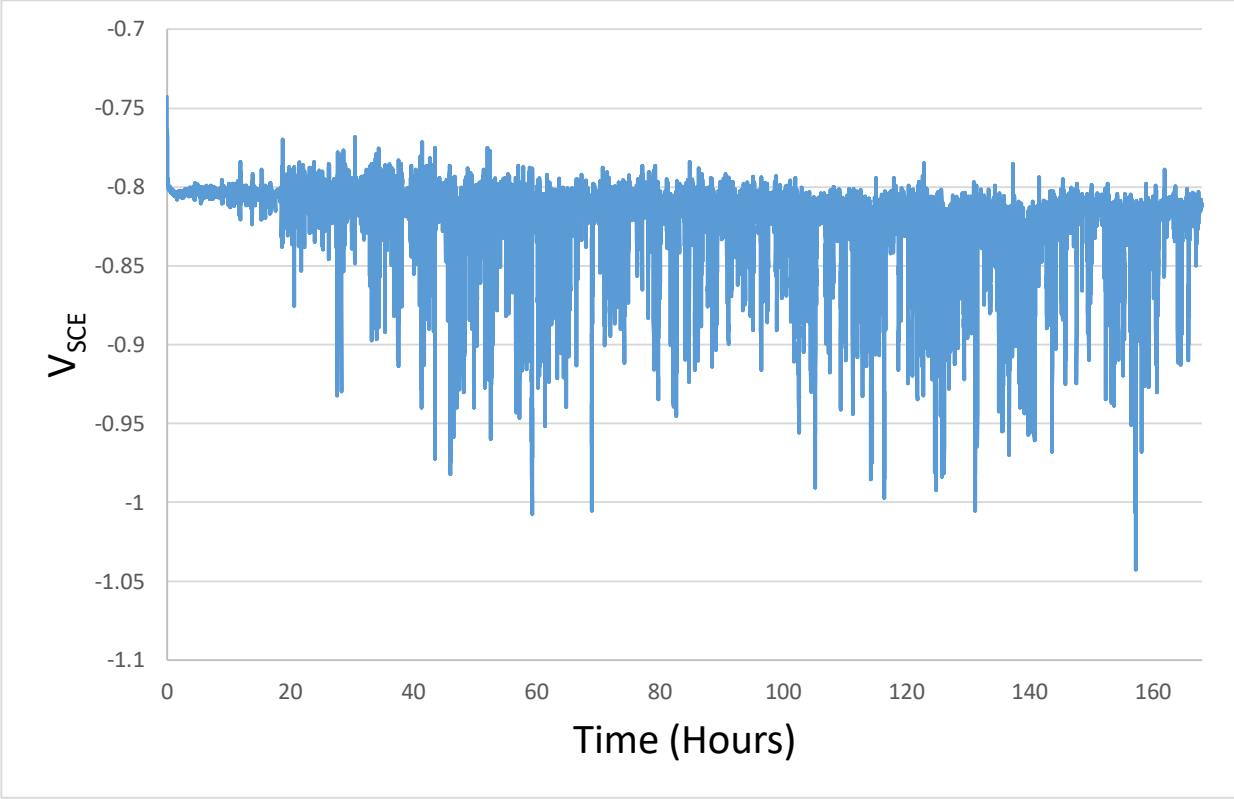

Figure 42: Voltage behavior of 500°C Anneal temperature test, Cu UM2. This test suggests that 500°C is insufficient to remove erratic behavior.

Results

Anode Efficiency

An important measurement of the effectiveness of sacrificial anodes is their efficiency. For the majority of the tests, the samples were weighed on a Sartorius gk-3102 scale before and after the test, and the mass loss calculated. This scale could measure the weights of the samples to the milligram. These measurements are in Tables 2-4. Samples were weighed three times, and the median value taken as the weight. The predicted corrosion rate was compared to the actual weight loss. First, we calculate the theoretical current capacity for 0.1% wt Al-Ga, usually measured in Amp hours per kilogram.

Equation 3: Theoretical current capacity of pure aluminum[11,12]

$$\frac{1hr}{3600s} * \frac{3 * 1.602 * 10^{-19} Coul}{1\ atom\ Al} * \frac{6.02 * 10^{23} atoms}{0.02698 Kg} = 2979 \left(\frac{A * hr}{Kg}\right)$$

Equation 4: Theoretical current capacity of pure gallium[11,12]

$$\frac{1hr}{3600s} * \frac{3 * 1.602 * 10^{-19} Coul}{1\ atom\ Al} * \frac{6.02 * 10^{23} atoms}{0.06972 Kg} = 1153 \left(\frac{A * hr}{Kg}\right)$$

Note the factor of 3, as gallium and aluminum both ionize to a +3 state. Next, these values are combined via the rule of mixtures to calculate the theoretical current capacity of the alloy.

Equation 5: Theoretical current capacity of Al-Ga 0.1%wt

$$\frac{2979 * 99.9\%}{100\%} + \frac{1153 * 0.1\%}{100\%} = 2977 \left(\frac{A * hr}{Kg}\right)$$

Now, since all of the galvanostatic tests were done at 0.62mA, for 168 hours, calculate the expected mass loss, and compare this value to the measured mass loss.

Equation 6: the expected weight loss for 168 hour test:

$$\frac{168hr}{2977 \left(\frac{A * hr}{Kg}\right)} * \frac{6.2 * 10^{-4} A}{1} * \frac{1000g}{Kg} = 0.0349g$$

The mass loss for the samples varied between 0.040g and 0.032g Thus the measured anode efficiency ranged between 88%, and 109%, with the exception of one sample which had anomalous voltages. It is important to note a few sources of error which may exist. First, if the gallium does not leave the aluminum surface, as suggested by previous work, a theoretical current capacity of pure aluminum might be more accurate.[14] Second, for the samples which may exhibit segregation, those areas with higher concentrations of gallium are more likely to activate first, and thus a higher effective concentration of gallium would again affect the current capacity. Errors may also have arisen due to particles of the sample falling off, and sample electrolyte remaining within sample pores. Additionally, the scale used to measure the weight loss was only accurate enough to record to the nearest milligram of mass loss.

Table 2: Mass Loss of as Cast Samples

	UL Steel 1	UR Air 1	UL Cu 1	BR steel 1	BL Air 1	BL Cu 1
Before (g)	8.130	8.124	8.032	8.329	8.245	8.347
After (g)	8.092	8.090	7.997	8.289	8.206	8.308
Net Loss (g)	0.038	0.034	0.035	0.040	0.039	0.039
% Efficiency	92	102	100	88	90	90

Table 3: Mass Loss of Annealed Samples

	Air UL 1	UL CU 2	Air UL2	Air Cent1	Cu Cent1	Steel 2 UL	Steel 2 UR	Cu 1 BR
Before (g)	8.102	8.722	7.959	8.030	8.116	8.223	8.294	8.141
After (g)	8.064	8.684	7.925	7.995	8.084	8.191	8.256	8.108
Net Loss (g)	0.038	0.038	0.034	0.035	0.032	0.032	0.038	0.033
% Efficiency	92	92	103	100	109	109	92	106

Table 4: Mass Loss of Annealed and Ice Tested Samples

	Steel UR1	Steel BM2	Copper UL1	Copper BM1
Before (g)	8.350	8.069	8.176	7.995
After (g)	8.318	8.034	8.147	7.961
Net Loss (g)	0.032	0.035	0.029	0.034
% Efficiency	103	100	120	103

Statistical Analysis of Anode Efficiencies.

The recorded mass loss of the samples exhibits a quite significant range of values, from 0.040g to 0.032g so it is hard to find an obvious correlation between the anode efficiencies and the various different tests. If there is a correlation, it should show itself by comparing the chilled+annealed mass loss, with its optimal voltage behavior, with the non-annealed samples, and their generally undesirable voltage behavior. Comparing these data sets, we find that the non-annealed samples have an average mass loss of 0.038g, while the chilled+annealed samples have an average mass loss of 0.035g. If we assume the mass loss of these sets follows a normal distribution and have identical variance, we can calculate a two-tailed p value of 0.103. Thus, we cannot say, to even a 90% confidence level, that there is a statistically meaningful difference between the anode efficiencies of the recorded weight loss of the chilled+annealed samples, and the non-annealed samples, but it certainly warrants further research.

Significance of Annealing

While the number of data points collected per data set was massive, the number of data sets was still quite small, especially considering the number of outliers. Thus, we need to be sure our results are significant. Five out of five of the chilled+annealed tests gave results which demonstrated the desired voltage behavior, while two out of six of the slow cooled tests (three as cast, three annealed) demonstrated desired results. A quick binomial statistical test with an assumed probability of 33% of a 'lucky' success (based upon the slow cooled samples), suggests that 0.39%(n=5, k=5, p=0.33) of the time it would be expected that the chilled+annealed test results were a lucky fluke.[33]

Equation 7: Probability mass distribution function.[34]

$$\Pr(\mathrm{X} = \mathrm{k}) = \binom{n}{k} p^k (1-p)^{n-k}$$

Equation 8: Inverse of the cumulative distribution function.[34]

$$\Pr(X \geq k) = 1 - \left(\sum_{i=0}^{k-1} \binom{n}{i} p^i (1-p)^{n-i} \right)$$

Figure 43: Probability mass distribution function, and the inverse of the cumulative distribution function.[34] The first equation describes the chance of a particular number of successful outcomes, while the second describes the chance of a number of successful outcomes or better. Pr is the probability of getting a successful outcome k times, n is the number of tests run, and p is the probability of a single successful outcome.

The cold water tests, however, further prove that the annealing process does help, as four of five of those tests show desired steady state voltage behavior at some point during the tests. If those results can be added, then the probability of the results being lucky falls to 0.032%. This suggests with great confidence that using chilled molds followed by a 600°C anneal does cause a significant effect.

The slow cooled+annealed results are less favorable. As three tests were performed, and two of them gave undesirable results, we might conclude that the annealing did not work on these samples. This of course seems contrary to the hypothesis that it is indeed gallium segregation that causes the undesirable voltage behavior, despite the annealing times being sufficiently long to the point where the gallium segregation should be gone. Thus, we can do some binomial statistical tests to check our significance. If an annealed sample, based upon the chilled+annealed results, has an assumed 10% chance of failure, then the probability of two of three samples being 'unlucky' is only 2.7% (n=3, k=2, p=0.1).[34] This would seem reasonable, however, one of the tests has such a strange result, it perhaps should instead be discarded as a testing failure. If that is done, the chances of one of the two remaining tests being 'unlucky' rises to 18%(n=2, k=1, p=0.1).[33] An 18% chance that the chilling of the sample molds is unnecessary and only the annealing process has an effect upon the anodes does warrant further testing.

According to the Navy's specifications, the acceptable voltage range of low-alloy sacrificial anodes for short tests such as these is between -0.800 to -0.850 V_{SCE}.[10] Thus we can compare the data with this metric, and get an idea how desirable each sample would be as a sacrificial anode, and thus compare the various sets of heat treatment and conditions. This data is simplified displayed in Table 5, but discussed in detail below.

The three slow cooled samples exhibited average voltages of -0.914, -0.894, and -0.809 V_{SCE}, and out of the 60,480 collected data points, 30,899 were below -0.850 V_{SCE} 7,653 were above -0.800 V_{SCE}. This translates to only 36.3% of the data points being within the acceptable range, most of which were from a single sample.

The copper chilled samples without the anneal exhibited average voltages of -0.794, -0.830, and -0.822 V_{SCE}. Out of the 60,480 data points: 8,218 were below -0.850 V_{SCE}, and 19,376 were above -0.800 V_{SCE}. 54.4% of these data points were in the optimal range, with most those above -0.800 V_{SCE} from a single sample.

The steel chilled samples were mostly similar to the copper chilled samples, with average voltages of -0.808 and -0.809 V_{SCE}. Out of the 40,320 data points: 2,618 were below -0.850 V_{SCE}, and 11,095 were above -0.800 V_{SCE}. 66.0% of data points in acceptable range.

The slowly cooled and then annealed samples exhibited average voltages of -0.883, -0.781, and -0.821 V_{SCE}. Out of the 60,480 data points: 19,408 were below -0.850 V_{SCE}, and 16,721 were above -0.800 V_{SCE}. This means only 40% of the data points for these samples were in the acceptable range, and most of those on the single well behaved sample.

Of the copper chilled and annealed samples, the voltage averages were -0.822, -0.822, and -0.819 V_{SCE}, and out of 60,480 data points only 43 were below -0.850 V_{SCE} 27 were above -0.800 V_{SCE}. Using this metric, 99.9% of the data points gathered were within the acceptable range.

The steel chilled and annealed samples were effectively identical, with average voltages of -0.822 and -0.822 V_{SCE}. Out of 40,320 data points only 33 were below -0.850 V_{SCE} 18 were above -0.800 V_{SCE}. 99.9% of the data points were thus within the acceptable range.

The cold water tests must be broken down into four distinct sections: cold, warm, and the two transitory periods. The transitory periods vary slightly between the tests, and the voltage behavior change of the samples, while usually quite sudden, happens at slightly different times as well. In order to minimize errors, we will look at only the data points for which the temperature is constant for all the samples. Thus, we will define 'cold' to be between 24 and 96 hours, and 'warm' from 120 hours to test completion. As all of the cold water tests were done using chilled and annealed samples, and that It is expected that the copper chilled and steel samples will be effectively identical, so we will not differentiate between them for this analysis.

The 'cold' sections exhibited average voltages of -0.836, -0.839, -0.802, and -0.817 V_{SCE}. Out of 34,560 data points, 8,799 were below -0.850 V_{SCE} and 15,093 were above -0.800 V_{SCE}. For these 'cold' sections, only 30.9% of the data points were within the acceptable range.

The' warm' sections had voltage averages of -0.855, -0.822, -0.801, and -0.815 V_{SCE}. Out of 21,941 data points, 3,238 were below -0.850 V_{SCE} and 3,710 were above -0.800 V_{SCE}. For these 'warm' sections, 68/3% of the data points were within the acceptable range. This is significantly worse than the other chilled+annealed samples which were not subjected to cold temperatures, as some of the samples did not revert completely to the steady voltage behavior.

Table 5: Exhibited Voltage Ranges of Differing Conditions

	Slow Cooled	Chilled	Slow Cooled+Anneal	Chilled+Anneal	'Cold'	'Warm'
% Above -0.80V_{sce}	12.7%	30.2%	27.6%	>0.1%	43.7%	16.9%
% Acceptable	36.3%	59.0%	40.3%	99.9%	30.9%	68.3%
% Below -0.85V_{sce}	51.1%	10.8%	32.1%	>0.1%	25.5%	14.8%

Erratic Behavior

The behavior of the samples in these galvanostatic tests seems to fall into two distinct modes: A steady, constant voltage behavior, and an erratic voltage behavior. These two behaviors likely correspond to different corrosion mechanics, as the samples which experience one or the other are visually different. The samples which exhibit steady voltages tend to have wide, shallow pits, while the samples which exhibit erratic behavior tend to have deep, narrow pits.

The erratic behavior seems to generally vary in voltage between -0.750 and -1.100 V_{SCE} which somewhat corresponds to the voltages expected of aluminum with its passive aluminum oxide layer (-0.730 V_{SCE}[12]), and pure aluminum with no protective layer, as the corrosion potential of pure aluminum is -1.418 V_{SCE}[35]. It could be theorized that the erratic behavior is a cyclic failure or detachment of the oxide layer within the pitted area, followed by a re-passivation of the surface. Since the surface area of the pits is much smaller than the measured test area, a voltage difference between the ideal case of pure aluminum with no oxide layer and the test results would be expected. However, these tests are insufficient to prove such behavior.

While visually we can see the difference in the voltage behavior in the graphs, we should mathematically compare the voltage behaviors as well. We can do this by comparing the standard deviation of the voltage data for each of the sets of data. This is not a perfect metric, as nearly all samples show a slight decrease in voltage over time, and the distribution is not entirely normal, but it will suffice to displace the variance in a quantitative way. The voltage decrease might be attributed to the increase in effective surface area caused by the corrosion process, and/or the change in electrolyte composition as the aluminum and gallium dissolve.

Taking the standard deviation of the three slow cooled samples gives σ = 0.058, 0.072, for the erratic samples and 0.011 for the sample which gave steady state behavior. For the chilled samples, σ = 0.029 and 0.021 for the two steel chilled samples, and σ = 0.028, 0.036, and 0.032 for the three copper chilled samples.

For the slow cooled + annealed samples, we get σ = 0.020, 0.019, and 0.004. For the chilled + annealed samples, σ = 0.005, 0.004, 0.004, 0.004 and 0.006. This clearly shows that the chilled+annealed samples exhibit much steadier voltage than the non-annealed samples. Interestingly,

in difference from the acceptable voltage range metric, the slow cooled + annealed samples would be considered 'better' than the chilled samples using this metric.

Most interestingly are the differences in standard deviation between the cold and warm sections of the cold water tests. These gave σ values of 0.060, 0.065, 0.039, and 0.052 for the 'cold' sections, and 0.044, 0.048, 0.002, and 0.005 for their respective 'warm' sections. This clearly shows that while all samples recovered somewhat, only two of the four can be said to have complete recovery. This helps confirm the notion that the erratic behavior is the preferred mode, and that the steady-state voltage behavior could be described as meta-stable. However, the work done here cannot correlate the discussed mechanisms in the literature[13,14,17,18,28] to the two different observed behaviors.

Table 6: Standard Deviation of Samples

	Slow Cooled	Copper Chilled	Steel Chilled	Slow Cooled+Anneal	Copper Chilled+Anneal	Steel Chilled+anneal	'Cold'	'Warm'
Test 1	0.058	0.028	0.029	0.020	0.005	0.004	0.060	0.044
Test 2	0.072	0.036	0.021	0.0190	0.004	0.006	0.065	0.048
Test 3	0.011	0.032	N/A	0.004	0.004	N/A	0.039	0.002
Test 4	N/A	N/A	N/A	N/A	N/A	N/A	0.052	0.005
Average	0.047	0.032	0.025	0.014	0.004	0.005	0.054	0.025

Future Work

While the improvement in voltage behavior is significant between the as-cast samples and chilled+annealed samples, it must be remembered that only the face directly adjacent to the chill was tested, and the grain sizes varied greatly from the back of the sample to the front. This method would be unusable for large bulk sacrificial anodes. More must be done to determine if simply having smaller grain sizes followed by an anneal would be sufficient for homogenizing the gallium concentration of the anode. Thus for commercial applications, it needs to be investigated if adding a grain refiner during the casting process followed by an anneal is sufficient to get optimal voltage behavior, while also insuring that the 2nd phase particles do not significantly affect the voltage behavior. If not, a fabrication method involving stacking multiple thin plates could be potentially used, perhaps from a continuous casting process which is set up to rapidly quench the material as it is formed.

We know from previous work that adding 0.1wt% germanium and/or other elements[11,12] stabilizes the voltage behavior without the chilling and annealing process. This is almost certainly not due to the other elements affecting the gallium segregation, but this should be investigated. Similarly, it needs to be asked if the voltage behavior of those anode compositions remains stable in cold water tests.

Conclusion

With this research we have looked into the galvanostatic testing of Al-0.1wt% Ga anodes to a finer granularity than done previously. We have found we can virtually eliminate the unwanted erratic voltage behavior with a 168 hour, 600^{o}C anneal. We also have some evidence that the erratic behavior can be brought back by subjecting the anodes to near 0^{o}C temperatures. We have also narrowed down the various possible causes for the difference in corrosion behaviors of the alloy, and have shown though simulations that we can likely attribute some of the erratic behavior to alloy segregation.

The conclusion of this work is that while casting samples using chilled molds and then annealing at 600^{o}C 0.1wt% Al-Ga sacrificial anodes does significantly improve the voltage behavior in galvanostatic tests; they are still unfit for use as sacrificial anodes for any application which may operate in cold water.

References

1. H. Le Guyader, "Consumable anode for cathodic protection, made of aluminum-based alloy," U.S. Patent 5 547 560, Aug. 20, 1996.
2. J.T. Reding and J.J. Newport, "The Influence of Alloying Elements on Aluminum Anodes in Seawater," Materials Protection (1966)
3. De Rincón, O. T., Salas, O., Sánchez, M., de Romero, M. F., Romero, G., Zamora, R., … Suárez, J. "Comparative Behavior Of Sacrificial Anodes Based On Mg, Zn, And Al Alloys In Brackish Water," NACE International, 2010, January 1.
4. N. Idusuyi and O. Oluwole, "Aluminum Anode Activation Research–A Review," *International Journal of Science and Technology,* 2012, vol. 2, p. 561-566.
5. ScienceLab.com, "Material safety data sheet Indium MSDS," http://www.sciencelab.com/msds.php?msdsId=9924359 May 21 2013.
6. F. P. Castronovo and H. N. Wagner, "Factors Affecting the Toxicity of the Element Indium," British Journal of Experimental Pathology, 52.5 (1971): 543–559.
7. S. Eliassen, "New concept for cathodic protection of offshore pipelines to reduce hydrogen induced stress cracking (HISC) in high strength 13%Cr stainless steels," *Corrosion Engineering, Science and Technology*, 39:1, p. 31-37.
8. Kitco.com, "Strategic Metals", https://www.kitco.com/strategic-metals/ Nov 16 2018.
9. J.P., Pautasso, H. Le Guyader, and V. Debout, "Low Voltage Cathodic Protection for High Strength Steels: Part 1 – Definition of a New Aluminum Galvanic Anode," Paper #725, Corrosion 98, NACE, 1998.
10. Military Specification MIL-DTL-24779D, "Detail Specification Anodes, Sacrificial, Aluminum Alloy," March 2015.
11. A. Druschitz, M. Maxfield, W. Monzel, and K. Tontodonato, "A Novel Approach for the Development of Low-Voltage, Aluminum, Sacrificial Anodes," in *Corrosion 2015*, Dallas, TX, 2015.
12. D. Baker, & A. Druschitz, "Understanding the Corrosion of Low-Voltage Al-Ga Anodes," *Virginia Tech*, June 26, 2015, http://hdl.handle.net/10919/53835.
13. J. Uruchurtu, "Electrochemical Investigations of the Activation Mechanism of Aluminum," Corrosion, Vol 47, Issue 6, pp. 472-479, 1991.

14. D.O. Flamini and S.B. Saidman, “Polarisation behavior of Al-Zn-Ga alloy in chloride medium,” J Appl Electrochem (2008) pp. 663-668.
15. C. Tuck, J. Hunter, and G. Scamans, "The Electrochemical Behavior of Al-Ga Alloys in Alkaline and Neutral Electrolytes," Journal of the Electrochemical Society, vol. 134, pp. 2970-2981, 1987.
16. E. Aragon, L. Cazenave-Vergez, E. Lanza, A. Giroud, and A. Sebaoun, "Influence of alloying elements on electrochemical behavior of ternary Al-Zn-Ga alloys for sacrificial anodes," British Corrosion Journal, vol. 32, pp. 263-268, 1997.
17. N. Murer and R. G. Buchheit, "Stochastic modeling of pitting corrosion in aluminum alloys," Corrosion Science, vol. 69, pp. 139-148, 2013.
18. Hunter II, “The Anodic Behavior of Aluminum Alloys in Alkaline Electrolytes,” Oxford, England, 1989.
19. D.J. McPhail, "The anodic behavior of aluminum alloys in alkaline solutions," PhD thesis, University of Canterbury, 1993.
20. E. Senel, J.C. Walmsley, S. Diplas, K. Nisancioglu, “Liquid metal embrittlement of aluminum by segregation of trace element gallium,“ Corrosion Science, Volume 85, pp. 167-173, 2014.
21. Keyvani, M. Emamy, M. Saremi, H. Sina, M. Mahta, “Influence of casting temperature on electrochemical behavior of Al-Zn-In sacrificial anodes,” Iran. J. Chem. Chem. Eng., 24. 1-8, 2005.
22. B. Straumal, S. Risser, V. Sursaeva, B. Chenal, W. Gust, “Grain Growth and Grain Boundary Wetting Phase Transitions in the Al-Ga and Al-Sn-Ga Alloys of High Purity,” Journal de Physique IV Colloque, 05 (C7), pp.C7-233-C7-241, 1995.
23. P. Mason, Thermo-Calc Software, http://www.thermocalc.com, 2014.
24. J. L. Murray, “The Al−Ga (Aluminum-Gallium) system,” Bulletin of Alloy Phase Diagrams, 4(2): pp. 183-190, 1983.
25. Gulliver, G.H, “The quantitative effect of rapid cooling upon the constitution of binary alloys,” *J. Inst. Met*, *9*(1), pp. 120-157, 1913.
26. E. Scheil, "Bemerkungen zur schichtkristallbildung," *Zeitschrift für Metallkunde,* (1942), pp. 70-72.
27. Z. Ashitaka, P. Skeldon, G. E. Thompson, K. Shimizu, and H. Habazaki, "Enrichment behavior of gallium in heat and surface treatments of Al–Ga foils," *Corrosion Science,* vol. 44, pp. 2725-2735, 2006.
28. D. O. Flamini, S. B. Saidman, and J. B. Bessone, "Aluminum” activation produced by gallium," *Corrosion Science,* vol. 48, 2006, pp. 1413-1425.
29. ASTM D1141-98(2013), “Standard Practice for the Preparation of Substitute Ocean Water,” ASTM International, West Conshohocken, PA, www.astm.org, 2013.
30. ASTM E122-17, “Standard Practice for Calculating Sample Size to Estimate, With Specified Precision, the Average for a Characteristic of a Lot or Process,” ASTM International, http://www.astm.org/cgi-bin/resolver.cgi?E122-17, 2017.
31. National Institutes of Health, ImageJ, https://imagej.nih.gov/ij/.
32. National Oceanic and Atmospheric Administration, “Can the ocean freeze,” https://oceanservice.noaa.gov/facts/oceanfreeze.html, August 2018.
33. J. Stangroom, “Binomial test calculator,” https://www.socscistatistics.com/tests/binomial/Default2.aspx, 2018.
34. W. J. Stewart, “Probability, Markov Chains, Queues, and Simulation: the Mathematical basis of performance modeling,” Princeton University press, pp. 115-118, 2011.
35. D. R. Lide, “CRC Handbook of Chemistry and Physics,” (87th ed.), Boca Raton, FL: CRC Press. ISBN 0-8493-0487-3.

Appendixes

Appendix A: Voltage Comparisons

All tests done at a current of 0.62mA on a test area of 1 cm^2

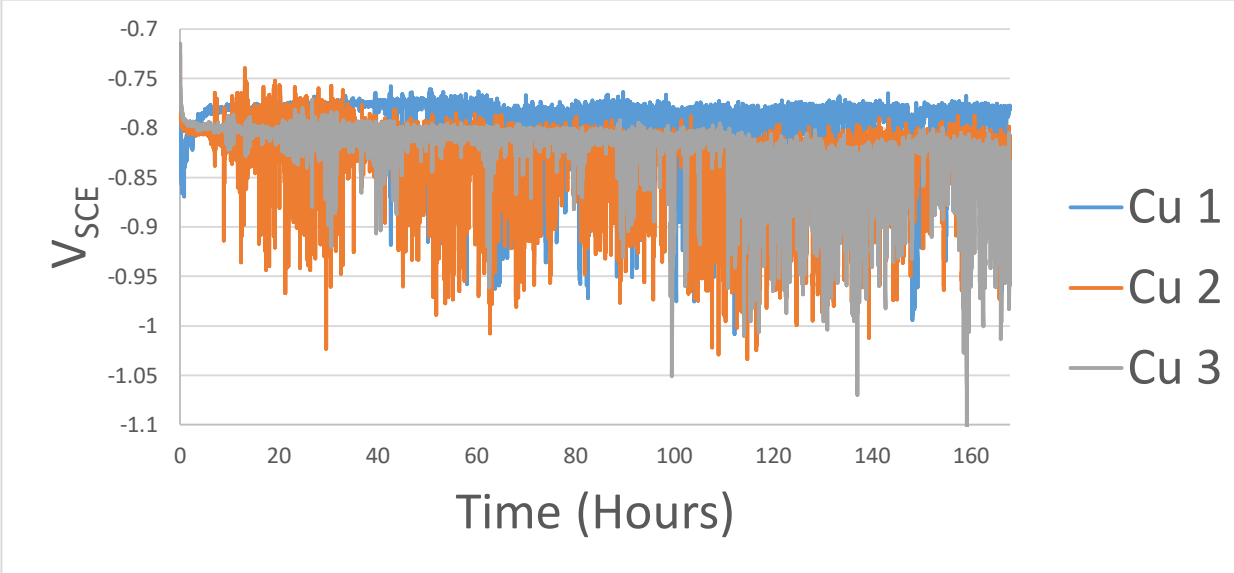

Figure 44: Voltage comparison of the three copper-chilled samples with respect to time. No anneal.

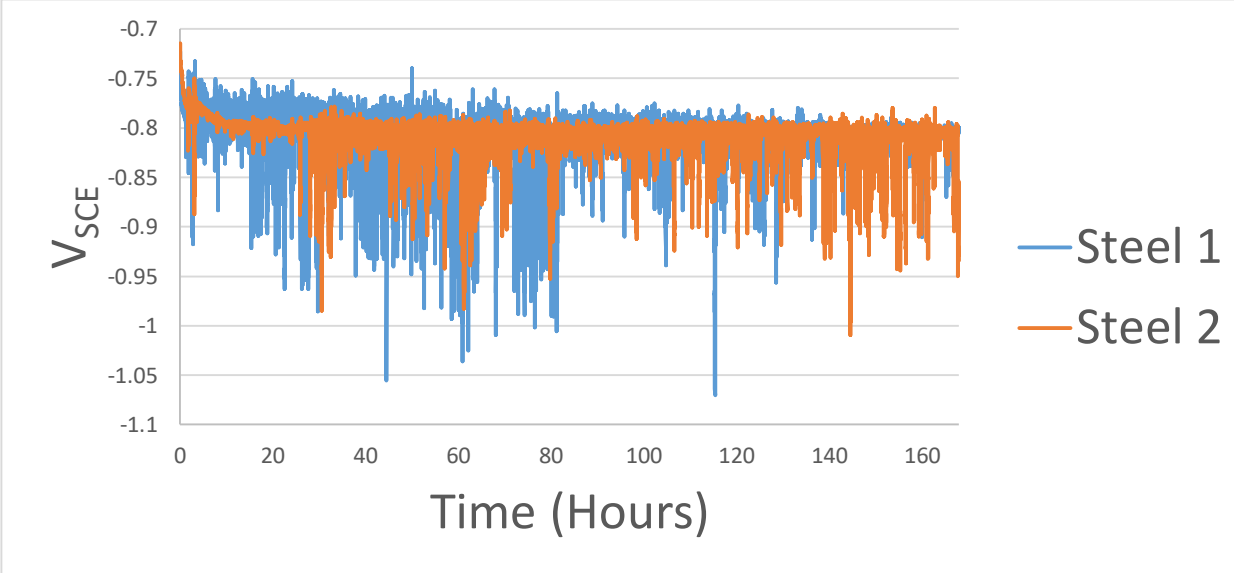

Figure 45: Voltage comparison of the two steel chilled samples with respect to time. The third steel dataset was lost. No anneal.

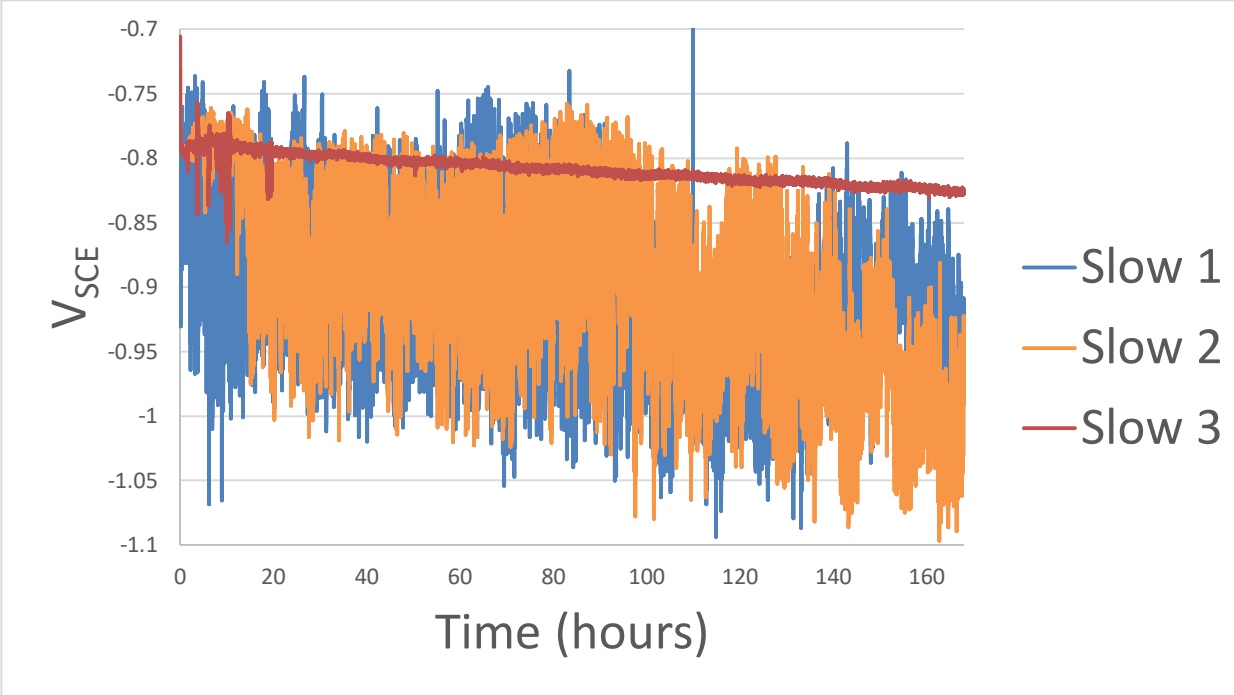

Figure 46: Voltage comparison of the slow cooled samples with respect to time. No anneal.

Appendix B: Spectrography results

Figure 47: Composition of Al 0.1wt% Ga test anodes. Data gathered using an optical emission spectrometer after anodes were cast. Test was performed on a piece of alloy apart from the test samples. The equipment used can only measure gallium concentration up to 0.048%, thus its reading of only 0.048%.

Info:	: Concentrations Created on: 10/7/2016 10:42:41 AM														
ID:	QualityOK:		Quality:		QualityVersion:		SampleNo:	Kidd_Al-Ga_Heat 1							
Symbol:	Si	Fe	Cu	Mn	Mg	Cr	Ni	Zn	Ti	Ag	B	Ba	Be	Bi	Ca
Unit:	%	%	%	%	%	%	%	%	%	%	%	%	%	%	%
9.Measurement:	0.0078	<0.0020	0.0058	<0.0020	0.00064	<0.0020	<0.0020	<0.0020	<0.0010	<0.00050	0.00036	<0.0010	<0.00030	<0.0030	0.0043
10.Measurement:	0.0072	<0.0020	0.005	<0.0020	0.00054	<0.0020	<0.0020	<0.0020	<0.0010	<0.00050	0.00041	<0.0010	<0.00030	<0.0030	<0.00020
11.Measurement:	0.0085	<0.0020	0.0072	<0.0020	0.0007	<0.0020	<0.0020	<0.0020	0.0017	<0.00050	0.00042	<0.0010	<0.00030	<0.0030	0.00076
12.Measurement:	0.0087	<0.0020	0.006	<0.0020	0.00079	<0.0020	<0.0020	<0.0020	<0.0010	<0.00050	0.00052	<0.0010	<0.00030	<0.0030	0.00078
13.Measurement:	0.0091	<0.0020	0.0067	<0.0020	0.00061	<0.0020	<0.0020	<0.0020	<0.0010	<0.00050	0.00063	<0.0010	<0.00030	<0.0030	0.00068
14.Measurement:	0.0082	<0.0020	0.0063	<0.0020	0.00062	<0.0020	<0.0020	<0.0020	<0.0010	<0.00050	0.00049	<0.0010	<0.00030	<0.0030	<0.00020
average:	0.0083	<0.0020	0.0062	<0.0020	0.0007	<0.0020	<0.0020	<0.0020	<0.0010	<0.00050	0.0005	<0.0010	<0.00030	<0.0030	0.0016
Symbol:	Co	Ga	In	Li	Mo	Na	P	Pb	Sn	Sr	V	Zr	Sb	Hg	Al
Unit:	%	%	%	%	%	%	%	%	%	%	%	%	%	%	%
9.Measurement:	<0.0010	>0.048	<0.0020	<0.00002	0.0018	<0.00050	<0.0020	<0.0050	<0.0020	<0.0010	<0.0020	<0.0020	<0.0070	<0.0020	99.89
10.Measurement:	<0.0010	>0.048	<0.0020	<0.00002	0.0013	<0.00050	<0.0020	<0.0050	<0.0020	<0.0010	<0.0020	<0.0020	<0.0070	<0.0020	99.89
11.Measurement:	<0.0010	>0.048	<0.0020	<0.00002	0.0011	<0.00050	<0.0020	<0.0050	<0.0020	<0.0010	<0.0020	<0.0020	<0.0070	<0.0020	99.89
12.Measurement:	<0.0010	>0.048	<0.0020	<0.00002	0.0015	<0.00050	<0.0020	<0.0050	<0.0020	<0.0010	<0.0020	<0.0020	<0.0070	<0.0020	99.89
13.Measurement:	<0.0010	>0.048	<0.0020	<0.00002	0.0019	<0.00050	<0.0020	<0.0050	<0.0020	<0.0010	<0.0020	<0.0020	<0.0070	<0.0020	99.89
14.Measurement:	<0.0010	>0.048	<0.0020	<0.00002	0.0024	<0.00050	<0.0020	<0.0050	<0.0020	<0.0010	<0.0020	<0.0020	<0.0070	<0.0020	99.89
average:	<0.0010	>0.048	<0.0020	<0.00002	0.0017	<0.00050	<0.0020	<0.0050	<0.0020	<0.0010	<0.0020	<0.0020	<0.0070	<0.0020	99.89

Appendix C: Gallium Test Results

NSL ANALYTICAL

TEST REPORT

THE REPORTED TEST RESULTS RELATE ONLY TO THE ITEM(S) TESTED

ANAB ACCREDITED

Virginia Tech
445 Old Turner Street, 213 Holden Hall
Blacksburg, VA 24060
ATTN: Alan Druschitz

Request ID: R-20171113-058
Date: 11/16/2017
PO Number: P3284086

Client Description Aluminum Alloy

Page 1 of 1

Sample No. S-171113-105 Customer ID: N/A

Tests	Results/Units	Method
Ga	0.092 %	ICP-MS

Methods noted with an * fall outside of NSL's ISO 17025 Scope of Accreditation.

Definitions: NC - Nonconforming value, Min - Minimum, Max - Maximum. All quantitative analytical results are subject to variability due to the nature of testing. Estimated Uncertainty data is available upon request

Reporting Officer :

Lisa Simko, Technical Specialist

These results relate only to the items tested and this report shall not be reproduced, except in full, without the written consent of NSL Analytical Services, Inc.
The recording of false, fictitious, or fraudulent statements or entries on this document may be punished as a felony under the federal statutes, including Federal Law, Title 18, Chapter47.

NSL Analytical Services
4450 Cranwood Parkway
Cleveland, Ohio 44128

For current Terms and Conditions, please visit http://nslanalytical.com/terms-and-conditions

Figure 48: Commercial test results of gallium content of the Al-Ga alloy.

Appendix D: Raw Voltage Data for Galvanostatic Tests

All tests done at a current of 0.62mA on a test area of 1 cm^2

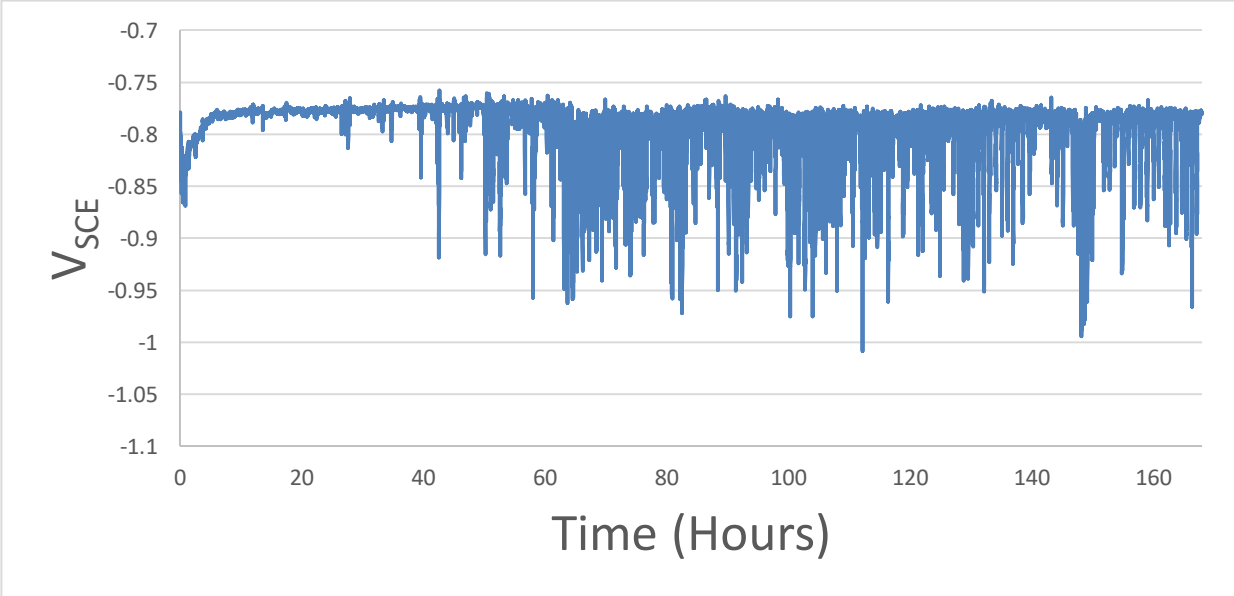

Figure 49: Voltage behavior of copper chilled sample, Cu BR2. Mass loss not recorded.

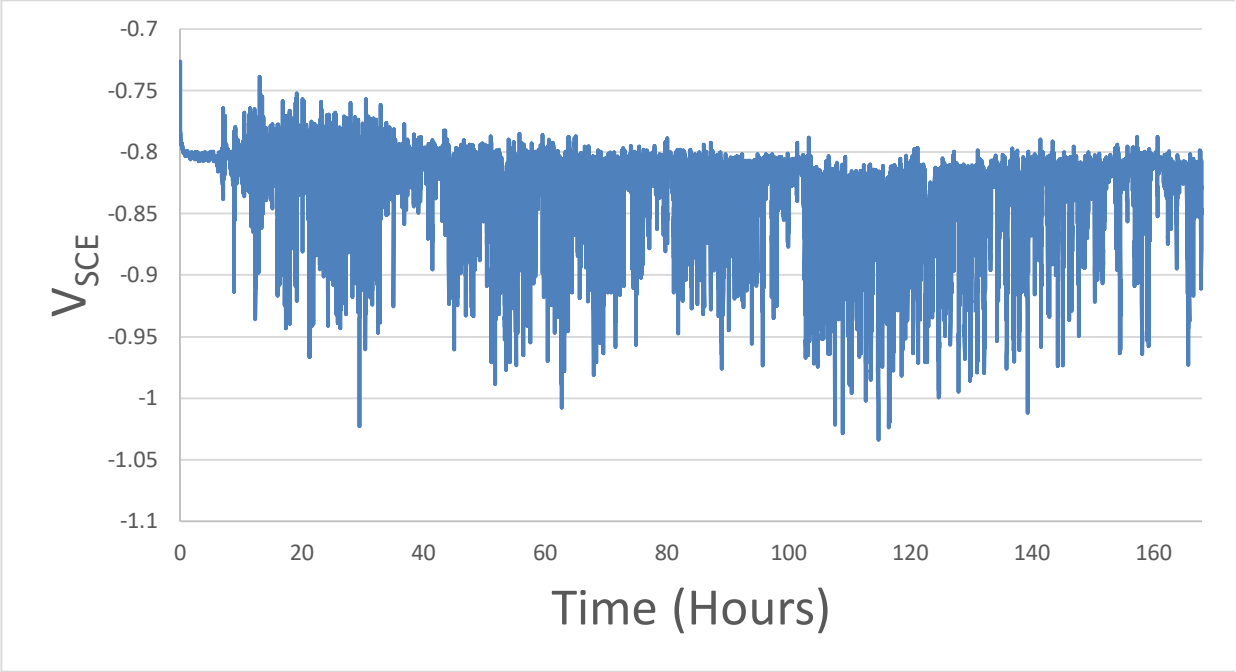

Figure 50: Voltage behavior of copper chilled Sample, Cu UL1. Mass loss: 0.035g

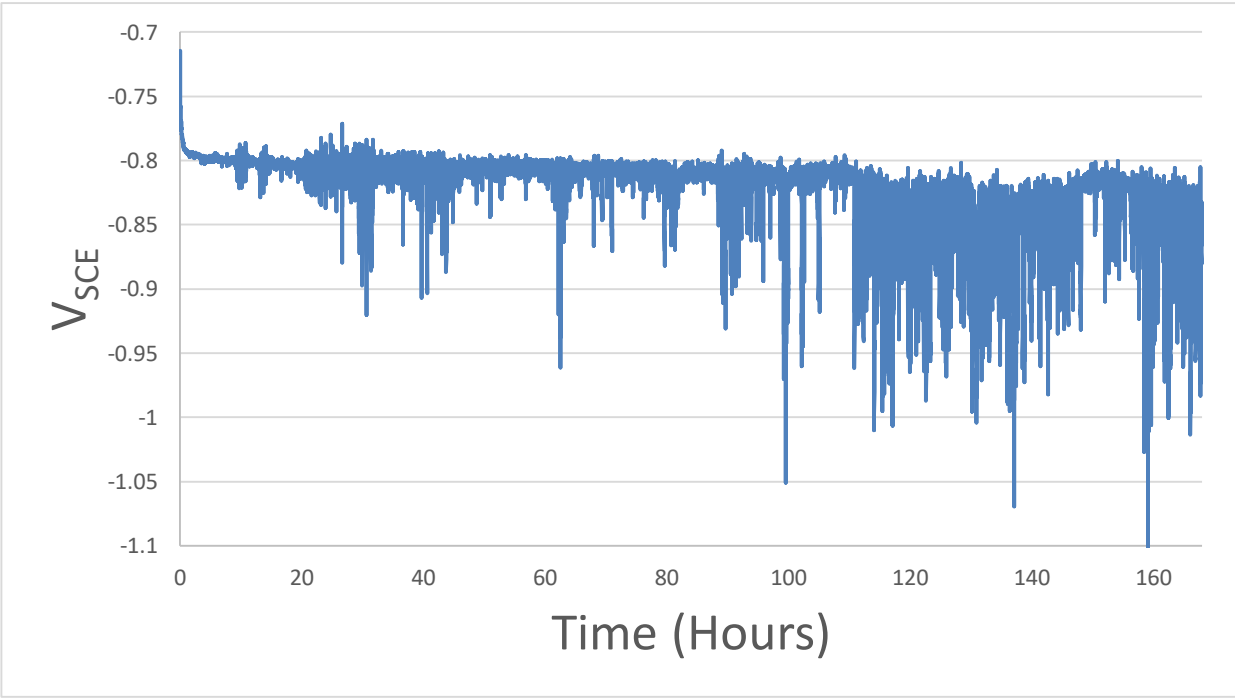

Figure 51: Voltage behavior of copper chilled sample, CU BL1. Mass loss 0.039g

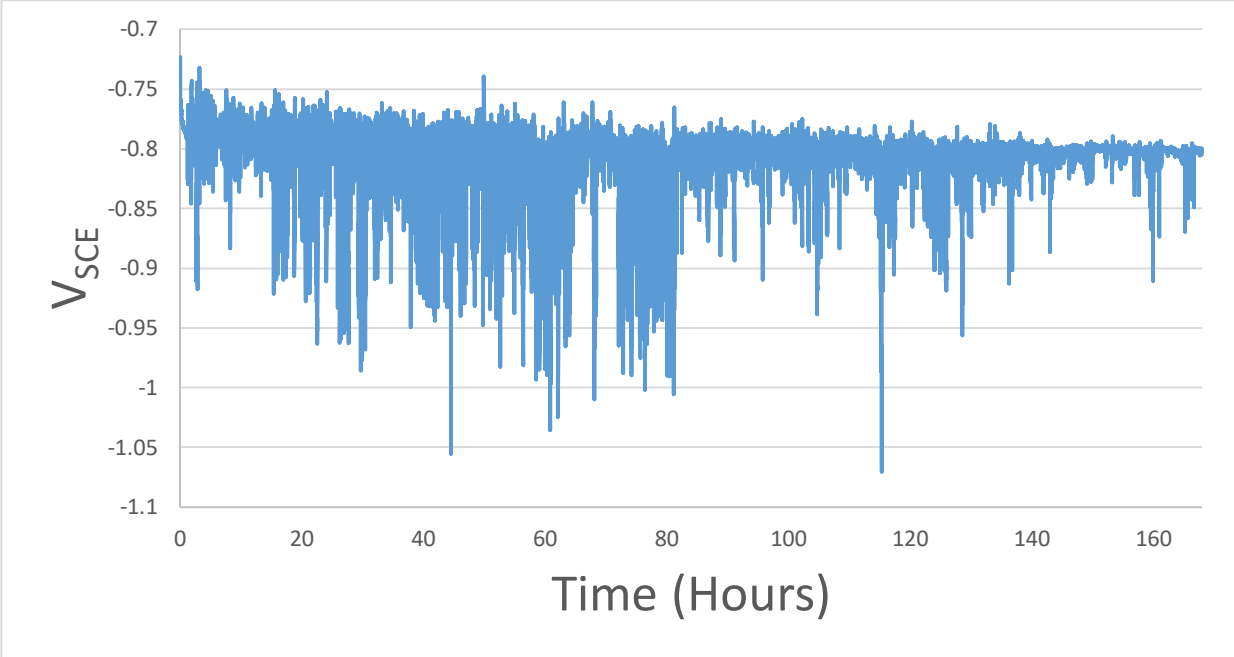

Figure 52: Voltage behavior of steel chilled sample, Steel BR2. Mass loss not recorded.

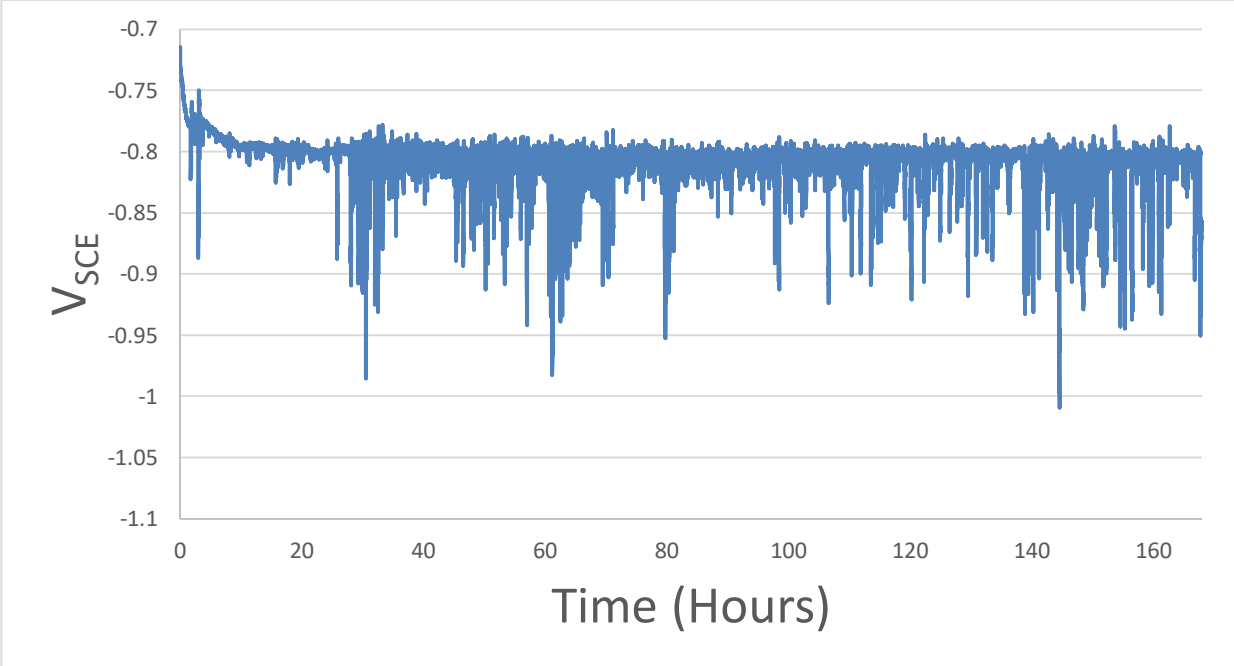

Figure 53: Voltage behavior of steel chilled sample, Steel UL1. Mass loss: 0.038g

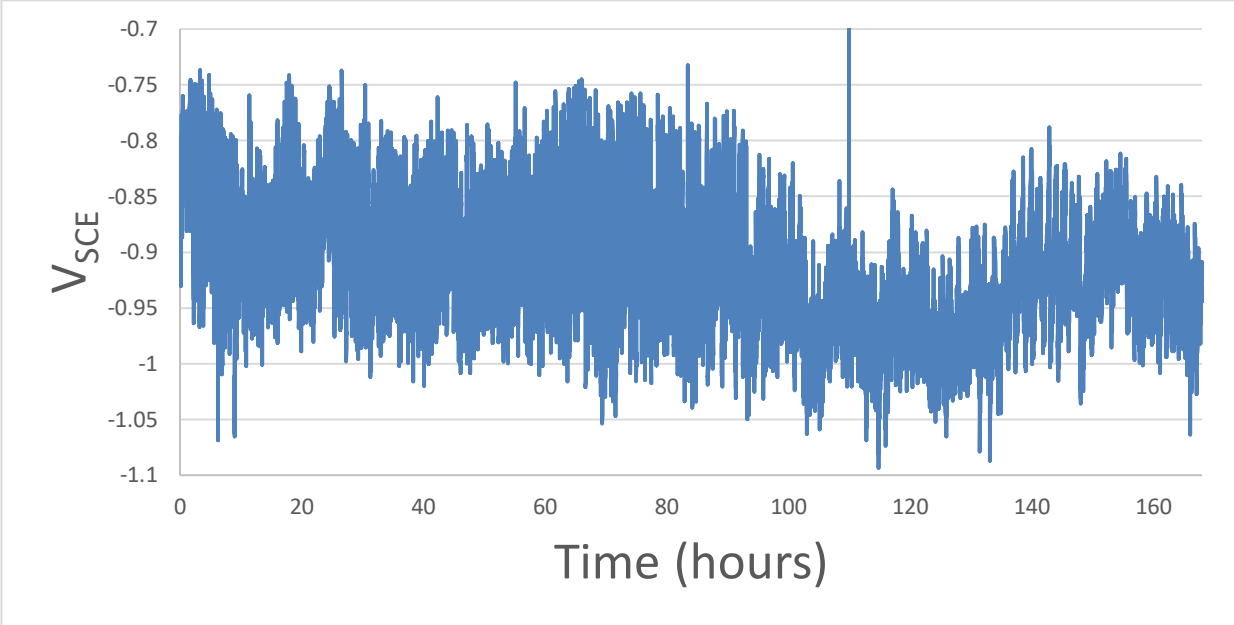

Figure 54: Voltage behavior of slow cooled sample, Air BL2. Mass loss not recorded.

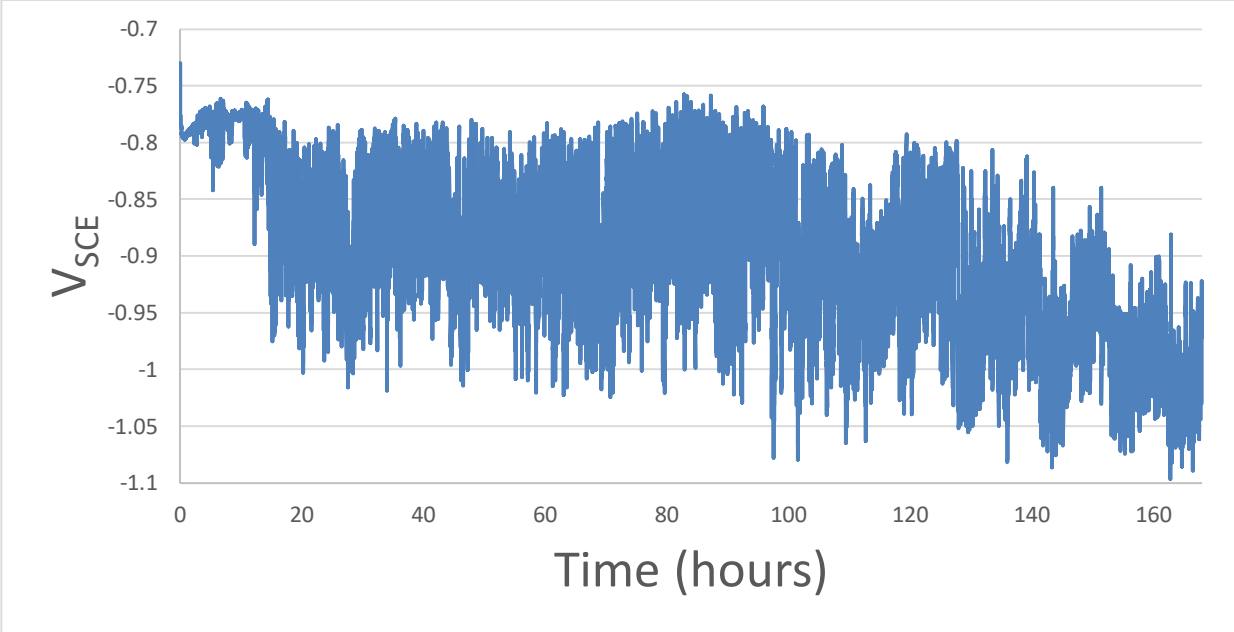

Figure 55: Voltage behavior of slow cooled sample, Air UR1. Mass loss: 0.034g

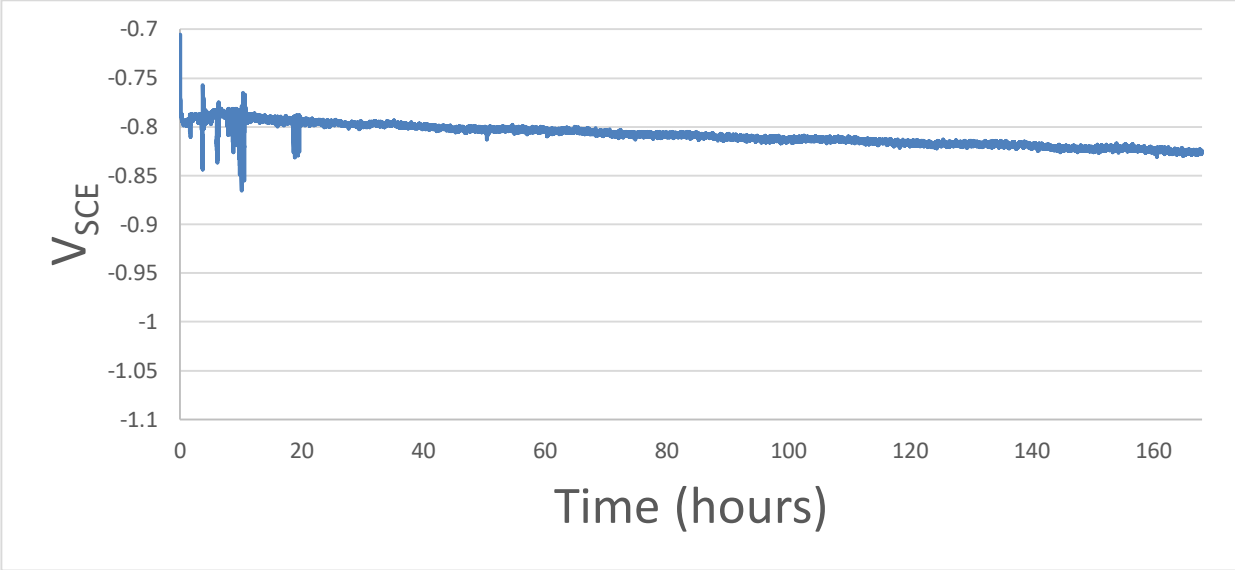

Figure 56: Voltage behavior of slow cooled sample, Air BL1. Mass loss: 0.039g

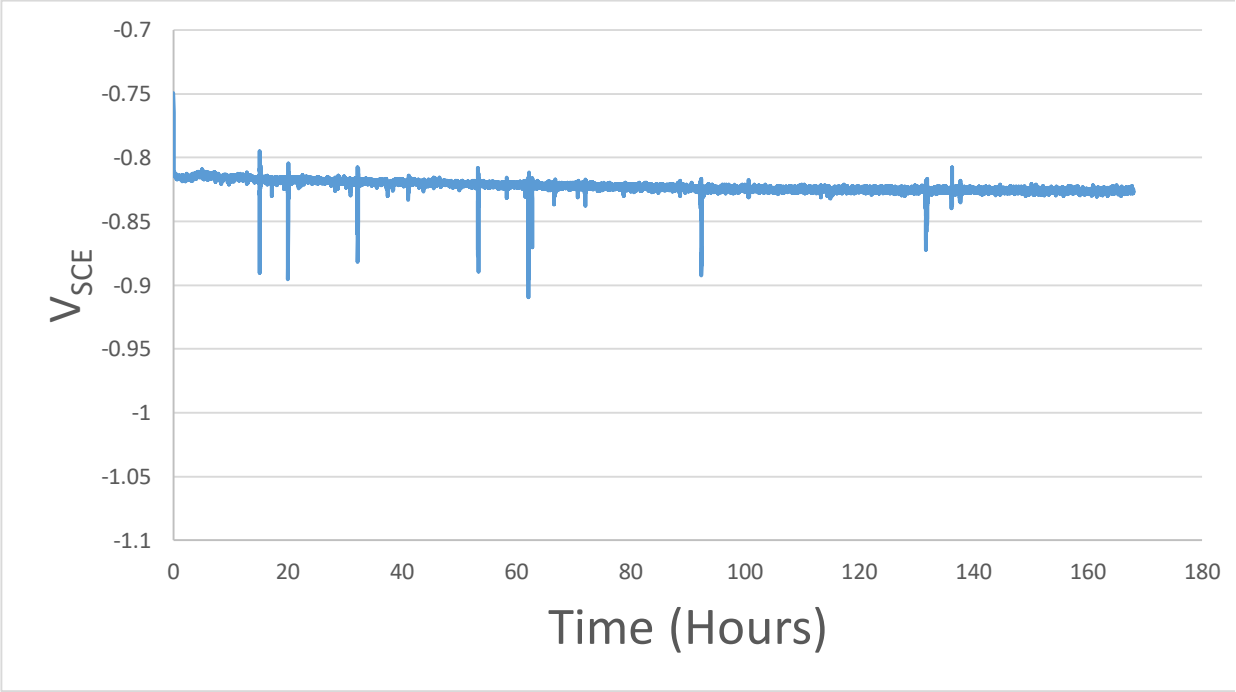

Figure 57: Voltage behavior of copper chilled and annealed sample, Cu UL2. Mass loss 0.038g

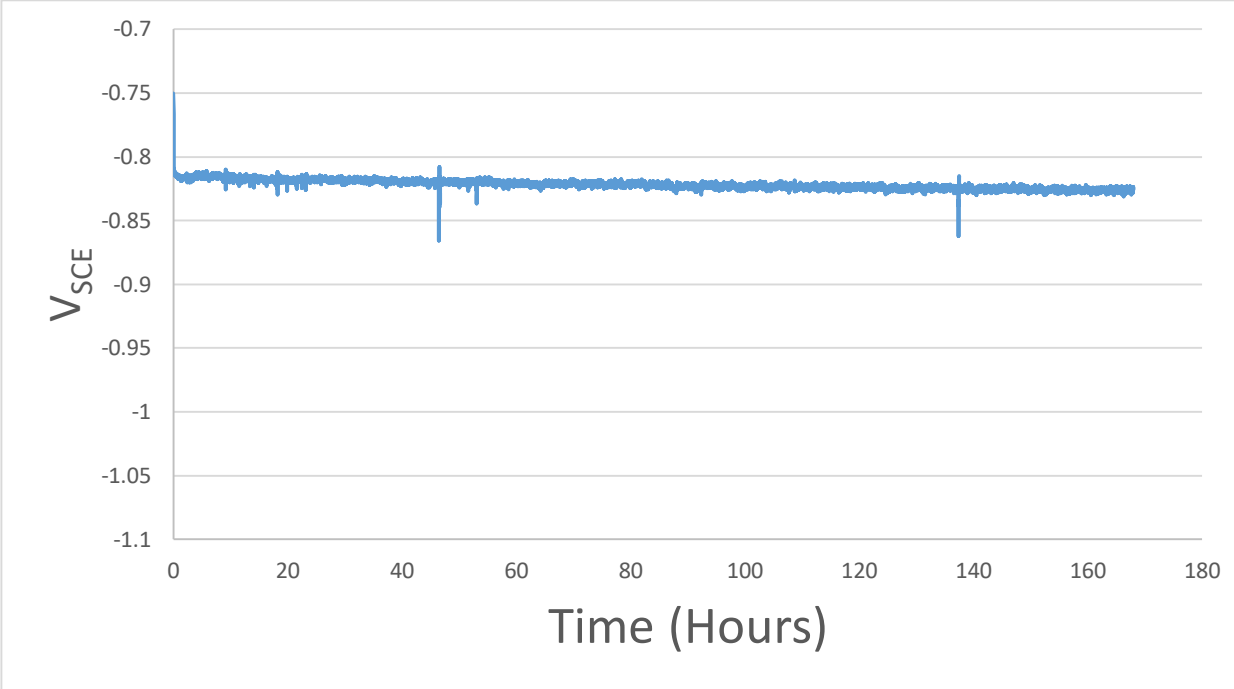

Figure 58: Voltage behavior of copper chilled and annealed sample, Copper CENT1. Mass loss 0.032g

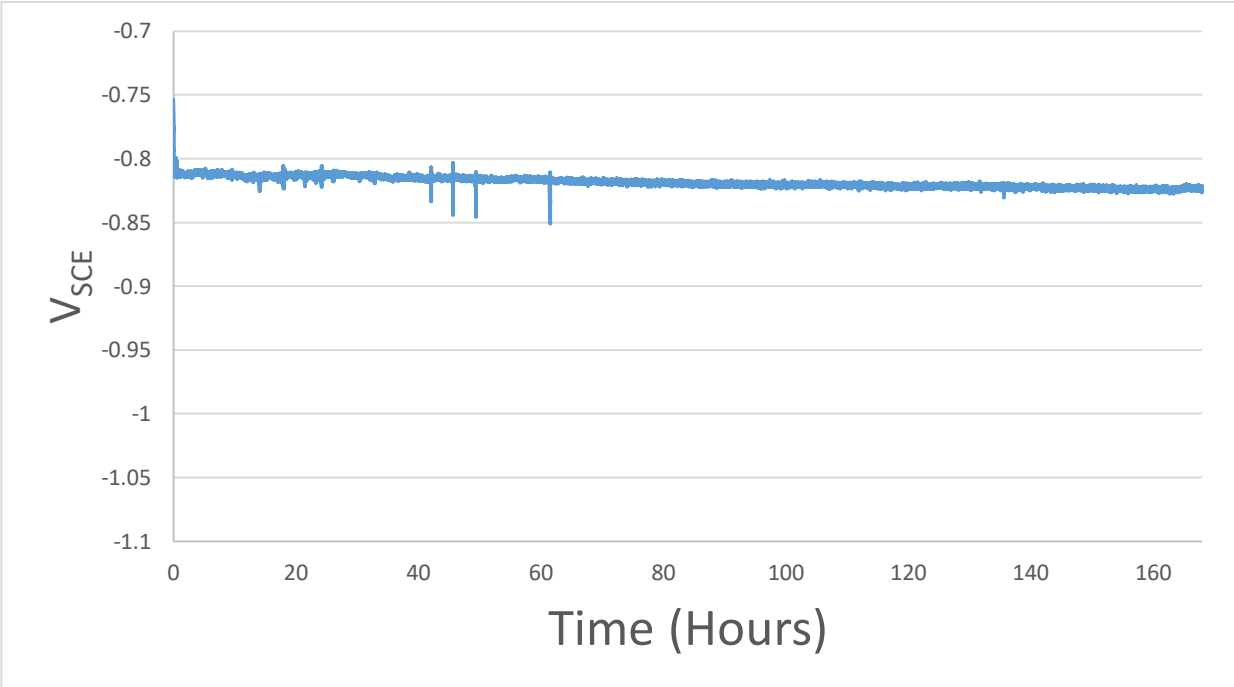

Figure 59: Voltage behavior of copper chilled and annealed sample, Cu BR1. Mass loss 0.033g

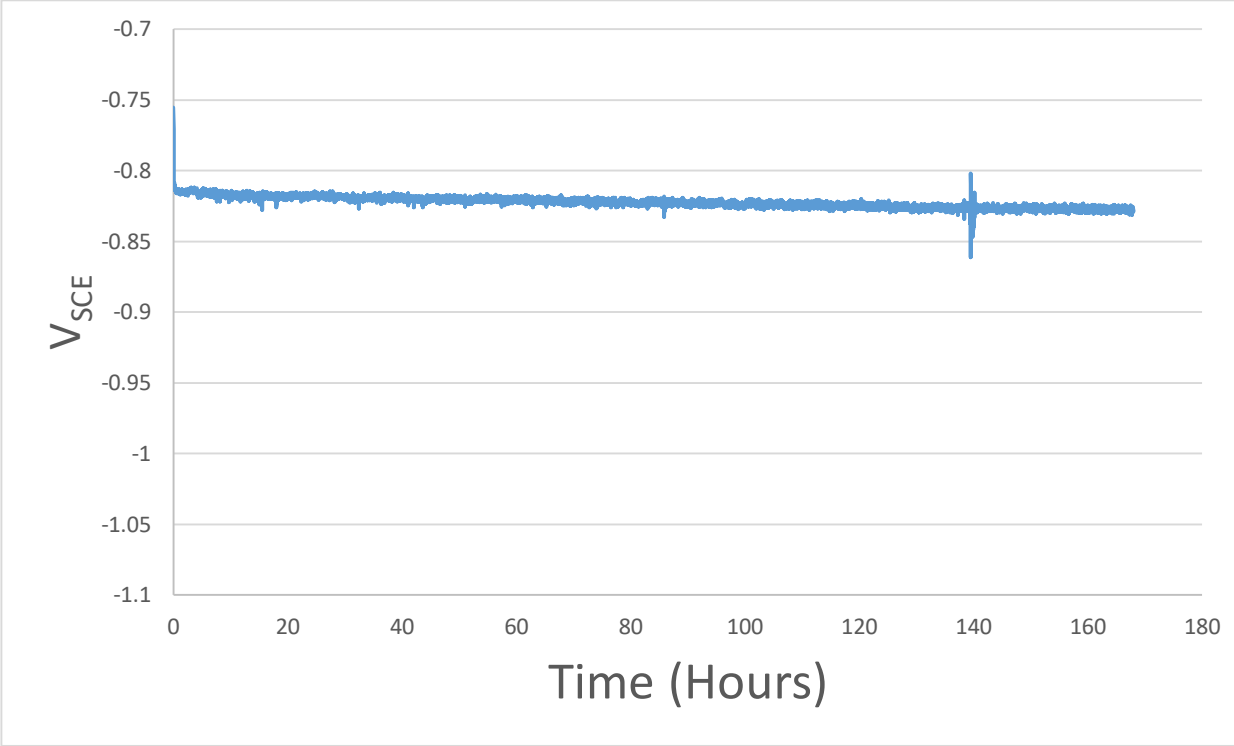

Figure 60: Voltage behavior of steel chilled and annealed sample, Steel UL2. Mass loss 0.032g

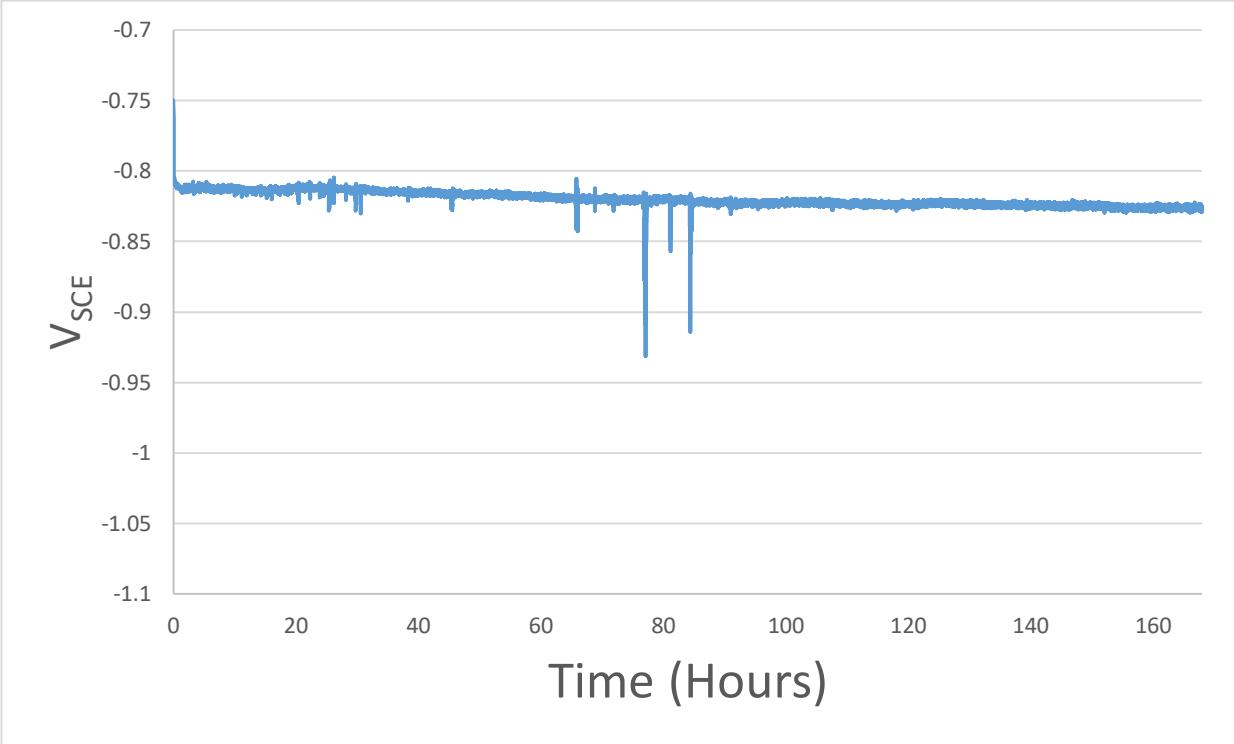

Figure 61: Voltage behavior of steel chilled and annealed sample, Steel UR2. Mass Loss: 0.038g

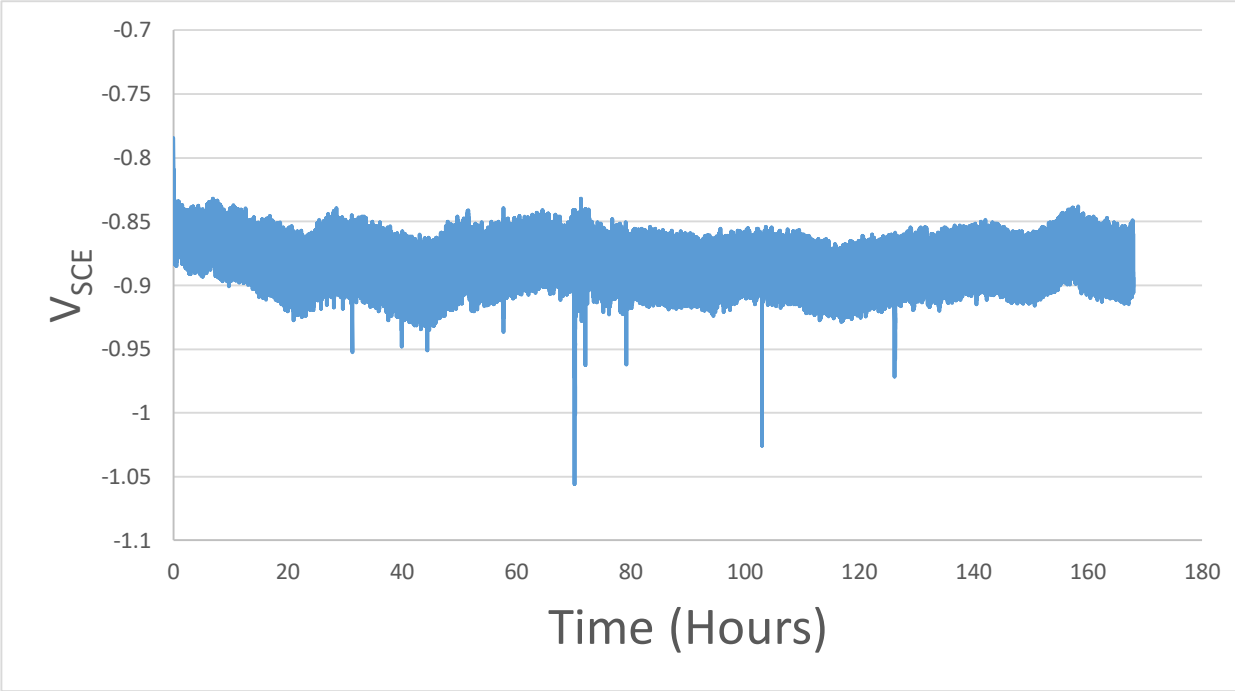

Figure 62: Voltage behavior of slow cooled and annealed sample, Air UL1. Mass loss: 0.038g

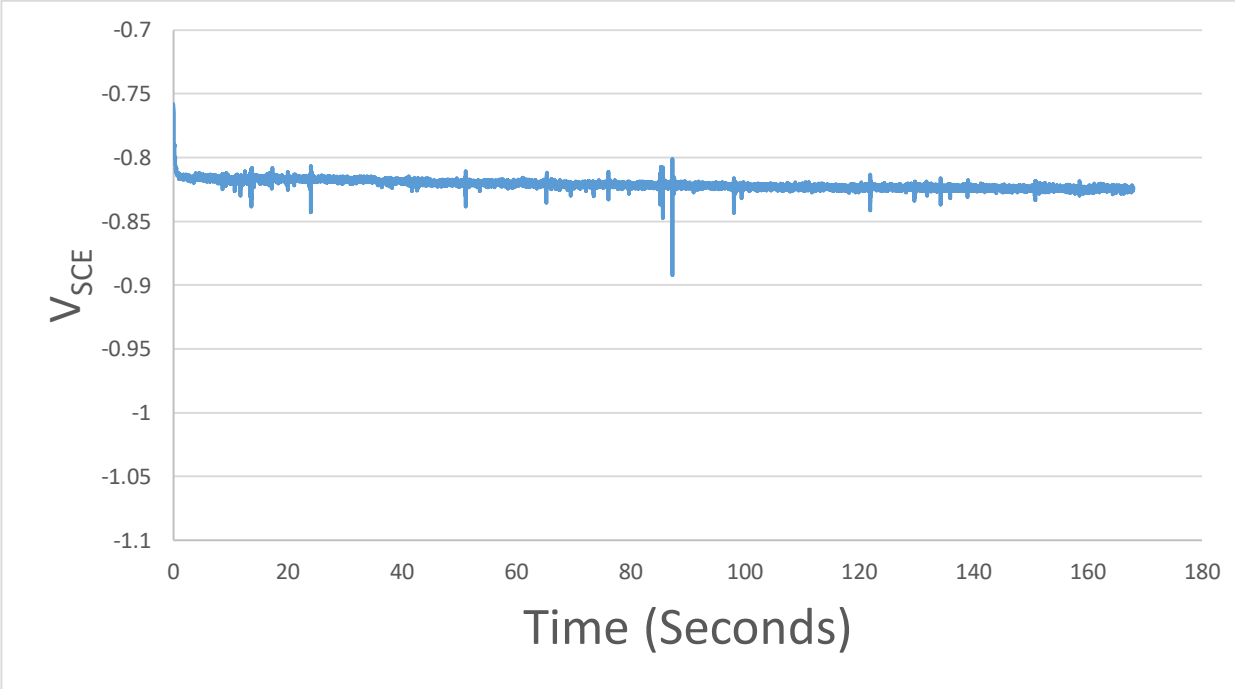

Figure 63: Voltage behavior of slow cooled and annealed sample, Air UL2, Mass loss 0.034g

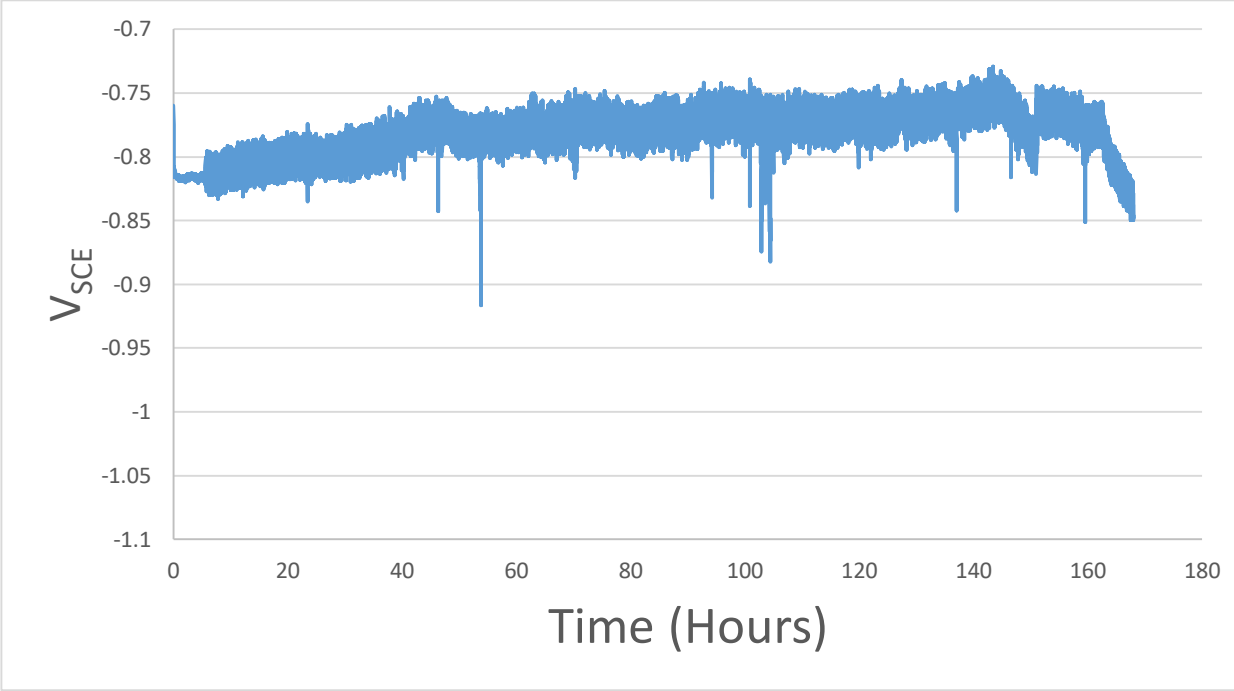

Figure 64: Voltage behavior of slow cooled and annealed sample, Air CENT1. Mass loss: 0.035g

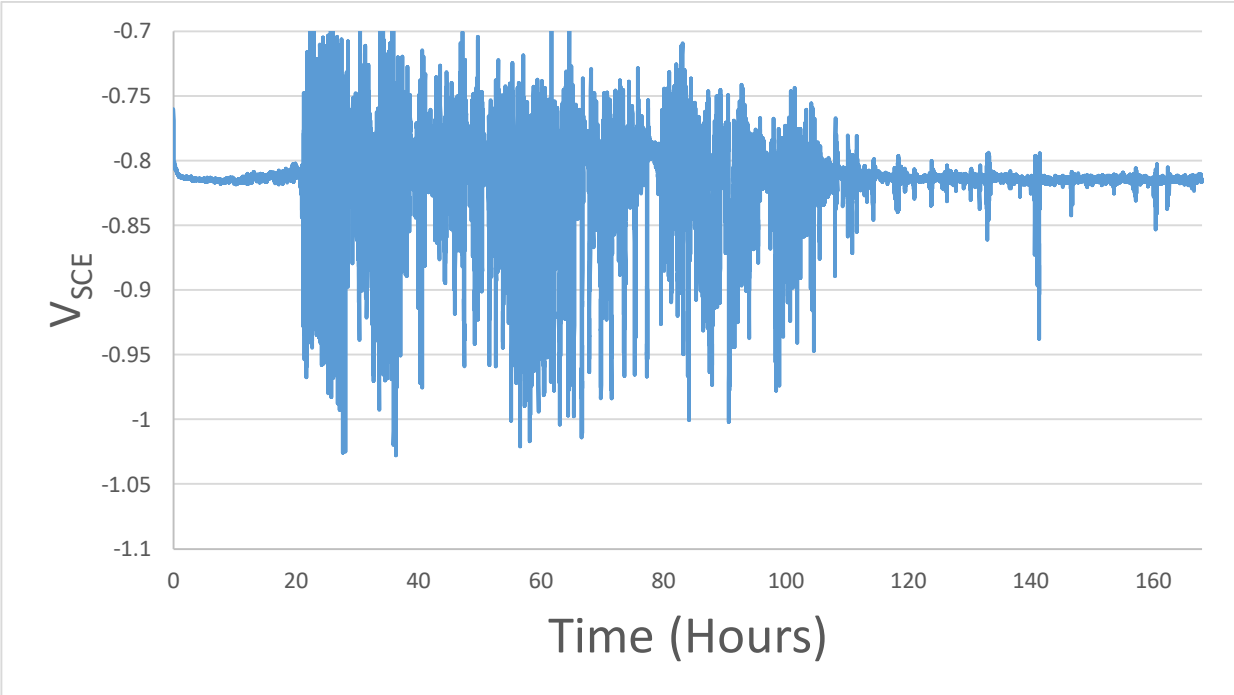

Figure 65: Voltage behavior of copper chilled, annealed, and ice tested sample. CU BM1. Mass loss: 0.034g

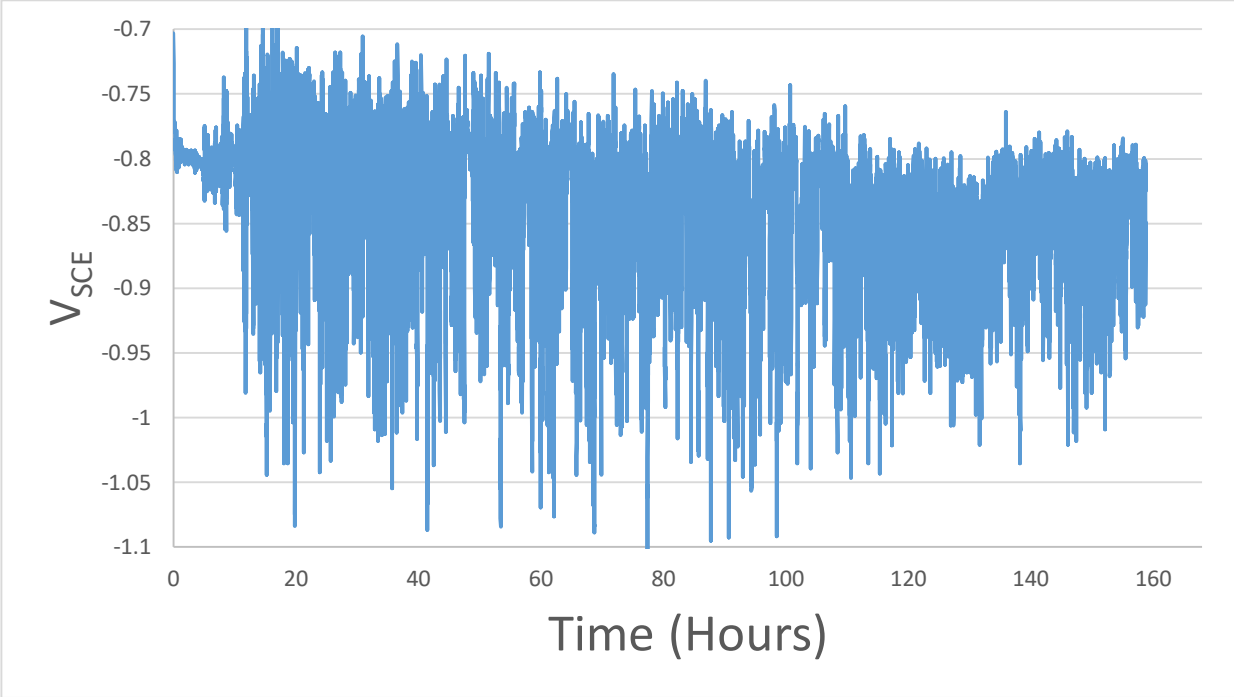

Figure 66: Voltage behavior of steel chilled, annealed, and ice tested sample, Steel UR1. Mass loss: 0.032g

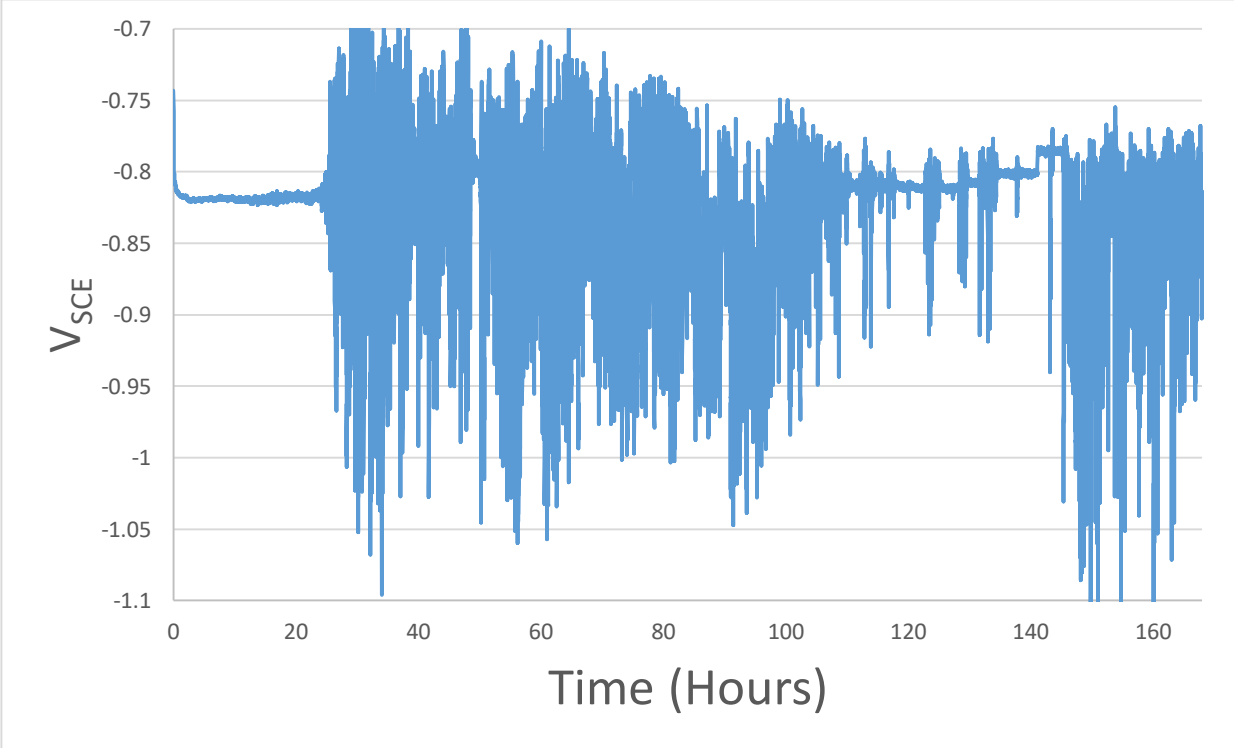

Figure 67: Voltage behavior of steel chilled, annealed, and ice tested sample, Steel UM1. Mass loss not recorded.

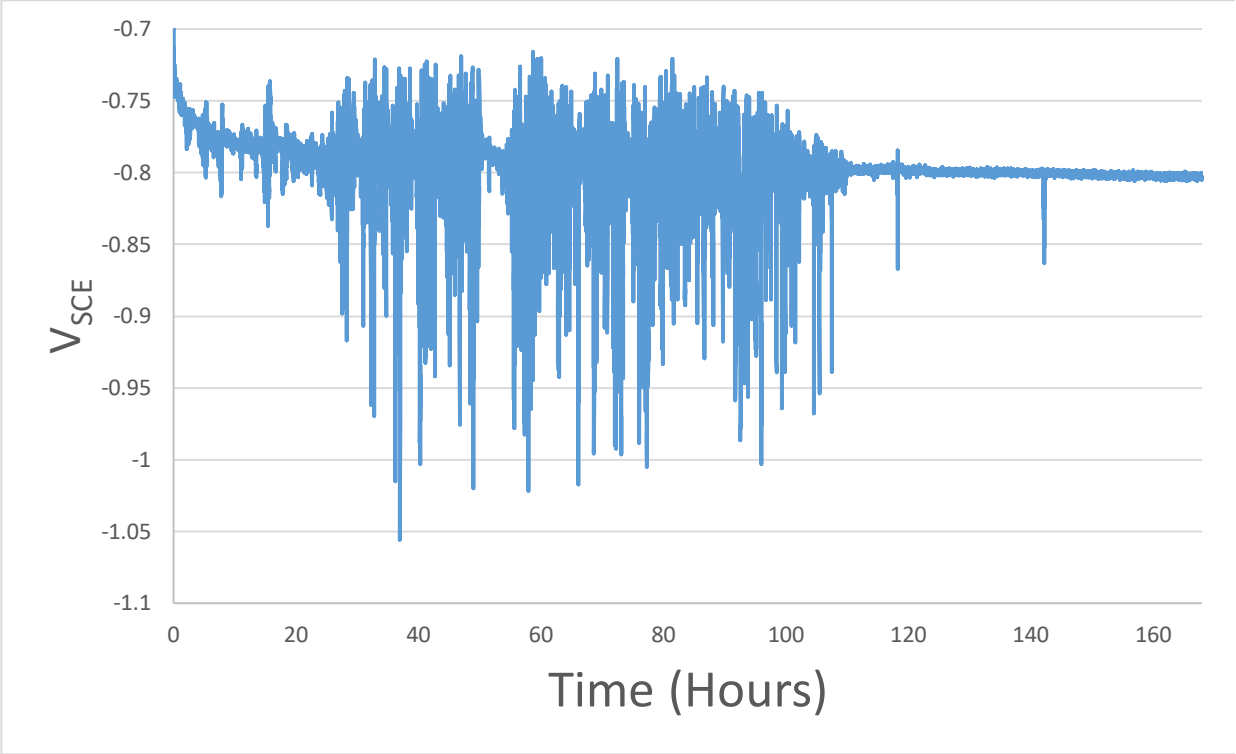

Figure 68: Voltage behavior of steel chilled, annealed, and ice tested sample, Steel BM2. Mass loss: 0.35g

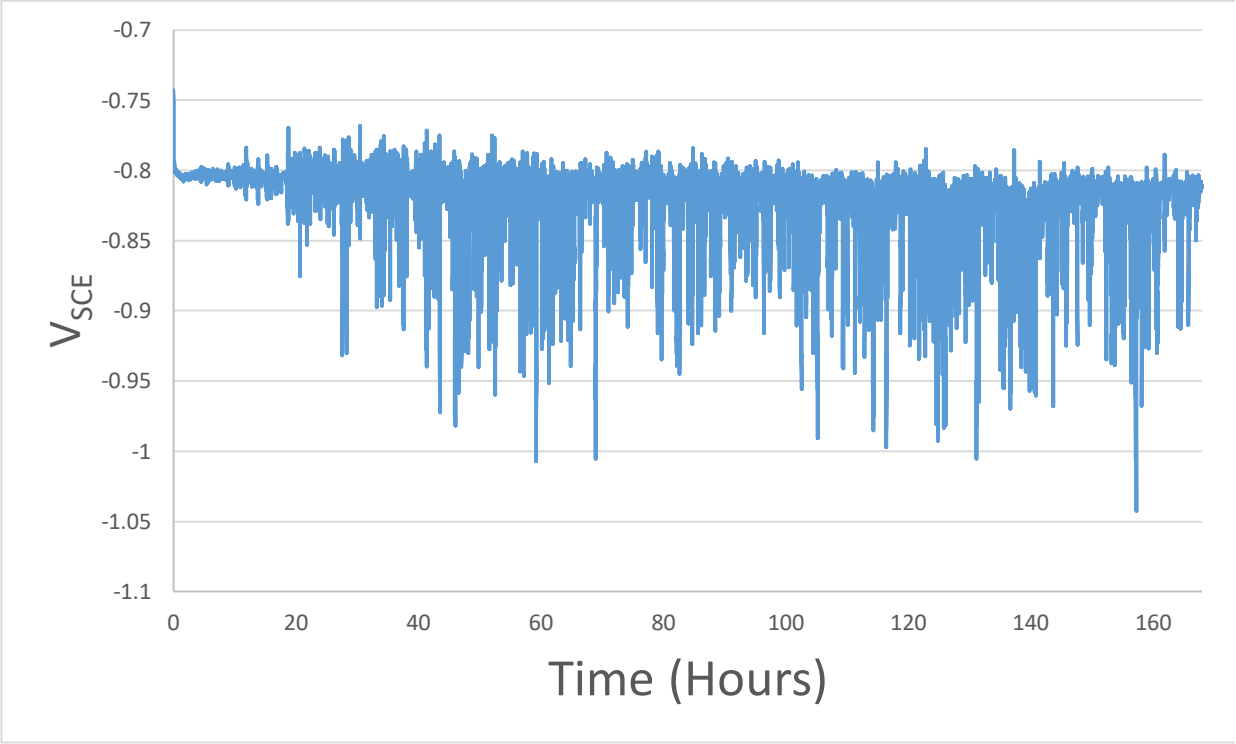

Figure 69: Voltage behavior of 500°C anneal temperature test, Cu UM2. Mass loss: 0.045g

Appendix E: Pictures of Corroded Samples

All pictures are of an area with length and width of 2.2 cm.

Figure 70: Picture of corroded surface of copper chilled sample, Cu BR2. Mass loss not recorded.

Figure 71: Picture of corroded surface of copper chilled sample, Cu UL1. Mass loss: 0.035g

Figure 72: Picture of corroded surface of copper chilled sample, CU BL1. Mass loss: 0.039g

Figure 73: Picture of corroded surface of steel chilled sample, Steel BR2. Mass loss not recorded.

Figure 74: Picture of corroded surface of steel chilled sample, Steel UL1. Mass loss: 0.038g

Figure 75: Picture of corroded surface of steel chilled sample, Steel BR1. Mass loss: 0.040g. Galvanostatic corrosion data lost.

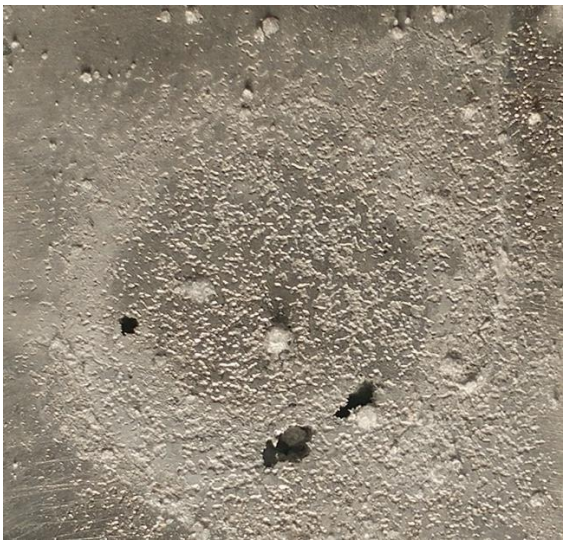

Figure 76: Picture of corroded surface of slow cooled sample, Air BL2. Mass loss not recorded.

Figure 77: Picture of corroded surface of slow cooled sample, Air UR1. Mass loss: 0.034g

Figure 78: Picture of corroded surface of slow cooled sample, Air BL1. Mass loss: 0.039g

Figure 79: Picture of corroded surface of copper chilled and annealed sample, Cu UL2. Mass loss: 0.038g

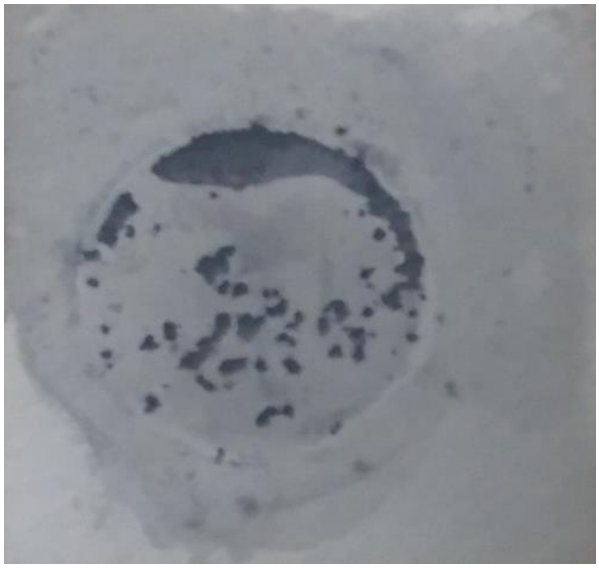

Figure 80: Picture of corroded surface of copper chilled and annealed sample, Copper CENT1. Mass loss: 0.032g

Figure 81: Picture of corroded surface of copper chilled and annealed sample, Cu BR1. Mass loss: 0.033g

Figure 82: Picture of corroded surface of steel chilled and annealed sample, Steel CENT2, unknown testing failure. Test stopped from circuit overload. Mass loss not recorded. Sample gathered iron rust from testing equipment seen in Figure 83.

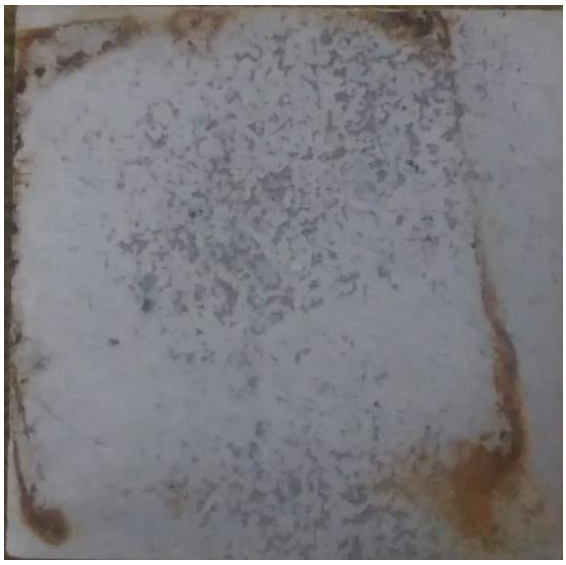

Figure 83: Picture of back of steel chilled and annealed sample, Steel CENT2. Iron rust from testing equipment visible.

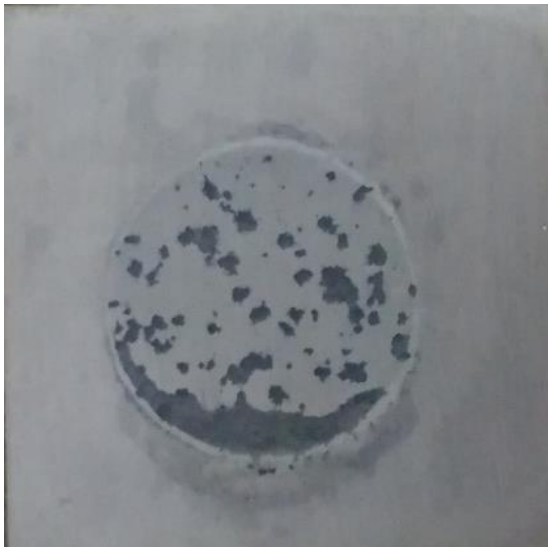

Figure 84: Picture of corroded surface of second steel chilled and annealed sample, Steel UL2. Mass loss: 0.032g

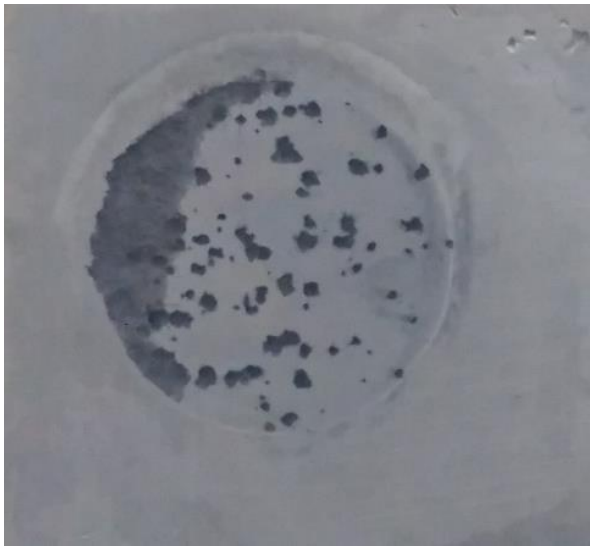

Figure 85: Picture of corroded surface of third steel chilled and annealed sample, Steel UR2. Mass Loss: 0.038g

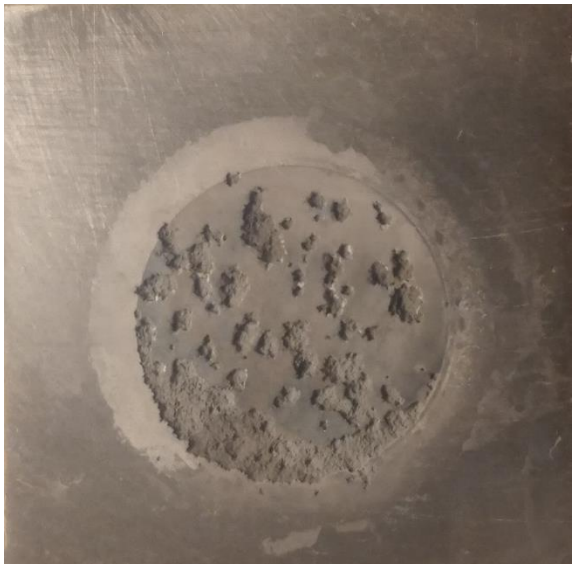

Figure 86: Picture of corroded surface of slow cooled and annealed sample, Air UL1. Mass loss: 0.038g

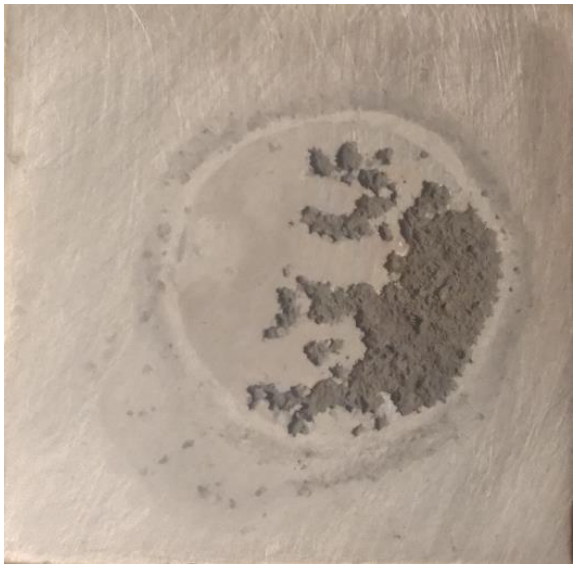

Figure 87: Picture of corroded surface of slow cooled and annealed sample, Air UL2, Mass loss: 0.034g

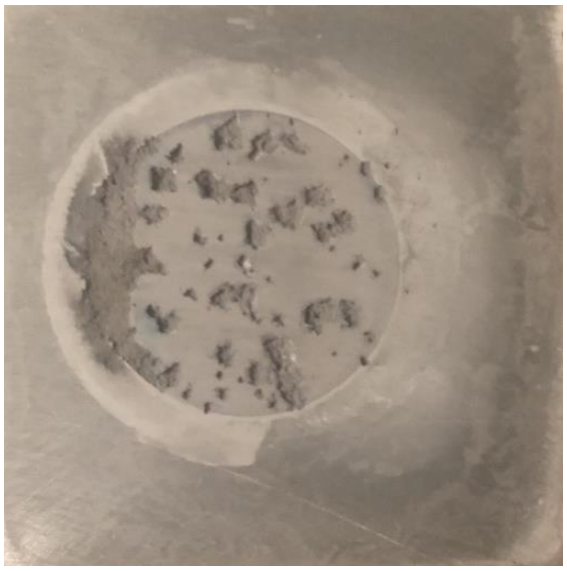

Figure 88: Picture of corroded surface of slow cooled and annealed sample, Air CENT1. Mass loss: 0.035g

Figure 89: Picture of corroded surface of copper chilled, annealed, and ice tested sample, Cu UL1. Mass loss: 0.029g. Unknown test failure, suspected contaminate buildup on platinum electrode from different set of experiments.

Figure 90: Picture of corroded surface of copper chilled, and ice tested sample. Cu BM1. Mass loss 0.034g

Figure 91: Picture of corroded surface of steel chilled, annealed, and ice tested sample, Steel UR1. Mass loss: 0.032g

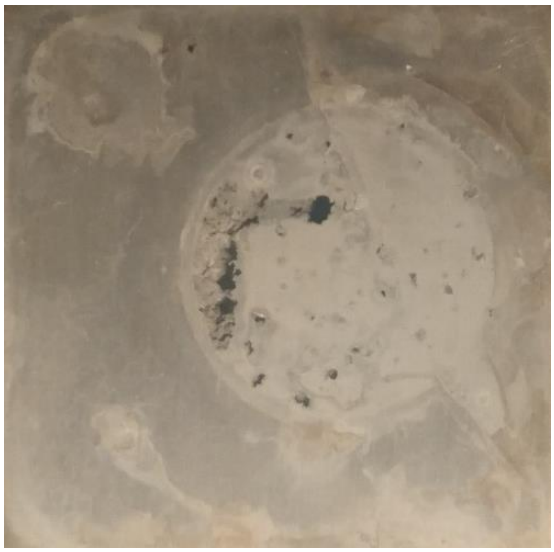

Figure 92: Picture of corroded surface of steel chilled, annealed, and ice tested sample, Steel UM1. Mass loss not recorded.

Figure 93: Picture of corroded surface of steel chilled, annealed and ice tested sample, Steel BM2. Mass loss: 0.35g

Figure 94: Picture of corroded surface of the 500^{o}C anneal temperature test, Cu UM2 Mass loss: 0.045g

Appendix F: Pictures of Etched Samples

All pictures are of an area with length and width of 2.2 cm.

Figure 95: Picture of front of etched copper chilled sample, Cu Cent2.

Figure 96: Picture of back of etched copper chilled sample, Cu Cent2.

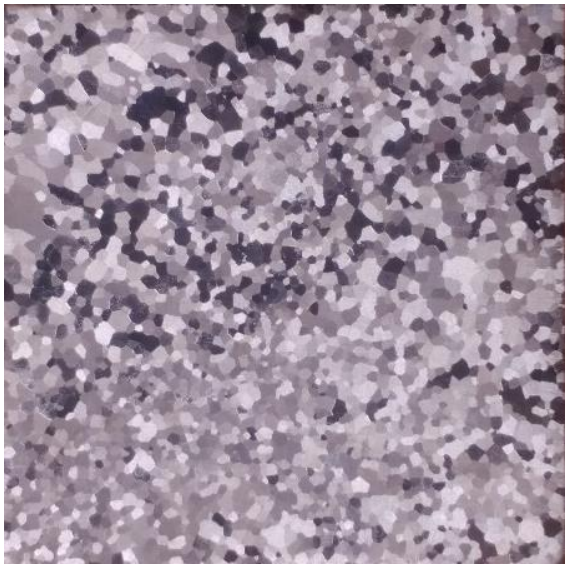

Figure 97: Picture of front of etched steel chilled sample, Steel Cent2.

Figure 98: Picture of back of etched steel chilled sample, Steel Cent2.

Figure 99: Picture of front of etched slow cooled sample, Air Cent2.

Figure 100: Picture of back of etched slow cooled sample, Air Cent2.

Figure 101: Picture of front of etched and annealed copper chilled sample, Cu ML1.

Figure 102: Picture of back of etched and annealed copper chilled sample, Cu ML1.

Figure 103: Picture of front of etched and annealed steel chilled sample, Steel ML2.

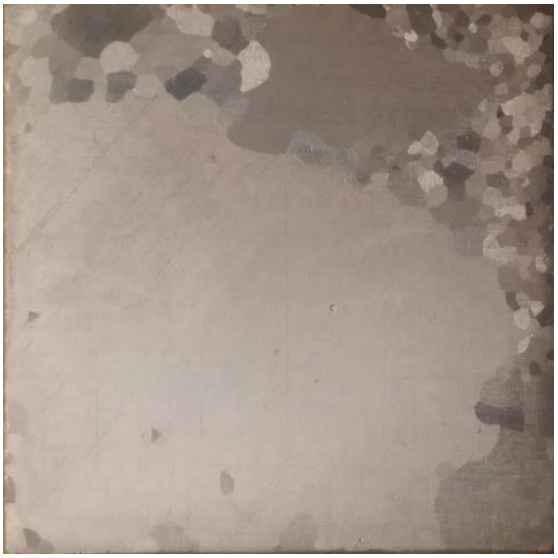

Figure 104: Picture of back of etched and annealed steel chilled sample, Steel ML2.

Figure 105: Picture of front of etched and annealed slow cooled sample, Air MR2. This sample did not etch properly, so the grains are difficult to see.

Figure 106: Picture of back of etched and annealed slow cooled sample, Air MR2. This side etched better, but the grains still have less contrast than they should.

Appendix G: Example Thermo-Calc Programs

Aging of gallium segregation program

@@This program simulates Al-Ga diffusion at low temperatures and long times.

```
go da
switch
TCAl4
def-spec Al Ga
rej ph *
res ph liq fcc_l12
get
app
MOBAL3
def-spec Al Ga
rej ph *
res ph liq fcc_l12
get
go d-m
set-cond
GLOBAL
T
0
450

N
enter-region alga
enter-grid
ALGA
50e-6
LINEAR
80
enter-phase
ACTIVE
ALGA
MATRIX
fcc_l12
```

enter-comp
ALGA
FCC_L12
al
weight_per
GA
func
0.1+0.05*erf(2000000*(x-.000025)/25);
set-sim-t
3.154e7
YES
3154000
1E-07
1E-07
s-s-c
0
1
2
NO
pot
YES
YES
.5
2
NO
YES
NO
save
sim
post
s-d-a y w-p Ga
s-d-a x dis glob
s-p-c time
0,1000,100000,3e7
Plot

Gallium solubility program

@@ This program calculates the solubility limit of gallium in Aluminum at 298K

go da
switch tcal
d-s al ga
define-sys al ga

```
get
go poly
set-cond
T = 298 p = 100000 n = 1
change-sta
PHASES
ort
fixed
0
comp-eq
li-eq
SCREEN
VWCS
exit
```

Steady cooling rate solidification

@@ This program assumes a 0.5^{o} steady-state cooling rate and simulates a 0.1mm diameter grain

```
go da
switch
TCAl4
def-spec Al Ga
rej ph *
res ph liq fcc_l12
get
app
MOBAL3
def-sys Al Ga
rej ph *
res ph liq Fcc_l12
get
go d-m
set-cond
glob
T
0
1500-0.5*TIME;
*
N
enter-region alga
```

enter-grid
ALGA
50e-6
geo
80
1.1
enter-phase
ACTIVE
ALGA
matrix
liq
enter-phase
inact
ALGA
no
fcc_l12
Al
1E-05
CLOSED_SYSTEM
enter-composition
ALGA
liq
al
w-p
Ga lin .1 .1
set-sim-time
1800
YES
10
1E-07
1E-07
s-s-c
0
1
2
yes
pot
YES
YES
.5
1.5
NO

```
YES
NO
save
sim



post

s-d-a y w-p Ga
s-d-a x dis glob
s-p-c time


plot


set-title AL-GA 0.5 percent
enter-function fs=1-iww(liq);
enter function fs=1-iww(liq);
s-d-a x fs
set-axis-text
x
n
Fraction Solid
s-d-a y t-c
s-p-c
interface
alga
Upper
s-s-s x n 0 1
s-s-s y m 620 680
plot
select_plot
2
s-d-a y w-p Ga
s-d-a x dis glob
s-p-c time
1125,1130,1135,1140,1145,1150,1155,1175,1800
plot
exit
```